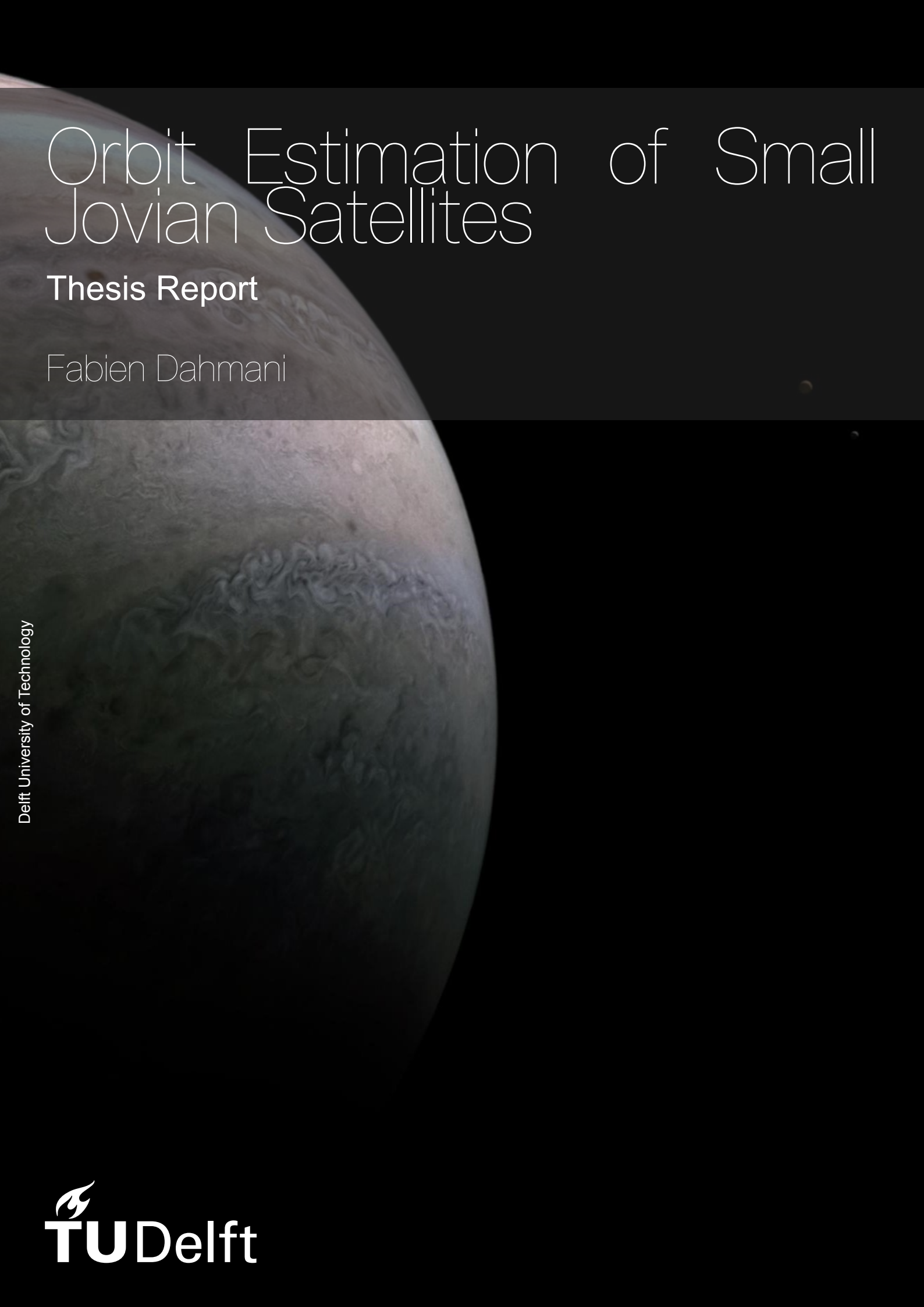

Orbit Estimation of Small Jovian Satellites

Thesis Report

Fabien Dahmani

Delft University of Technology

TU Delft

Orbit Estimation of Small Jovian Satellites

Thesis Report

by

Fabien Dahmani

to obtain the degree of Master of Science
at the Delft University of Technology,
to be defended publicly on Monday February 19, 2024 at 01:00 PM

Student Number:	4824555	
Thesis committee:	Ir. K.J. Cowan MBA	Committee chair
	Dr. Ir. D. Dirkx	Supervisor
	Dr. Ir. J.G. De Teixeira da Encarnação	External Examiner

The cover picture was taken by NASA's Juno mission, demonstrating Jupiter, along with the Jovian moons Io and Europa. Image credit: NASA

TU Delft

Preface

After five and a half years in Delft, these are the final official words I will be writing as a student. The next one will be my name at the bottom of my diploma when I am officially graduated. Despite a minor interruption due to the COVID-19 pandemic, it was one of the best periods of my life so far, and I am very curious about what future opportunities will cross my path, now that I have overcome this challenge. Before that however, I want to take a few words to express my thanks to the people who were invaluable to realizing this project, and by extension, my master, and supported me throughout this journey.

First of all, I want to thank my exceptional supervisor, Dominic Dirkx. Not only did he provide accurate and clear advice when discussing how to move forward, but he was also always ready to help debug any problems I identified within the tudat library, such that I could quickly move forward. Finally, he provided many motivating words and helpful insights during the tedious process of processing the raw observation files. For all of this: thank you, Dominic!

Secondly, I would like to extend my deepest gratitude to my uncle, Etienne Huyghe, who aided me significantly by proofreading this thesis and making sure I did not misspell my very own name.

A third thank you goes out to my friends, that were invaluable in keeping a perfect balance between work and fun during my period in Delft, one of the most important aspects of success.

Last, but most definitely not least, I cannot thank my parents enough for their unwavering support throughout my studies. They have always been my strongest believers and fiercest supporters, and they have sacrificed on many occasions to accommodate me. This journey would have most definitely not been possible without them. Of course, this gratitude also extends to my brother, Nathan, not in the least for the occasional comedic relief.

Fabien Dahmani
Delft, February 2024

Abstract

The primary motivation for this work was the lack of open-source or clearly motivated studies describing the orbit estimation of natural satellites. The capability to accurately model the trajectory of the moons of Jupiter is crucial for properly understanding the evolution of the Jovian system and, by extension, the solar system. Considering the small Jovian moons remain relatively unknown, they will be the focus of this study. The goal of this project was to develop a framework for the full estimation process, based on the Tudat software library, starting from raw astrometric observations, to be made available publicly.

The first step was designing a new data processing algorithm, capable of uniformising the observational data. These measurements are reported in a wide variety of formats, with differences in time format, time scale, orientation, and observation type, amongst others. The developed software was able to produce Tudat-compatible observations with limited user interaction. These processed measurements were then analyzed and validated, first by examining the mean residuals with respect to existing ephemerides to detect remaining biases in the data, before comparing the standard deviation of these residuals to those reported in their original publication, whenever available.

Secondly, the estimation framework was set up. Based on the processed astrometric observations, the orbits of three minor Jovian satellites, Himalia, Elara, and Amalthea were estimated as case studies. Each of these posed its own set of challenges, but together they yield a good representation of the full range of outer moons. The SPICE kernel ephemerides were used to evaluate the quality of these orbital solutions.

Estimating Himalia's orbit proved the easiest, as it is the minor moon that is observed the most, in combination with its relatively slow dynamics. One problem was the fact that there was a remaining unmodeled bias in the oldest, i.e. pre-1960, observations due to errors in converting from old to new frames. Removing these observations and replacing them with simulated measurements with realistic residuals both proved to reduce the difference with respect to the SPICE benchmark to within the uncertainty level of this very benchmark. This proves that the framework allows to accurately estimate the ephemerides of Himalia, although no conclusions could be drawn on the exact contribution of the old observations.

Elara's orbit is in many ways similar to that of Himalia, as they are part of the same orbital group. However, a close approach with this more massive Himalia in 1949 had a significant impact on Elara's trajectory. Therefore, estimating Elara's orbit is not limited to its initial state. Instead, Himalia's gravitational parameter is determined concurrently to optimize the solution. However, even when determining this gravitational parameter, it became apparent that the current dynamical model could not perfectly capture the dynamics at the close approach, due to the limited amount of data before the event, leading to an error of several hundred km. This is still well below the residual of the observations, however.

Finally, Amalthea proved to be the most difficult body to get an accurate orbital solution for. Since Amalthea is an inner moon, as opposed to the outer moons Himalia and Elara, its angular velocity is over 500 times higher. This logically makes both timing and position errors significantly more impactful. Additionally, the very limited amount of data, which is constrained to just a few campaigns of several nights, further hamper accurate orbit determination. By limiting the step size of the update in the estimated initial state between iterations to a standard deviation of 100 km by defining the a-priori covariance, a stable solution, accurate to several 100 km could be found. A preliminary investigation of the contribution of simulated spacecraft data indicated that the few available spacecraft observations of Amalthea have a large impact, which warrants further studies.

Thus, through determining and analyzing the orbit of these three case studies, the quality of the developed framework is ascertained. The solutions proved to lie within the uncertainty region of the ephemerides published in SPICE. Inaccuracies in the estimated orbit could always be linked to deficiencies in the input data, thus not taking away from the quality of the framework.

Contents

1

Introduction

Since its inception, mankind has been studying the motion of the heavens, trying to understand the dynamics governing the night sky. Gradually, a theory emerged that the solar system is not a steady-state solution, but rather a complex dynamical system that is continuously evolving. Logically, this led brave individuals to wonder backward, dreaming of the origins of the solar system and how it developed from there. Answering these questions could not only help us predict the future of our planet but also understand how life flourished on Earth and how likely it is to occur on other bodies. One of the main limitations of this study is the slow dynamics involved. Uranus, with an orbital period of 84 years, has yet to complete its third orbit since its discovery. Clearly, 2 rotations are not sufficient to draw any conclusions on the long-term evolution of its dynamics.

There is an alternative within the solar system, however. Jupiter and its moons can be compared to the Sun, the planets, and asteroids. They both have a small number of massive bodies, containing more than 95% of the mass in orbit, orbiting with low eccentricities and inclinations. Within this same plane, there are smaller bodies orbiting closer to the primary. Finally, a number of small bodies that are thought to stem from outside the system have more eccentric, inclined, and distant orbits. For the Jovian system, these are the Galilean, inner and outer moons respectively. The main advantage of studying the evolution of the Jovian system is the rapid dynamics, where moons take hours to days to orbit, instead of years, as well as having expansive datasets.

Thus, determining the orbits of the Jovian satellites is an active field of research (e.g. Jacobson, 2014; Lainey et al., 2004; Lieske, 1980). Throughout the past decades, this facilitated improvements in our understanding of tidal mechanics (e.g. Lainey et al., 2009) and geological phenomena (e.g. Sohl et al., 2002) amongst others, and for the speculation of the development of life on the icy moons with subsurface oceans (Chyba and Phillips, 2002). However, most of this research is centered around the Galilean moons, whereas significantly fewer publications discuss the orbit estimation of the small Jovian moons, except for those describing the ephemerides published by the Jet Propulsion Labratory (JPL) (e.g. Brozović and Jacobson, 2017; Jacobson, 2000) and by the Institut de Mécanique Céleste et de Calcul des Éphémérides (Institute of celestial mechanics and of the calculation of ephemerides, IMCCE) (e.g. Emelyanov, 2005a; Emelyanov et al., 2022). However, neither of these covers in-depth how these ephemerides were obtained, apart from the general working principles and a rough overview of the data employed. Therefore smaller institutions, independent scientists, and astronomers have to rely on the results of these publications, without being able to estimate their own ephemerides easily.

In order to fill this gap, the main goal of this study is to develop a fully open-source framework for orbit estimation, specifically for the minor Jovian satellites, starting from raw observations, and demonstrate its functionality. The estimation process was applied to three case studies, which were Himalia, Elara and Amalthea, which together represent a wide range of natural satellites. The observations required for these estimations were taken from the Natural Satellite Data Center (NSDC), which contains a large amount of observations about the solar system moons. The first part of this project was then concentrated on robustly processing these data into a usable format. The second phase then revolved around

properly setting up the estimation process. The JPL ephemerides, in the form of SPICE kernels, were used as a benchmark to evaluate the quality of the fit, and as a basis for an initial guess and simulations. The results of the solution were then used to compare with some of the existing numbers on uncertainty, accuracy, and conclusions drawn. Logically, the first point of comparison is the small amount of data that is available from the quality of the existing ephemerides. Another important comparison was determining the mass of Himalia from Elara's orbit. These two bodies had a close encounter in 1949, based on which the gravitational parameter from Himalia was calculated (Emelyanov, 2005b). Both software and observation files were made available in the repository[1].

1.1. Research Goal

As mentioned, this study aimed to demonstrate the full estimation process. The main research goal is defined as:

- To accurately estimate the state of the Jovian minor moons, specifically that of the case studies Himalia, Elara and Amalthea, based on raw NSDC observations.

This objective can be broken down into the following sub-goals:

- To Process the raw observations into uniform tudat-readable files.
- To accurately model the dynamic environment of the (selected) Jovian moons.
- To reach a convergent estimate of the orbit of the (selected) Jovian moons.
- To perform a preliminary assessment of the influence of Spacecraft observations on the generation of Amalthea ephemerides.
- To determine the mass of Himalia.

1.2. Report Outline

How these goals were achieved will be discussed in this thesis report. The main content will be presented chapter 2 in the form of a Journal article, while the conclusions will be reported in chapter 3. The general working principles of the astrometric data processing algorithm will be discussed Appendix A. The motivation behind the selection of integrator and propagator settings will be covered in Appendix B. Finally, some additional variations of the estimation process are briefly introduced in Appendix C, to further support the choices in the estimation set-up of the case studies covered in the article and contextualize the results.

[1] https://github.com/FDahmani/Estimationframework

2

Journal Article

The core work of this project is provided in the format of a journal article, following the template of Astronomy and Astrophysics.

Astronomy & Astrophysics manuscript no. output
February 5, 2024

Orbit Estimation of the Small Jovian Satellites

An open-source study

F. Dahmani[1]

Faculty of Aerospace Engineering (AE), Delft University of Technology, Kluyverweg 1, 2629 HS Delft
e-mail: f.dahmani@student.tudelft.nl

February 5, 2024

ABSTRACT

Context. Accurately modeling the orbit of the Jovian moons proves crucial in understanding solar system long-term dynamics. Although the Galilean moons have been the subject of many studies and missions, not as much is known about the minor moons of Jupiter. Given the swift increase in publicly available and accurate observations, open-source software would allow for rapid advances in science instead of relying on publications and ephemerides by established institutions.
Aims. We sought to develop a new observation processing and estimation framework, available to any and all researchers without an in-depth understanding of coding in plug-and-play fashion and demonstrate its functionality through an in-depth analysis of data and estimated orbit of several representative applications.
Methods. To achieve this goal, we developed a new processing algorithm that was added to the tudat software library and combined with its existing estimation functionality. The orbits of three minor moons, Himalia, Elara and Amalthea, were estimated as case studies to demonstrate the process and its results. A comparison was then made to existing JPL ephemerides, the SPICE kernels, for validation purposes.
Results. Using the estimation framework we managed to accurately estimate the ephemerides of these three moons, statistically indistinguishable from those of the benchmark. The orbital fit for Himalia proved most accurate, where the positional difference with respect to SPICE was kept below 20 km for the past 40 years. The orbits of Amalthea and Elara could be determined up to several hundred km, mostly due to the limited quantity and quality of data. Furthermore, we estimated Himalia's gravitational parameter to be 0.144 km^3s^{-2} based on its 1949 close approach with Elara, well within the range 0.13 ± 0.02 km^3s^{-2} reported in earlier studies. Finally, we verified the suspicion that Amalthea's ephemerides improved greatly with the available mission data, increasing the agreement with SPICE to below 30 km, while the older Himalia data did not significantly affect its results.

1. Introduction

Studying the Jovian satellites and their orbits allows us to answer fundamental questions about the solar system, its evolution, and many of its physical phenomena. Amongst others, accurately determining their ephemerides helps in advancing tidal (e.g. Lainey et al. 2009), geophysical (e.g. Sohl et al. 2002), and astrobiological research (e.g. Chyba & Phillips 2002). Furthermore, the Jovian system can be considered a miniature version of the solar system, considering they have similar dynamics and orbiting bodies, and thus conclusions on its evolution can be extrapolated to the solar system as a whole (Heller et al. 2015). This is beneficial given the faster dynamics, where some moons complete a full rotation in a few hours, as opposed to the nearly 150 years for Neptune. An active area of research is thus to understand how the Jovian, and by extension Solar, system came to be. This, in turn, is expected to shed light on the conditions that allowed for the development of life on Earth, and whether similarly favorable circumstances could have nurtured life elsewhere, such as moons containing subsurface oceans (e.g. Chyba & Phillips 2001).

The majority of these studies focus on the four Galilean satellites, the largest in the Jovian system, containing over 99.997 % of the mass in orbit around Jupiter. Due to their size and brightness, they were discovered early, have more extensive observational datasets and have been the target of multiple (future) missions, such as JUICE and Europa Clipper, as well as being observed abundantly by earlier missions, such as Voyager (Smith et al. 1979) and Cassini (e.g. McCord et al. 2004), while passing through the Jovian system. Subsequently, many studies have estimated their orbit, both to answer scientific questions (e.g. Lainey et al. 2009) and to prepare for missions (e.g. Dirkx et al. 2016).

The small moons of Jupiter however did not enjoy the same level of attention, mostly as a result of them being harder to observe, as they are small and faint. Many of these were only discovered after the year 2000, and new ones are still being found to this date, as increasingly small bodies can be detected due to improvements in both telescopes and image processing techniques (Sheppard et al. 2023). Others have not been observed (often) since their discovery, and are considered lost (Brozović & Jacobson 2017). Nevertheless, properly understanding the motion of these satellites can be crucial in uncovering the evolution of the Jovian system, including their origin. The small Jovian moons can be roughly split into two groups: the inner moons and the outer moons. The inner moons are hard to detect due to their faintness and their proximity to Jupiter, all orbiting with a semi-major axis of 3 Jupiter radii or lower, which causes a lot of noise in the observations. Apart from their short period of up to 16 hours, they have orbits similar to the Galilean moons, i.e. low eccentricities and inclinations. The outer Jovian satellites on the other hand are significantly farther from Jupiter, to the point where the Sun plays a considerable role in their dynamics. Furthermore, these objects usually have high inclinations and eccentricities (Nicholson et al. 2008). Unlike the regular satellites, i.e. the major and inner satellites, these outer moons are thought to

stem from outside the Jupiter system (e.g. Gaspar et al. 2011). Studying their orbital evolution can thus provide insight into orbital stability and capture mechanics (Nesvorny et al. 2003). The outer moons are grouped into families with similar orbital properties and are thought to stem from the same parent body (Sheppard & Jewitt 2003).

Determining the orbits of these minor satellites currently relies primarily on classical Earth-based astrometric observations (e.g. Jacobson 2000; Lainey et al. 2004). These observation sets are supplemented by occasional measurements by spacecraft. Several spacecraft have visited the Jovian system, and despite not being the main focus, have observed minor satellites while they passed through the Field of View (FOV), during dedicated mission extensions (Bindschadler et al. (2003)) or targeted observations depending on mission and instrument availability. Recently there has been an increase of precision in observations. First of all, new space-based telescopes, such as Hubble and Gaia, have not only reported highly accurate angular positions of the moons themselves but Gaia's observations were also used for improving the catalog of background stars allowing for a more accurate data reduction (Mallama et al. 2004; Robert et al. 2017; Brown et al. 2021; Shang et al. 2022). Note however that while these space-based telescopes can observe the positions of the minor satellites with high accuracy, they are usually not used for discovering new moons, as their time is in high demand, while extensive observation campaigns are required for detecting new satellites. Furthermore, there has been a strong interest in alternative observing techniques, including mutual events and approximations (Morgado et al. 2016; Fayolle et al. 2022), which are more accurate than the classical methods (e.g. Morgado et al. 2019).

Several iterations of estimating the orbit of the minor Jovian moons have been made in the past. NASA's Jet Propulsion Laboratory (JPL) continually publishes updated ephemerides on the SPICE system (e.g. Brozović & Jacobson 2017 and earlier iterations). Alternatively, the IMCCE, in collaboration with the Russian Sternberg Institute, provides ephemerides on the MULTISAT system (Emelyanov 2005a; Emelyanov et al. 2022). Additionally, the rise in new observation types allows for new estimation efforts. Using eclipses of Amalthea and Thebe by the galilean satellites showed promising results (Saquet et al. 2016), although more events are required for accurate long-term solutions. Only one other eclipse of Thebe was reported to date (Catani et al. 2023). We are not aware of any publication of data containing mutual approximations containing minor moons at the time of writing. Due to the limited availability of data from mutual events and approximations for now, especially for the small satellites, they are not incorporated into this study. However, they prove great potential for future improvements of the ephemerides. One main limitation within these previous studies is the lack of in-depth explanation covering the steps and choices made within the estimation process, apart from the top-level decisions. Important choices include for example how the integration and propagation were set up, how the observations were weighted and how the input data was corrected. These former studies would mention for example that a weighted least-squares methodology was used, based on the residuals of the observations, without expanding upon the actual calculation of these weights. Alternatively, bias corrections are applied without properly motivating these values. This hampers any attempt at reproducing the results, especially if one aims for a slightly different use case, where it will likely be unclear which corrections, steps are values are required in this new case. Furthermore, all earlier estimation efforts were fully closed-source. This means any future study by third parties would have to start from scratch, based on the very limited instructions published, with only the final estimation result to compare with.

In this study, we focussed on demonstrating the estimation process, fully open-source, for the orbits of 3 specific moons as case studies, representing the full set of small (Jovian) satellites. These case studies will be Himalia, Elara and Amalthea. Himalia was the first outer Jovian satellite to be discovered and has an orbital period of about 250 days. Elara, which was discovered not long after, is part of the same orbital family, and thus has a similar orbit. However, this moon is particularly interesting due to its close approach with Himalia in 1949. The change in its path after this interaction allowed for the estimation of the mass of Himalia (Emelyanov 2005b; Brozović & Jacobson 2017). Finally, Amalthea was the first inner moon to be discovered and has significantly faster dynamics with an orbital period of just 12 hours. This poses more stringent constraints on the requirements of the model, propagator and integrator.

To facilitate the estimation process, we made use of the Tudat (TU Delft Astrodynamics Toolbox) software, specifically its Python interface TudatPy. This open-source software library contains a lot of functionality to enable astrodynamics research, as well as estimation and optimization studies. This software has been used extensively in prior studies (e.g. Dirkx et al. 2014; Bauer et al. 2016), including for modeling Jovian environments comparable to the study at hand (e.g. Dirkx et al. 2016; Fayolle et al. 2021, 2023).

This article will be structured as follows. First, the data employed will be discussed in section 2. Then we will move on to discussing the dynamical model in section 3. section 4 then covers how we set up the estimation procedure, including the specifics of every case study. Next, the results of this estimation process will be presented and discussed in section 5. Finally, we will draw conclusions and present recommendations for future studies in section 6.

2. Data

This section will detail the observations and databases used in estimating the orbits of the satellites. subsection 2.1 will introduce the SPICE system, while subsection 2.2 will cover the NSDC database, the main source of natural satellite observations used in this study. Finally, subsection 2.3 will conclude the section by discussing spacecraft observations of Amalthea.

2.1. SPICE

Throughout this study, SPICE data has been used as a benchmark and a basis for simulations. SPICE is an information system containing many ephemerides and other properties of solar system bodies in sets called kernels, developed by NASA's Navigation and Ancillary Information Facility (NAIF) (Acton 1996). Through Tudat's SPICE interface, the calculated states of all bodies in these kernels can easily be requested at any given epoch within the ephemerides' window. Comparing these natural satellite positions retrieved from SPICE with those found from observation or estimation can be used to get an idea about their quality, as will be explained more in depth in section 5. It is important to note that while SPICE Kernels are high-accuracy, they are the result of an estimation process themselves, based on available data, and are therefore not perfect. For example, the uncertainty of Himalia's reported position was estimated to be 56 km in 2010 (Brozović & Jacobson 2017). Hence they are

a good benchmark for lower precision data (e.g. a single observation), but they can not be considered as absolute truth at higher precisions. In this study, a series of standard kernels have been loaded, as shown in Table 1, which include information on positions, masses, and orientations of the planets and the major natural satellites, as well as leap seconds. Additionally, the 'jup344.bsp' kernel was loaded, as it is the most complete data set for the Jovian system ephemerides, containing estimated positions of many, including minor, moons from the year 1800 to 2200.

2.2. NSDC

The observations used in this study were taken from the Natural Satellite Data Center (NSDC) [1]. This online database provides many sets of observations of the solar system moons from many campaigns, albeit in various reporting layouts. Although earlier studies have used these data sets (e.g. Emelyanov 2005a), no open-source tool was available to process and uniformize this data at the time of writing. Therefore, the first step in this project was to develop software that could perform this function. This functionality was later added to the TudatPy library and is henceforth available publicly [2].

In the NSDC database, the observations of the Jovian moons are divided into 4 categories: the inner moons, the Galilean moons, the most prominent outer moons (up to and including JXIII), and the other outer moons (JXVII and onwards). This distinction is logical, considering most observation campaigns observed multiple moons, although generally within the same category. As the principal satellites of this study will be Amalthea, Elara, and Himalia, it was chosen to process all files within the inner and prominent outer categories. All raw and processed observations are available in the repository, together with the rest of the estimation framework [3].

For the inner satellites, 11 files have been analyzed, collectively resulting in 1387 observations across the four moons. While these span a period of 27 years, some further files were discarded as their period of observation lay significantly outside this window. Although adding them would be advantageous in studying the longer-term effects and quality of the orbital fit, their sporadic nature combined with the significant increase in computational load motivated this decision. These 11 files are denoted in Table 2 by their NSDC file identifier, along with the mean and standard deviation of their difference in RA and DEC with SPICE after processing. This analysis shows that there are no significant biases remaining in the processed files, as the means are close to 0 µrad. Furthermore, these values are comparable to those in the original publications of this data (e.g. Kulyk et al. 2002 for ji0002). Figure 1 shows the residual between Amalthea's observed angular position and that retrieved from Spice at the same epoch, color-coded by their NSDC identifier. These data will be used as input in estimating Amalthea's orbit. One can already clearly notice the concentration of the observations at a limited number of epochs.

As outer moons are often easier to observe, considering they are much further away from Jupiter, more observations are available, spanning a significantly larger period and at a higher accuracy. For this study data will be included from 1900 up until

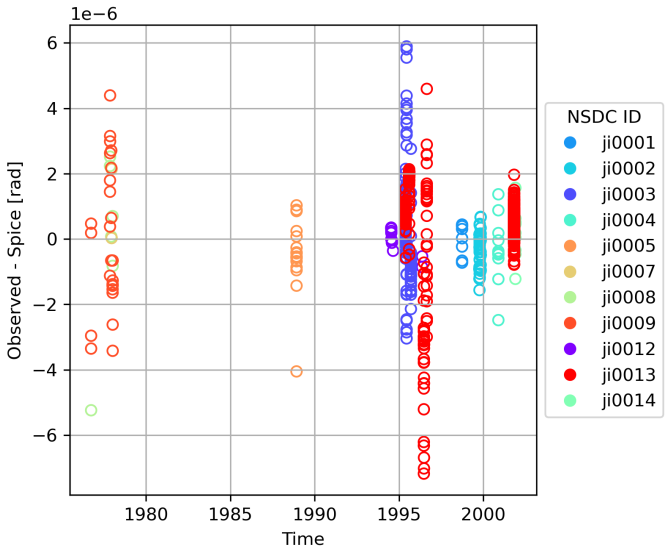

Fig. 1: Difference in Right Ascension between Amalthea observations and Amalthea's position from Spice, sorted per original NSDC file. The details and original study for each of these files can be found in Table 2. The declination residuals are similar and were omitted for clarity.

2023. This duration is not problematic, as opposed to Amalthea where estimating such a long stint would take close to 24 hours, considering the slower dynamics (Himalia's period is 500 times longer than that of Amalthea) reduce the computational load as a larger time step can be selected. The results from the outer Jovian moons NSDC files are shown in Table 3 added to the end of the paper, where we can observe the increase in quantity and quality of data over time. The observations used as input for estimating the orbits of Himalia and Elara can be found in Figure 2 and Figure 3 respectively. It can be seen that older data is significantly less precise and sparser. Especially for Elara, there are just a few usable observations before its 1949 close approach with Himalia. Note that there are no substantial systematic differences between residuals in right ascension and declination, instead being clumped together.

2.3. Spacecraft Observations

Although no missions specifically targeting the smaller Jovian moons have ever been launched, several have been able to capture images of Amalthea and the other inner moons, due to their close proximity to Jupiter. The epochs of these observations that are used to generate ephemerides can be found in JPL's database [4].

2.3.1. Voyager

Both Voyager missions observed Amalthea during their Jupiter gravity assists. These images were crucial in improving the physical model (e.g. Veverka et al. 1981) and ephemerides (Jacobson 2014 and earlier versions) of Amalthea, as they were significantly more accurate than the current best Earth-based alternatives. Voyagers 1 and 2 had closest approaches of respectively 417 000 and 558 000 km to the moon (Campbell & Synnott 1985), with at least 19 observations across both missions. With

[1] http://nsdb.imcce.fr/obspos/obsindhe.htm
[2] https://docs.tudat.space/en/latest/_src_user_guide/state_estimation/observation_simulation/loading_real_data.html#natural-satellite-data-center-astrometry
[3] https://github.com/FDahmani/Estimationframework
[4] https://ssd.jpl.nasa.gov/sats/obs_data.html

Table 1: Standard Spice kernels loaded within this estimation study.

Kernel	Contents
pck00010.tpc	Orientation and Shape data of natural bodies
inpop19a_TDB_m100_p100_spice.tpc	Masses of solar system planets
inpop19a_TDB_m100_p100_spice.bsp	Ephemerides of solar system planets
NOE-5-2021.tpc	Jupiter rotation and mass, Galilean moons and Amalthea masses
NOE-5-2021.bsp	Jupiter, Galilean moons and Amalthea ephemerides
naif0012.tls	Leap second kernel

Table 2: Means and standard deviations in Right Ascension and Declination of processed observations of NSDC files on the Inner Jovian satellites, along with the number and period of these observations.

NSDC Identifier	RA $\mu \pm \sigma$ (μrad)	RA $\mu \pm \sigma$ (μrad)	#Obs	Observation Period	Reference
ji0001	-0.22 ± 0.56	-0.02 ± 0.50	35	1998 - 1998	Ledovskaya et al. (1999)
ji0002	-0.44 ± 1.02	0.18 ± 0.96	154	1999 - 2000	Kulyk et al. (2002)
ji0003	0.48 ± 1.54	-0.48 ± 1.06	165	1995 - 1995	Veiga & Vieira Martins (1996)
ji0004	-0.92 ± 2.97	0.37 ± 1.81	121	2000 - 2000	Kulyk et al. (2002)
ji0005	-0.27 ± 1.40	-0.11 ± 0.68	153	1988 - 1988	Nicholson & Matthews (1991)
ji0007	0.12 ± 0.85	0.04 ± 0.32	10	1977 - 1977	Ianna et al. (1979)
ji0008	-0.09 ± 2.58	-0.52 ± 1.74	6	1976 - 1978	Mulholland et al. (1979)
ji0009	0.04 ± 2.18	-0.88 ± 1.33	24	1976 - 1978	Mulholland et al. (1979)
ji0012	-0.08 ± 0.38	0.04 ± 0.51	10	1994 - 1996	Mallama et al. (2004)
ji0013	0.22 ± 1.82	0.04 ± 1.15	651	1995 - 2001	Veiga & Vieira Martins (2005)
ji0014	-0.38 ± 1.83	-0.52 ± 0.88	58	2001 - 2002	Kulyk (2008)

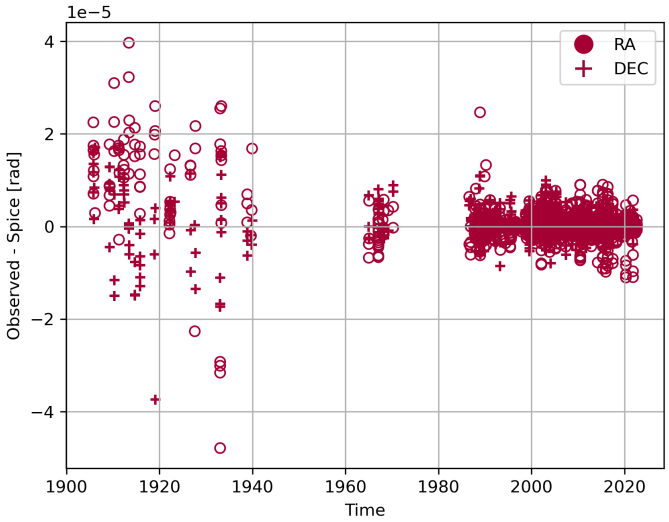

Fig. 2: Difference in Right Ascension and Declination between Himalia observations and Himalia's position from Spice, sorted per original NSDC file.

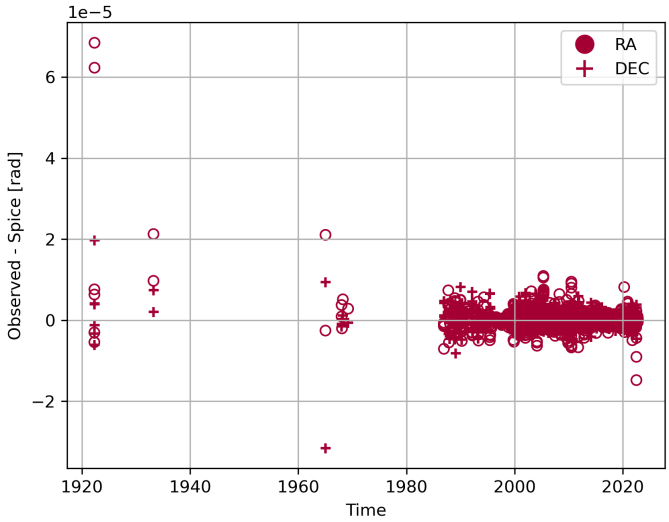

Fig. 3: Difference in Right Ascension and Declination between Elara observations and Elara's position from Spice, sorted per original NSDC file.

an uncertainty of half a pixel in these observations, as reported by JPL, they were accurate up to several km (Smtih et al. 1979).

2.3.2. Galileo

Despite failure during the deployment of the High-Gain Antenna (O'Neil et al. 1993), the Galileo mission proved robust and successful, getting two extensions to its nominal mission. Throughout its 8-year stint orbiting Jupiter, it has been able to observe Amalthea at least 26 times with its SSI instrument, with an accuracy of up to 20 kilometers at Perijove (uncertainty of twice the pixel scale of 10 km, Thomas et al. 1998). Furthermore, during Galileo's final mission extension, it performed an Amalthea flyby at a closest approach of 230 km (Weinwurm 2006) on November 5th, 2002. Although the high radiation dose forced the spacecraft to go into safe mode 16 minutes after the flyby, it already captured a lot of useful radio science, fields, and particles data and observations (Bindschadler et al. 2003) which allowed for improving the models of Amalthea's physical properties such as density, indirectly contributing to orbit determination.

2.3.3. Cassini

The Cassini spacecraft produced a total of over 26000 pictures during its Jupiter swingby in 2000-2001. Despite not being the intended target of these images, Amalthea would theoretically

be present in quite some of them, due to its close proximity to Jupiter. To help prepare for Galileo's 2002 Amalthea flyby mentioned before, a study was performed to detect Amalthea amongst these observations (Cooper et al. (2006)). They reported 239 Amalthea observations, which led to an estimation of its orbit with a precision of several km.

3. Dynamical Model

This section will delve deeper into the model that will be used to represent the Jovian system in this study. subsection 3.1 will introduce the gravitational accelerations working on the minor moons. Afterwards, the equations describing their motion will be discussed in subsection 3.2. Finally, the section is concluded by discussing the settings of the integrator and propagator, including the specific properties of the different case studies.

3.1. Acceleration models

The gravitational attraction of any body j on another body i can be described by (Lainey et al. 2004):

$$\ddot{\boldsymbol{r}}_{ij} = \ddot{\boldsymbol{r}}_{\bar{i}\bar{j}} + \ddot{\boldsymbol{r}}_{\bar{i}\hat{j}} + \ddot{\boldsymbol{r}}_{\hat{i}\bar{j}} + \ddot{\boldsymbol{r}}_{\hat{i}\hat{j}} \tag{1}$$

where $\bar{i}$ and $\bar{j}$ represent the point masses of the bodies, while $\hat{i}$ and $\hat{j}$ stand for their extended bodies. In this equation, the gravitational force is broken down into the acceleration on the point mass $\bar{i}$ due to point mass $\bar{j}$, $\ddot{\boldsymbol{r}}_{\bar{i}\bar{j}}$, the acceleration of the point mass $\bar{i}$ due to the extended body $\hat{j}$, $\ddot{\boldsymbol{r}}_{\bar{i}\hat{j}}$, and the acceleration on the extended body $\hat{i}$ due to point mass $\bar{j}$, $\ddot{\boldsymbol{r}}_{\hat{i}\bar{j}}$. The final term, the acceleration $\ddot{\boldsymbol{r}}_{\hat{i}\hat{j}}$ caused by the extended body $\hat{j}$ on the extended body $\hat{i}$ is considered negligible due to the multiplication of the small zonal terms involved (Krivov 1993; Dirkx 2022). The remaining three terms are then equal to:

$$\ddot{\boldsymbol{r}}_{\bar{i}\bar{j}} = \mu_j \nabla U_{\bar{j}}(\boldsymbol{r}_{ij}) \tag{2a}$$

$$\ddot{\boldsymbol{r}}_{\bar{i}\hat{j}} = \mu_j \nabla U_{\hat{j}}(\boldsymbol{r}_{ij}) \tag{2b}$$

$$\ddot{\boldsymbol{r}}_{\hat{i}\bar{j}} = -\frac{\mu_i}{\mu_j} \ddot{\boldsymbol{r}}_{\bar{j}\bar{i}} \tag{2c}$$

Within the scope of this work, all three study cases are minor moons, which means $\frac{\mu_i}{\mu_j} \approx 0$ for all bodies j that exert a meaningful attraction on the small satellites i. The gravitational potential of point mass $\bar{j}$ is given by:

$$U_{\bar{j}}\left(\mathbf{r}_{ij}\right) = \frac{1}{r_{ij}} \tag{3}$$

Whereas the gravitational potential function of the extended body $\hat{j}$ can be described by the spherical harmonics expansion, which is equal to (Lainey et al. 2004):

$$U_{\hat{j}}\left(\mathbf{r}_{ij}\right) = \sum_{l=0}^{\infty} \sum_{m=0}^{l} U_{j,lm} \tag{4a}$$

$$U_{j,lm} = \left(\frac{R^l}{r^{l+1}}\right) P_{lm}(\sin\phi)\left(C_{lm}\cos m\theta + S_{lm}\sin m\theta\right) \tag{4b}$$

3.2. Equations of Motion

The equations of motion govern the dynamics of the propagated moons. In their simplified version, in the absence of non-gravitational forces, the equation becomes a straightforward summation of the gravitational forces by all bodies, which in reality is limited to those exerting a significant attractive force. This total acceleration can be broken down in that by the central body Jupiter (J), and the perturbation by the third bodies (j). In a Jupiter-centered ECLIPJ2000 inertial orientation, this becomes (Dirkx 2022):

$$\ddot{\boldsymbol{r}}_i = \ddot{\boldsymbol{r}}_{iJ} + \sum_{j=1}^{N(j\neq J)} \ddot{\boldsymbol{r}}_{ij} \tag{5}$$

where

$$\ddot{\boldsymbol{r}}_{iJ} = -(\mu_i + \mu_J)\left(\frac{\boldsymbol{r}_{iJ}}{r_{iJ}^3} - U_{\hat{J}}\left(\mathbf{r}_{iJ}\right) + U_{\hat{i}}\left(\mathbf{r}_{Ji}\right)\right) \tag{6a}$$

$$\ddot{\boldsymbol{r}}_{ij} = -\mu_j\left(\left(\frac{\boldsymbol{r}_{ij}}{r_{ij}^3} - U_{\hat{j}}\left(\mathbf{r}_{ij}\right) + U_{\hat{i}}\left(\mathbf{r}_{ij}\right)\right) - \left(\frac{\boldsymbol{r}_{Jj}}{r_{Jj}^3} - U_{\hat{j}}\left(\mathbf{r}_{Jj}\right) + U_{\hat{J}}\left(\mathbf{r}_{jJ}\right)\right)\right) \tag{6b}$$

The main question remaining from Equation 5 is which bodies j should be taken into account and to what degree and order should the spherical harmonics of the different bodies be expanded. Based on a preliminary analysis, where the propagated orbits with and without a specific body or zonal harmonic term were compared. Only when this difference proved to affect the state by multiple km, which is an order of magnitude more precise than the best-case expected quality of the fit, they were added to the environment. For the three case studies, these influential accelerations are:

- Spherical Harmonic acceleration by Jupiter up to degree and order (8,0)
- Point mass accelerations by the Galilean moons
- Point mass accelerations by the Sun and Saturn

Additionally, for propagating Elara, given its deviation in orbit due to the 1949 close approximation:

- Point mass acceleration by Himalia

By integrating these equations it is possible to determine the position of the body at any epoch, i.e. propagate their state. The inverse problem, namely determining the model parameters based on a series of observed positions, will be discussed in section 4.

3.3. Numerical Integration and Propagator Settings

In order to avoid introducing additional errors, it is important to properly set up the integration and propagation. The integrator refers to the tool or method used to solve the differential equation Equation 6, while the propagator is a broader instrument to calculate the state of the body at a later epoch, based on the current state, the integrator and the environment. Due to the difference in dynamics, these vary slightly per study case, and will thus be discussed separately. One setting in common between the study cases however is the selection of the Runge-Kutta Dormand-Prince 8th order integrator (Dormand & Prince 1980). While

other estimation studies employed the Runge–Kutta–Nystrom or the Gauss–Jackson method (e.g. Jacobson 2000; Brozović & Jacobson 2017) due to their low integration errors for long propagations, the RKDP8 integrator was chosen as it was the most accurate and stable integrator available within the Tudat library.

3.3.1. Amalthea

Amalthea's state was propagated and subsequently estimated from 1976 up until 2003. This period was chosen to maximize the amount of observations included in the timespan. However, to minimize the propagation error increasing over time, the initial epoch was taken on January 1st 1990, and propagating both forward and backward from there. Due to the short orbital period, a constant time step of 6 minutes was used.

3.3.2. Himalia

As Himalia has a significantly lower angular velocity than Amalthea, the time step for its propagation was taken at 180 minutes. Due to the reduction in computational requirements, this allowed for the expansion of the time of propagation to 1900 - 2023. The initial epoch was taken at 1980, a good point of distinction between the plentiful and accurate modern data, versus the sparse and imprecise older observations.

3.3.3. Elara

Like Himalia, a step size of 180 minutes was chosen for Elara as their orbital periods are comparable. Additionally, the same period was considered. However, unlike Himalia, the starting Epoch was taken as the 15th of July, 1949, which was the date of the close approach. This ensures that the propagation error is minimal at this crucial epoch.

4. Estimation Set-up

This section will be dedicated to discussing the process of estimating the orbit of the moons based on the observational data discussed in section 2 and the dynamics covered in section 3. The first step will be discussing the least square estimation process that will be used for finding the best fit in subsection 4.1, before covering how weights are calculated and assigned in subsection 4.2. Afterwards, we will briefly explain how an initial guess for the initial state is generated to improve the rate of convergence. Finally, we will cover the specific steps from data to final fit in subsection 4.4, once again discussing the specifics per moon. An overview of how the different processes in this work come together towards a final solution of the orbits is shown in Figure 4.

4.1. Least Squares Estimate

In the estimation process, the observations and dynamical model are combined in fitting the orbit to the data. This entails that the best combination of estimated parameters is iteratively found, in order to minimize the residual between calculated (i.e. propagated based on the dynamical model) and real observations. A least squares methodology was used in this study, following the notation and methodology by (Montenbruck & Gill 2000).

First, one can define $\mathbf{z}$ as the vector containing the observations and relate it to the dynamical model through:

$$\mathbf{z} = \mathbf{h}(\mathbf{x}_0) + \boldsymbol{\epsilon} \tag{7}$$

where $\mathbf{h}(\mathbf{x}_0)$ corresponds to the function that returns the expected observation value (e.g. angular position) at the same epoch t as the observation based on the initial state $\mathbf{x}_0$. $\boldsymbol{\epsilon}$ on the other hand represents a vector containing the measurement errors, which is assumed to be a random distribution around a zero mean. The goal of orbit fitting is then to find $\mathbf{x}_0$ that minimizes the residual between $\mathbf{z}$ and $\mathbf{h}(\mathbf{x}_0)$, which is done here by minimizing the sum of the squares of these residuals, known as the loss function.

$$J(\boldsymbol{x}_0) = \boldsymbol{\rho}^T \boldsymbol{\rho} = (\mathbf{z} - \boldsymbol{h}(\boldsymbol{x}_0))^T (\mathbf{z} - \boldsymbol{h}(\boldsymbol{x}_0)) \tag{8}$$

Determining $\mathbf{x}_0$) leading to the minimum value of this function is complicated however due to the highly non-linearity of $\mathbf{h}(\mathbf{x}_0)$. Linearizing this equation around a reference or a-priori state $\mathbf{x}_0^{ref}$ provides a solution by simplifying the equation. The residual $\boldsymbol{\rho}$ can be approximated close to this reference state by:

$$\rho \approx \Delta\mathbf{z} - \mathbf{H}\Delta\mathbf{x}_0 \tag{9}$$

$\Delta\mathbf{z}$ represents the discrepancy between the actual observed measurements and the expected observations at epoch t based on the reference initial state. $\Delta\mathbf{x}_0$ on the other hand is the difference between the reference initial state and the initial state that is being estimated. Finally, $\mathbf{H}$ depicts the change in or sensitivity of the expected observations at epoch t, due to changes in the initial state, and is known as the design matrix or the Jacobian.
Replacing this approximation for the residual into the loss function and differentiating to find the minimum, results in the following solution for the least squares problem:

$$\Delta\boldsymbol{x}_0^{\text{lsq}} = \left(\boldsymbol{H}^T\mathbf{W}\boldsymbol{H}\right)^{-1}\left(\boldsymbol{H}^T\mathbf{W}\Delta\mathbf{z}\right) \tag{10}$$

In this equation, the weight matrix $\mathbf{W}$ was added to to account for the relative importance and accuracy of observations. This matrix, along with how it was determined in this study will be covered in subsection 4.2. This process will be iterated by using the newfound initial state as reference state until either the maximum amount of iterations is reached, or until the change in loss function between two iterations is lower than a prescribed tolerance. Furthermore, the state covered in this section can be altered to include parameters that influence either the dynamics or the observations, such as the gravitational parameter of the central body. This does not change the fitting process but allows for more freedom in finding an accurate solution, at the cost of a higher complexity due to the increased dimensionality. Finally, we introduce the covariance matrix. This matrix represents the uncertainty in the estimated parameters and the relation between them and is defined as:

$$\mathbf{P} = (\mathbf{H}^T\mathbf{W}\mathbf{H})^{-1} \tag{11}$$

which is the first part of Equation 10. Apart from quantifying the reliability of this solution, it can be used to convey existing knowledge, which is information about the quality of the initial guess, the parameters, and the orbit into the least-squares problem. This is done by adding this knowledge in the form of an a-priori covariance matrix $\mathbf{P}_0^{-1}$ into Equation 11, as follows:

$$\mathbf{P} = (\mathbf{H}^T\mathbf{W}\mathbf{H} + \mathbf{P}_0^{-1})^{-1} \tag{12}$$

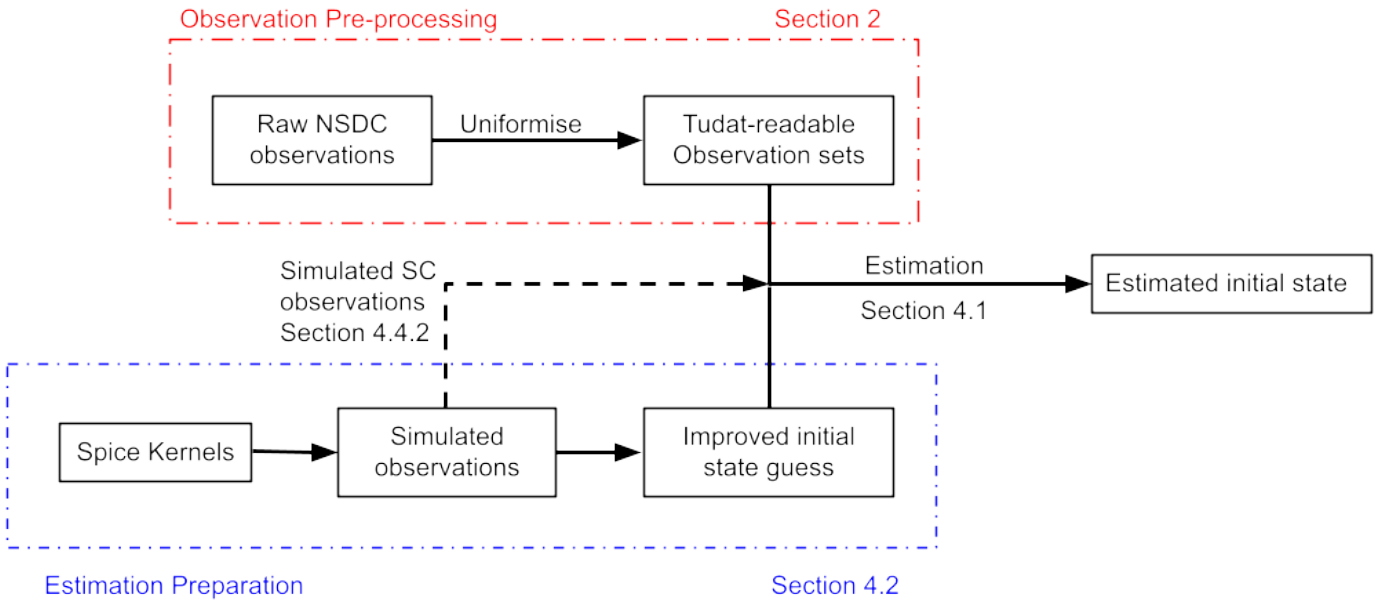

Fig. 4: An overview of the flow of the estimation process.

Implementing this new covariance matrix instead of the first part in Equation 10 results in Equation 13. Low values in $\mathbf{P}_0$, indicating a low a priori uncertainty, lead to a high $\mathbf{P}_0^{-1}$, thus dominating the first part of the equation. Taking the inverse then leads to this first factor becoming smaller with decreasing uncertainty. Thus, low a-priori uncertainties constrain the magnitude of the change in estimated parameters. Inversely, a higher uncertainty in the a-priori knowledge means the new observations are more influential. This equation nicely demonstrates the relative contribution of new and older data or observations, based on their quality.

$$\Delta \boldsymbol{x}_0^{\text{lsq}} = \left(\boldsymbol{H}^T \mathbf{W} \boldsymbol{H} + \mathbf{P_0^{-1}}\right)^{-1} \left(\boldsymbol{H}^T \mathbf{W} \Delta \mathbf{z}\right) \tag{13}$$

4.2. Weights

One important part of setting up this estimation procedure is properly defining the weight each observation should carry. In the previous section, the weight matrix $\mathbf{W}$ was introduced. This matrix contains the inverse of the variance of the observations on the diagonal. Off-diagonal entries indicate correlations between the uncertainty in observations. However, for the purpose of this study, the observations are assumed to be uncorrelated.

The general flow of determining these weights in the context of this study is demonstrated in Algorithm 1. The observations are grouped in arcs, which are measurements of the same publication taken less than 6 hours apart. Rather than directly relating the residual of a single observation with respect to the SPICE benchmark to the weight, which would assign extremely high weights to observations that are close to SPICE by chance, these residuals are averaged per arc. In this way, the weight, which is the squared inverse of this average residual, better represents the quality of the arc. A correction factor of $\sqrt{n}$ was applied to the noise, which is the average residual, to avoid dense arcs of observations, that can not be considered truly independent due to their proximity, completely dominating the solution, while not providing proportionately more new information. Detailed values of these weights are given in Appendix A.

Algorithm 1 Defining the weights of observations

for observation in dataset **do**
  if time since $ArcStartTime$ > 6 hours **then**
    n = length($CurrentArc$)
    $AverageResidual = \frac{\sum(\text{residuals of } CurrentArc)}{n}$
    $Noise = AverageResidual * \sqrt{n}$
    $Weight = \frac{1}{Noise^2}$
    Delete $CurentArc$
  end if
  Add observation to $CurrentArc$
end for

4.3. Initial guess generation

As a first step in the estimation process, an initial guess for the initial state is generated to ensure faster convergence. To produce this guess, ideal, error-free observations were simulated from SPICE, at intervals of 3 hours, for the duration of the propagation. A least squares estimate of the initial state was then made to minimize the residual between the propagated state and these simulated observations. This way, the initial state is shifted to account for disparities in the modeled environment with respect to the estimation process that resulted in SPICE, such as differences in integrator, propagator, and accelerations considered. For longer propagations, this process can be split into two steps, where a less accurate guess is generated first, based on a shorter propagation time. Using this method allows for a time-efficient estimation process, as fewer iterations are required when estimating the initial state with real observations. The outcomes of this initial guess generation will be discussed in section 5, together with the other results per study case.

4.4. Process

The Estimation Process itself consisted of loading the observations discussed in subsection 2.2 and assign them weights as discussed in subsection 4.2, to prevent the estimation from being dominated by randomly small residuals. A least-squares estima-

tion, as detailed in subsection 4.1, was then used to determine the initial state iteratively. An additional constraint was placed, allowing a maximum of five iterations to reach a final solution. Although this process was fairly similar for each of the moons, each had their own peculiarities, as will be discussed in this subsection.

4.4.1. Amalthea

There were two main difficulties in accurately determining Amalthea's orbit. On the one hand, its rapid dynamics mean any solution is sensitive to small changes in initial state, while the difference in both quantity and quality of data with respect to the outer satellites opposes accurate estimations. A number of solutions have been applied to solve these issues. Firstly, a constraint was placed on how much the estimator could vary the initial state between iterations of the estimation process by defining an a-priori covariance. A value of 100 km, which is believed to be roughly the accuracy of the a-priori knowledge of Amalthea, was used. In reality, we would expect the 'true' initial state to lie within several hundred km from the initial guess, which can be achieved with this a-priori constraint. To improve the quality of the data, an arc-wise bias correction was applied to the observations. The average residual of each arc, as calculated in Algorithm 1 in order to calculate the weights, is used as correction for this bias. This means that the average residual within such an arc is subtracted from each of the observations in the arc. This leads the arc to be centered around 0. The exact values of applied corrections can be retrieved in Appendix A.

4.4.2. Amalthea with simulated spacecraft observations

On top of estimating the orbit of Amalthea using on Earth-based observations, a preliminary investigation of the contribution of spacecraft observations on the ephemeris quality was made, as spacecraft data played an important role in determining Amalthea's ephemerides (Jacobson 2014). Therefore, additional data was simulated, in the form of 3D position observables, at the reported astrometry times of observations of Amalthea by Voyager, Galielo and Cassini [5]. Amalthea's position was retrieved from SPICE at these epochs, across both Voyagers. Based on the discussion in subsection 2.3, Gaussian noise with a standard deviation of 10 km was applied to represent the uncertainty in the Voyager data. For Galileo, this uncertainty was placed on 20 km, except for the close approach on 5th of November 2002, for which 1 km might be a better approximation of the data gathered leading up to the approach. Finally, a standard deviation of 5 km was used in simulating the more accurate Cassini data. Note that these are not the exact observations, rather a rough assumption, nor will the results demonstrate exactly the influence of spacecraft observations. Instead, this sidestep from the study on Earth-based observation is merely intended to get an initial feel for the order of magnitude of the contribution of these spacecraft measurements to the solution. No definite claims will be made, instead, the aim is to form a conclusion on whether these spacecraft observations warrant further investigation, where the actual observations would be employed.

4.4.3. Himalia

As Himalia has significantly slower dynamics than Amalthea, on top of having better quantity and quality of data as discussed in subsection 2.2, no a-priori constraints were necessary in order to quickly and accurately converge to a solution. Similarly, no arcwise bias correction was considered necessary. Although the older data would greatly benefit from it, as no prior corrections were applied to these observations as opposed to other studies (e.g. Jacobson 2000), the sparsity of the data means that most of these arcs would consist of only one or a few observations, which in turn results in simply setting the observations almost exactly equal to the SPICE kernels. By correcting the observations based on the SPICE kernels, while these same kernels are used as a benchmark, this estimation would result in overly positive results. For this reason, no arcwise biases were applied.

4.4.4. Elara

While Elara is in many ways, like its slow dynamics, similar to Himalia, the 1949 flyby requires some modifications to the estimation process. As mentioned by Emelyanov (2005b), this close approach can be used to estimate Himalia's gravitational parameter. The main problem was the scarcity and poor quality of data before the flyby. To combat this, the gravitational parameter of Himalia was estimated concurrently with fitting to SPICE to generate the initial guess, as explained in subsection 4.3. This means that the best combination of initial state and gravitational parameter is estimated in order to minimise the difference between the propagated orbit and SPICE. Since Elara's orbit is strongly influenced by this gravitational parameter, concurrently estimating is required to determine a closer fit. Furthermore, in this case, applying arcwise biases was once again relevant, as explained for Amalthea in subsubsection 4.4.1, due to the importance of pre-1949 observations. Although this likely results in an overestimation of the quality of old data, not correcting these observations like was done for Himalia, would be problematic as pre-encounter data is required to constrain the incoming leg at the close approach and thus the gravitational parameter of Himalia. If this correction would not be applied, the difference with SPICE would grow to 1000's of km, at which point no useful analysis can be performed. For this reason, arcwise biases are applied for all data sets containing data from before 1960, while keeping the effect this has on the quality of the fit in mind.

5. Results & Discussion

This section will be dedicated to presenting the results of the three case studies, four if you count studying the simulated spacecraft observations, introduced in section 4. The results will be introduced per moon, although similar discussions and plots will be present in each. The first topic will be evaluating the quality of the initial state guess and the dynamical model (referred to as the prefit), by comparing it to the SPICE kernel it is fitted to. Afterwards, a similar figure will show the orbital fit (after the estimation, postfit), comparing it to the same SPICE benchmark in order to properly visualize the effects of the estimation process. A comparison between the variance of the input data and the estimated solution will then shed some light on the reliability of the estimation process. In order to better understand the results, the discrepancies with respect to spice are then broken down into RSW components, after which the correlation between the estimated parameters, again in RSW for the initial state, is shown. Then, these results will be explained and contextualized, while making improvements where necessary. These results will be presented first for Himalia in subsection 5.1, while those for Elara will follow in subsection 5.2. The outcome of

[5] https://ssd.jpl.nasa.gov/sats/obs_data.html

the initial state estimation of Amalthea will be discussed subsection 5.3. For the final study case, where simulated spacecraft data was added to Amalthea's observation set, a slimmed-down discussion can be found in subsection 5.4. To keep the overview with the many study cases, especially now that variations will be introduced to the nominal study cases that were presented in subsection 4.4, Table 5 at the end of the article can be used. Here, the main differences between the runs, together with the most important results can be found. Note that the agreement with SPICE is represented here by the largest difference, while ignoring the in-orbit variations. The prefit solutions are also added and denoted by an ID containing '00'.

5.1. Himalia

Figure 5a shows the agreement of the prefit, i.e. the propagated initial state guess as determined as described in subsection 4.3, with SPICE. First of all, it can be noted that the difference between them is below 25 km for the modern times, while it steadily grows for earlier epochs. As a reminder, the uncertainty in the state of Himalia from the SPICE kernel was over 50 km for 2010, thus well above the difference noted here. These discrepancies likely stem from minor variations in the dynamical model. Secondly, the smallest difference is around 2010, which is the reference epoch of the SPICE kernels. This result is expected, considering the uncertainty of the Kernel is the lowest at that point, thus accurately estimating the state at that epoch, rather than the initial state epoch, leads to the lowest residual across the propagation. With these points, one can safely conclude that the quality of the prefit is mainly constrained by the uncertainty within the SPICE kernels, rather than the slight discrepancies within the dynamical model.

The rest of Figure 5 is dedicated to demonstrating the results of Him-01, the nominal Himalia run. In Figure 5b the postfit differences in position with respect to the SPICE benchmark can be seen. Immediately one can observe that the trajectory deviates from SPICE in almost linear fashion before roughly 1980, growing up to a discrepancy of about 500 km in 1900. Figure 5c shows us how this propagated estimated initial state compares to the residual of the observations. The error, i.e. the difference with respect to SPICE, lies well below the residual of most observations but grows with decreasing data quality. This indicates that the older observations do have a significant effect, pulling the solution in their, less precise, direction. Figure 5d teaches us that the less accurate observations cause a linear trend in the along-track component of the fit, which dominates the error before roughly 1980. After this point, the propagated uncertainty in the cross-track direction, which causes increasing variations within each orbit, but with a zero mean, has the strongest contribution to the total error. Inspecting the distribution of residuals in Figure 5e, it is once again clear that the many modern observations are significantly more accurate than those stemming from before the Second World War. On first glance, these observations could conceivably represent a Gaussian data distribution. A formal Kolmogorov-Smirnov test Kolmogorov (1933) however resulted in a p-value much below 0.01, which represent the chance that this sample would be observed if the measurements had a Gaussian distribution, thus indicating that this observation set most definitely can not be considered Gaussian. This is likely due to the data being sourced from many observational studies with varying accuracy. Note that the tails of the distributions of the modern measurements were cut from the plot, in order to better demonstrate the spread closer to the center. The observations from 1950 to 1980 are accurate but simply lack the numbers to significantly affect the solution.

Finally, it is worth investigating the correlation between the RSW state entries, as shown in Figure 6. One can immediately recognize the strong coupled relationship between the along-track position and the radial velocity. The radial position and along track velocity also show coupled behaviour, although less strong.

The postfit proved quite good, especially more accurate than the input data, although the solution was largely dominated by a linear trend caused by the inferior data quality of earlier observations. Although these observations have been used in past studies, they were always preprocessed and had biases of up to 1.5 arcseconds applied to correct for changes in observation reference frame and remaining biases (e.g. Brozović & Jacobson 2017). One could research the proper correction, like earlier studies, but a more interesting question might be: what would be the effect of correcting and subsequently employing these older observations? Figure 7 and Figure 8 show us the answer. These are the results of an estimation process, which will be referred to as Him-02, similar to that described in subsubsection 4.4.3, where all old (read: all datasets that contain observations before 1960) were removed. We see that the quality, i.e. the difference w.r.t SPICE, of the fit is significantly improved, as compared to Figure 5b. It is safe to conclude that this is an improvement by remembering that the estimated uncertainty in the SPICE kerels for Himalia is about 50-100 km. This improvement can be attributed to removing the linear trend. Instead, the new solution more closely resembles the prefit in Figure 5a. When comparing with the observation residuals, we see that the new fit is extremely accurate, as compared to SPICE, for the data-rich period. As this difference lies well within the uncertainty in these Kernels (Brozović & Jacobson 2017), the results of both solutions are statistically indistinguishable for this period. For epochs earlier in the 19th century, we notice that the error grows by an order of magnitude to 100 km, where it remains relatively constant. A similar level of discrepancy with respect to SPICE was reached when applying arcwise corrections to the old observations instead of simply removing them. To further improve our understanding of the contribution of the old observations on the orbital solution of Himalia, one final run was done, referred to as Him-03. Instead of simply removing the oldest observations, which might be overly pessimistic, or applying an arcwise correction, which might be overly optimistic, they were replaced by simulated observations, comparable to those simulated to represent the spacecraft measurements on Amalthea as introduced in subsubsection 4.4.2. Gaussian noise with a standard deviation of 4 μrad of added was added to these observations based on earlier reported average residuals (Jacobson 2000). The epochs of observations set 'jo0010', as introduced in subsection 2.2, were taken to represent the times of observation, as it is the primary old dataset. The postfit of this estimation is shown in Figure 9, which is almost exactly the same as the prefit seen in Figure 5a.

Although this seems to suggest that the oldest observations do further improve the fit, it is impossible to draw definite conclusions on their contribution as these differences are smaller than the uncertainty within these SPICE kernels. Inversely, as these solutions are statistically indistinguishable, there is also no definite proof that dropping the old observations deteriorates the solution. It is safe to conclude however that estimating the orbit of Himalia with uncorrected old observations significantly worsens the fit. Finally, it is noted that including the older data did not only reduced the quality of the fit at the time of observation but also had a negative impact on the precision of later epochs, thus

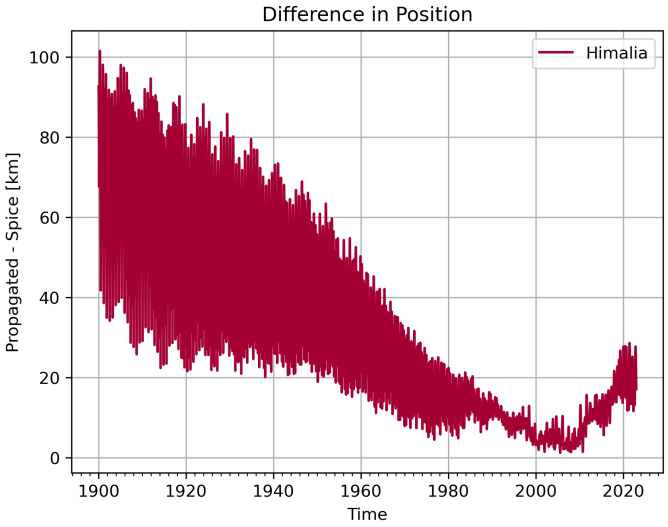

(a) Difference in the position of Himalia between propagated initial state guess and SPICE kernels for the prefit, Him-00.

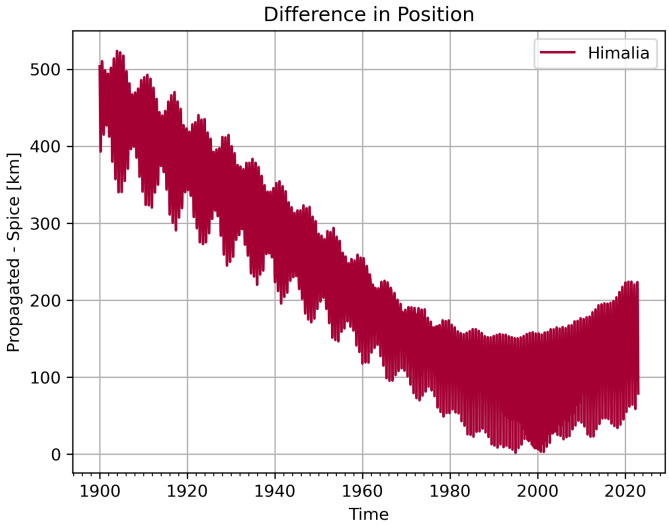

(b) Difference in the position of Himalia between propagated initial state estimate and SPICE kernels for the postfit, Him-01.

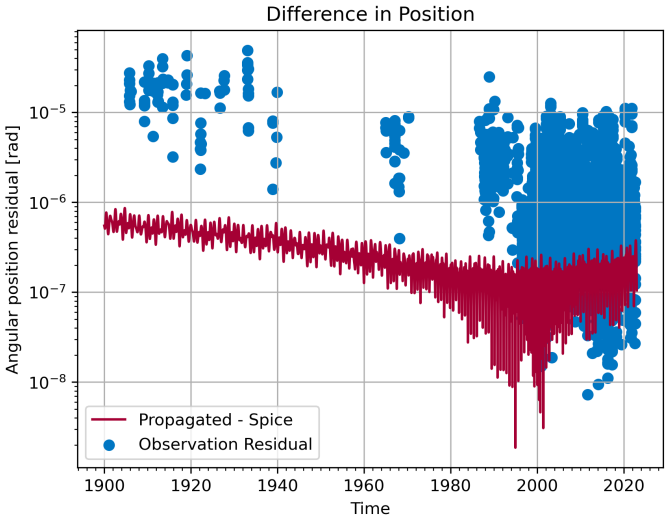

(c) Comparison between the quality of the Himalia's propagated postfit initial state vs the observation residuals, Him-01.

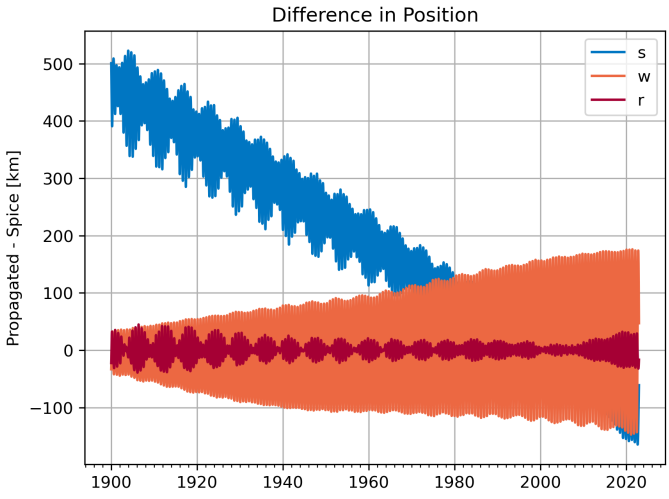

(d) Difference in the position of Himalia between propagated initial state estimate and SPICE kernels for the postfit, broken down into RSW components, Him-01.

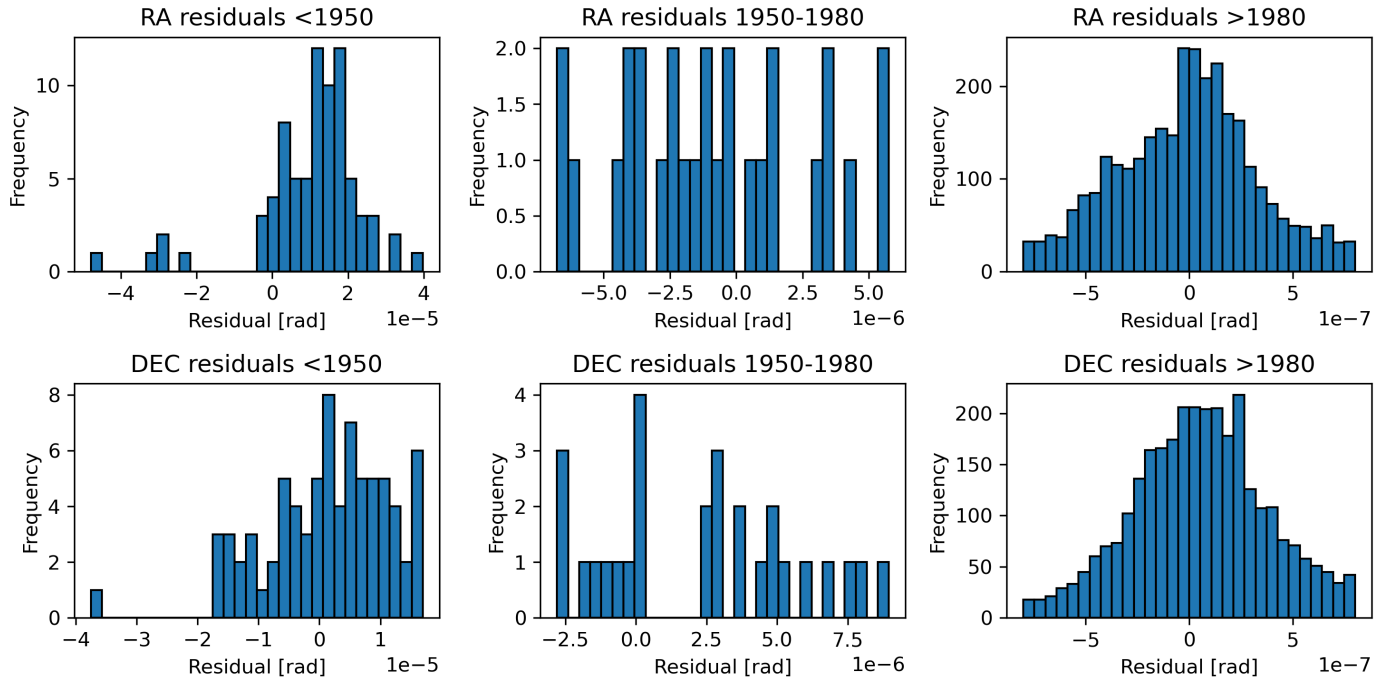

(e) The distribution of Himalia postfit residuals per period, Him-01.

Fig. 5: Results for the nominal run of Himalia, Him-01

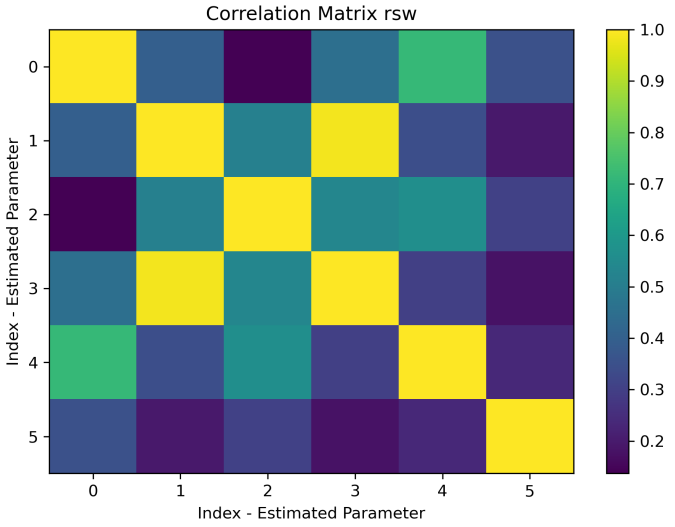

Fig. 6: Correlations between Himalia's estimated initial state parameters, Him-01.

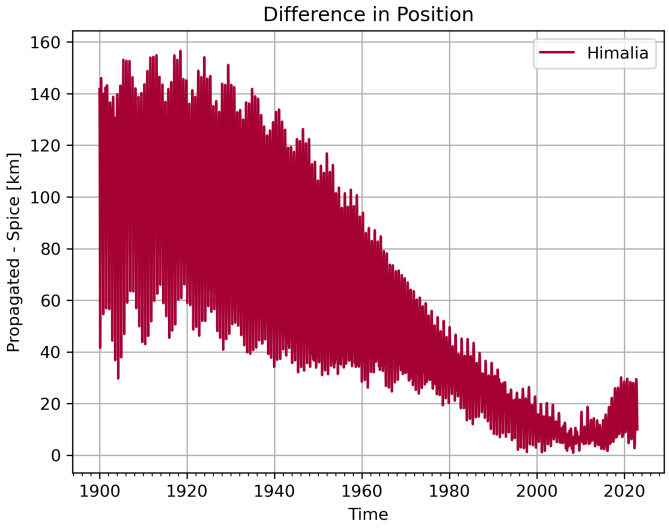

Fig. 7: Difference in the position of Himalia between propagated initial state guess and SPICE kernels for the postfit without the oldest data, Him-02.

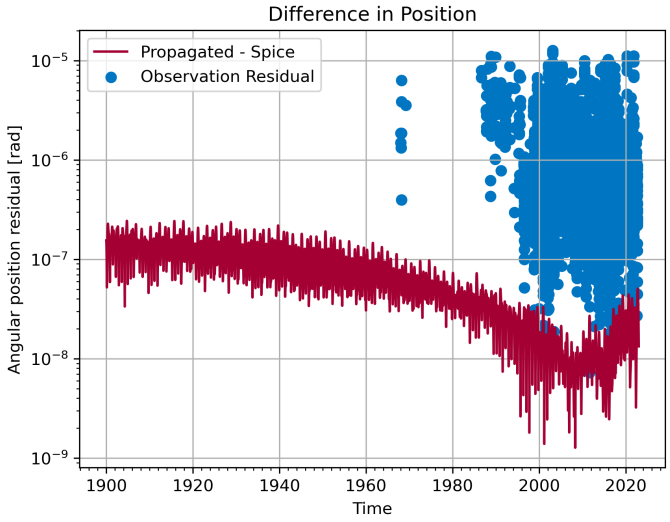

Fig. 8: Comparison between the quality of the Himalia's propagated postfit initial state without the oldest data vs the observation residuals, Him-02.

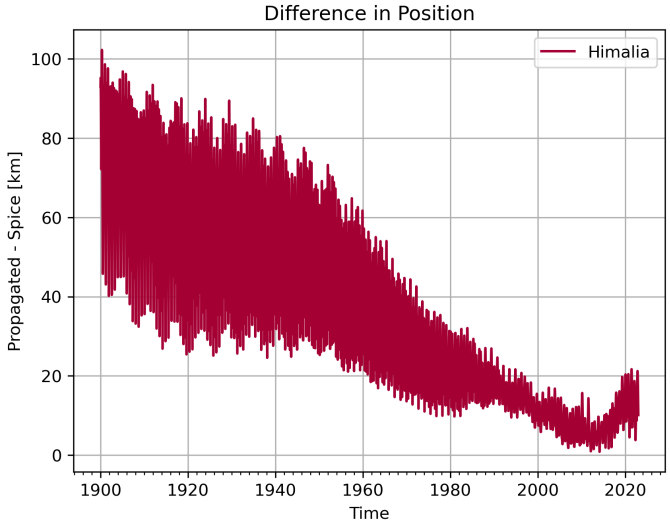

Fig. 9: Difference in the position of Himalia between propagated initial state guess and SPICE kernels for the postfit with simulated oldest observations, Him-03.

confirming that not using these observations is significantly better than using bad ones, as they still influence the orbit strongly.

5.2. Elara

One would expect many similarities between the results for Elara and Himalia, as they are part of the same group of moons. However, due to their 1949 close approach, and the fact that Himalia is significantly more massive, the propagation and estimation of Elara's state is affected by this event. In Figure 10a the prefit with respect to SPICE is shown. The difference remains well below 100 km after the close approach, while it quickly grows to 400 km propagating backwards from it. The initial guess for the gravitational parameter was set to 0.28 km^3s^{-2} (Emelyanov 2005b). After fitting to SPICE, this value was estimated to be 0.14km^3s^{-2}, close to 0.13km^3s^{-2} as reported for the SPICE ephemerides (Brozović & Jacobson 2017). This difference however plays a large part in explaining the prefit errors. Small differences in position, and thus also in experienced gravitational attraction lead to a growing discrepancy. Although estimating a new gravitational parameter partly absorbs this misalignment, it can not fully account for it, as the state after the event will be affected, in turn altering the other forces exerted by the other bodies, which explains the growing difference in position.

Figure 10b displays the postfit errors. We can again easily differentiate between before and after the Himalia close approach. Before the phenomenon, we can identify a linear trend, whereas after there is a relatively constant error, although there are increasing variations within the orbit. The magnitude of these discrepancies, together with the strong break at the epoch of the close approach, clearly indicates that the estimation process can not sufficiently capture the dynamics of this event. A value of

$0.132 km^3 s^{-2}$ was found for the gravitational parameter of Himalia, closer to SPICE than the prefit. Despite this, a difference of 200 km in state at this epoch causes a significant difference in accelerations leading to the observed errors. From Figure 10c we learn that the quality of the estimations correspond to the more accurate observations, whereas the fact that the quantity and quality of old data are lacking is highlighted once again. When breaking down the positional error into its components in Figure 10d, we see that the noteworthy behaviour, the linear trend and high per-orbit variation, is almost entirely in the along-track direction as was the case for Himalia. The distribution in residuals in Figure 10e portrays a different image than for Himalia. While the old observations are still sparse, they seem very accurate. This can simply be explained however by the applied arcwise bias that artificially improves the quality of the measurements, thus creating an overly optimistic image of the fit, although required due to the unique dynamics involved. Once again, the Kolmogorov-Smirnov test confirmed that these observations do not represent a Gaussian distribution, as would be expected.

Furthermore, Figure 11 demonstrates that the in-plane positions and radial velocity are strongly coupled. Noteworthy is that the gravitational parameter of Himalia is entirely decoupled from the initial state.

From these results, we can conclude that the old observations have a significant impact on the fit, skewing the outcome in their, inaccurate, direction. Another conclusion is that estimating Himalia's gravitational parameter well is important for accurate results, as was expected from observing the large influence of the close approximation both in pre- and postfit or considering the position error grow to several thousand km when not estimating this parameter and without a good initial guess. We saw that estimating this gravitational parameter was uncoupled from the initial state, meaning that both have to be very accurate to achieve a high-precision solution. This explains the change in the parameter between the prefit and postfit. When fitting to SPICE, the gravitational parameter partly absorbed the positional error, which means that the mass of Himalia is changed slightly to maintain a similar force experienced by Elara, for a difference in distance. When estimating using real observations this did not happen. Instead, the gravitational parameter was determined more accurately, i.e. closer to that of SPICE, than the state, leading to growing errors in position. To correct for this, we can repeat the estimation process fixing the value of Himalias gravitational parameter from the prefit, which better aligns with the dynamical model used in this study, and which lies within the uncertainty specified by Brozovic. The results of this estimation are displayed in Figure 12 and Figure 13.

From these plots, we learn that fixing the value of the gravitational parameter of Elara to the value found in the prefit improves the fit in terms of difference with respect to SPICE before the flyby by a factor of two. By once again placing our focus on the along-track component, we clearly see that the linear trend has disappeared, confirming our suspicion that it was due to a modelling error in the close approach, while the high variation in error within each orbit remains. This results is especially valuable in combination with the conclusions from our Himalia model. For Himalia we saw that the old observations did not prove a significant advantage in estimating its orbit. For Elara however, despite their similar trajectory, this conclusion does not hold. The results show that additional constraints, especially before the closest approach, can be highly valuable in reducing the magnitude of the error. Therefore, it is worth studying and applying corrections to the available old datasets, when high precision (i.e. below 100 km or 10^{-7} rad are desired.

Finally, it is worth noting that the results from this estimation process confirm the results by Brozovic and Jacobson. Both versions of the estimation process in this study resulted in a gravitational parameter of Himalia close to theirs of 0.13 ± 0.02 $km^3 s^{-2}$ with 0.144 and 0.132 $km^3 s^{-2}$ for the pre- and postfit respectively. This result is not surprising considering the methodology and data used are very similar. It is however a factor two smaller as those reported by Emelianov, who had less (accurate) data available at the time of his study, nearly 20 years ago. The change in residual of the observations of this change is however not statistically significant, and thus neither solution can be unambiguously treated as better (Brozović & Jacobson 2017).

5.3. Amalthea

The final case study was to estimate the orbit of Amalthea. Once again, the prefit is shown first in Figure 14a. The difference to SPICE is in the order of tens of km, corresponding to 10^{-8} rad. Although the uncertainty in the SPICE Kernel ephemerides of Amalthea is not published directly, the high accuracy compared to the observation quality, as shown in Table 2, shows that the modeling error is acceptable for this study.

Estimating the orbit of Amalthea was less straightforward, compared to that of Himalia, as the inversion was nearly ill-defined. This means that the available observations, which are very limited in number (212 compared to 2500 for Himalia) and not distributed evenly, do not sufficiently constrain the solution, especially in combination with the fast dynamics. Instead, small variations in input lead to vastly different solutions, as this small difference is propagated over thousands of orbits. This becomes apparent in the estimation process when the update in initial state, as was described in Equation 10, becomes increasingly large. In reality this means that the solution is too sensitive to changes in initial state in order to properly estimate it. To guarantee convergence, an a-priori covariance constraint of 100 km in each direction was posed, while two datasets that prevented a convergent result were discarded. The value of 100 km was chosen as it is expected to be roughly the uncertainty in the prior knowledge, i.e. the SPICE benchmark, although not concrete numbers have been published, another disadvantage of these closed-source studies. This constraint based on the a-priori covariance effectively prevents the estimator from taking too large steps. Finally, the postfit, Ama-01, as shown in Figure 14b was reached. Two things can be noted immediately, the almost linear trend to both sides and the two minima. By considering Figure 14c as well, it becomes clear that those minima correspond to two clusters of observations. A more complete understanding of these results can be found in the RSW breakdown in Figure 14d, where we once again detect a linear trend in the along-track direction. This demonstrates that the current fit does not adequately estimate the orbital period or, equivalently, the orbital energy, which causes a growing discrepancy over time. Note that this linear trend is then fitted such that it reaches a minimum at the two observation clusters. On the other hand, the cross-track direction shows an increasing variation per orbit when propagating backwards, related to the limited amount of data before 1990. When observing the distribution of residuals in Figure 14e, one can identify the seemingly random spread around the center. While the residuals for Himalia and Elara were not distributed normally, they did demonstrate a clear peak around 0, which is not the case for Amalthea. This once again demonstrates that Amalthea's data is not only lacking quantita-

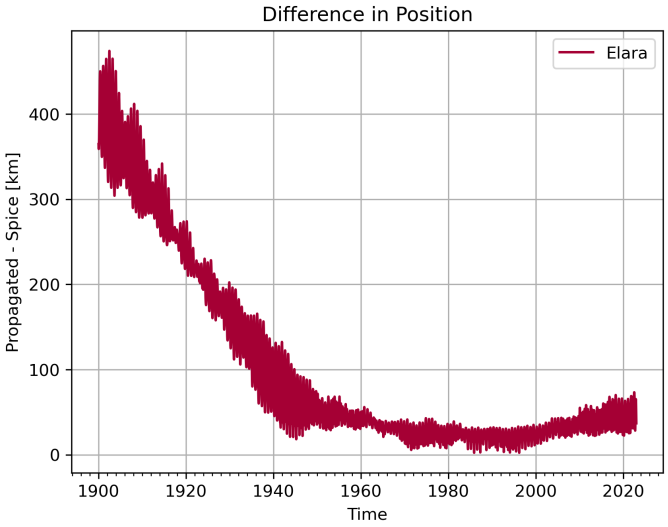

(a) Difference in the position of Elara between propagated initial state guess and SPICE kernels for the prefit, Ela-00.

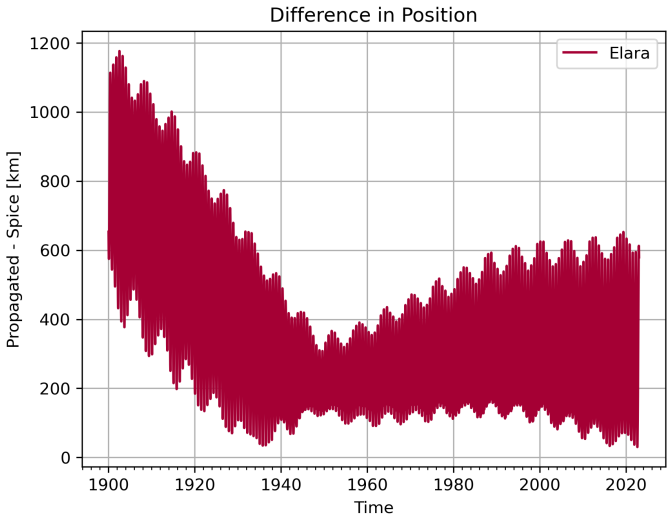

(b) Difference in the position of Elara between propagated initial state estimate and SPICE kernels for the postfit, Ela-01.

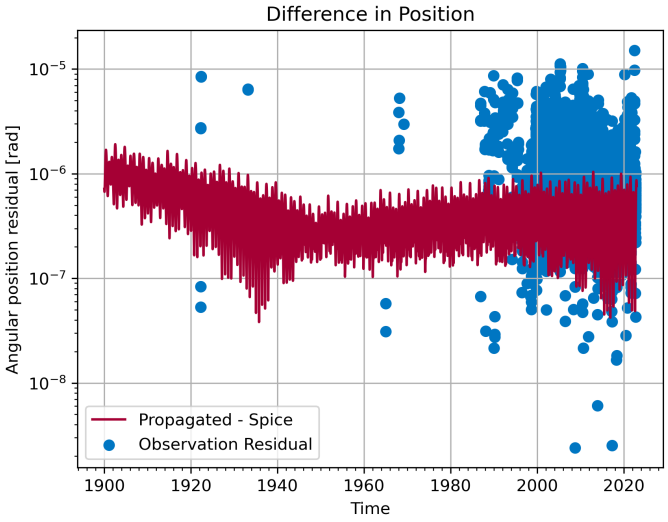

(c) Comparison between the quality of the Elara's propagated postfit initial state vs the observation residuals, Ela-01.

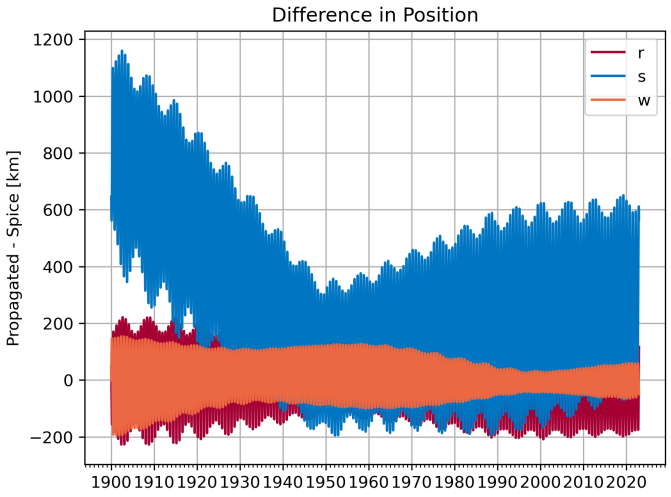

(d) Difference in the position of Elara between propagated initial state estimate and SPICE kernels for the postfit, broken down into RSW components, Ela-01.

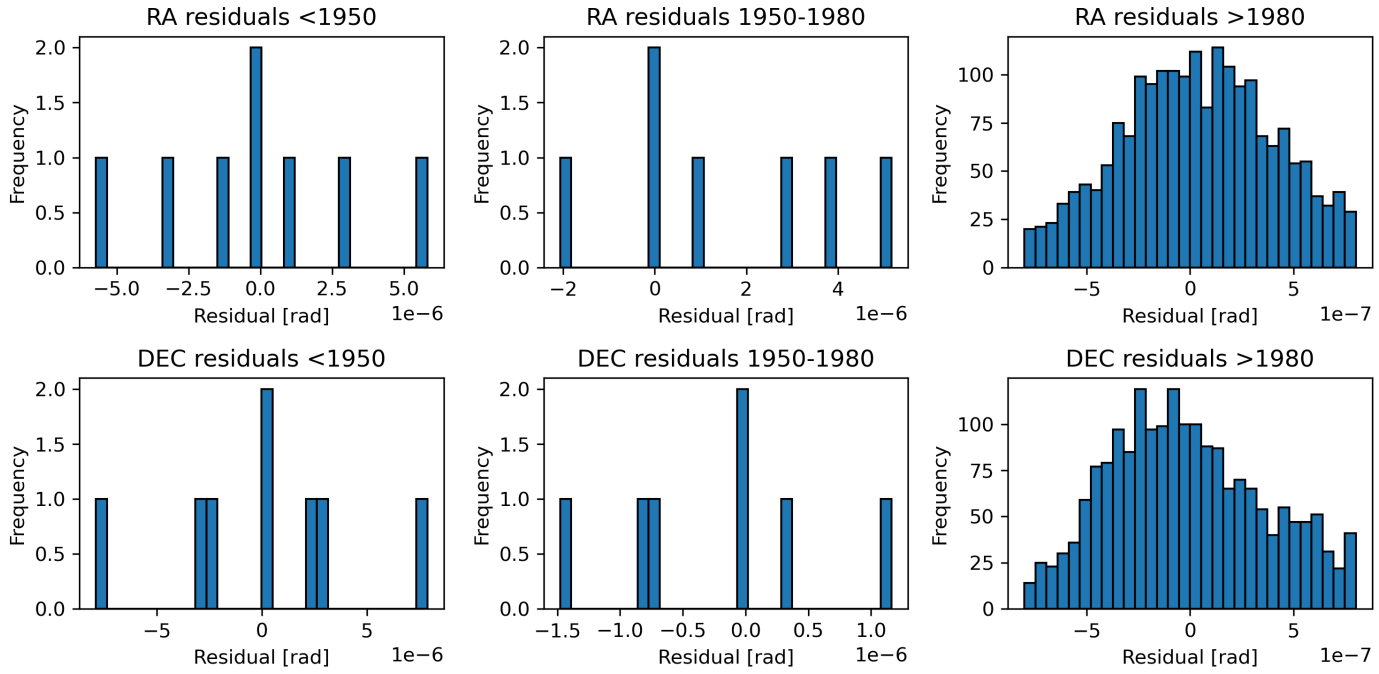

(e) The distribution of Elara postfit residuals per period, Ela-01.

Fig. 10: Results for the nominal run of Elara, Ela-01

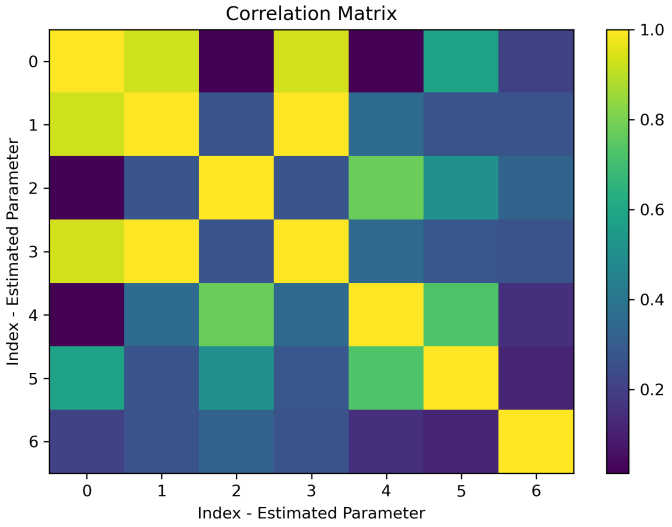

Fig. 11: Correlations between Elara's estimated initial state parameters and Himalia's gravitational parameter as the 6 entry, Ela-01.

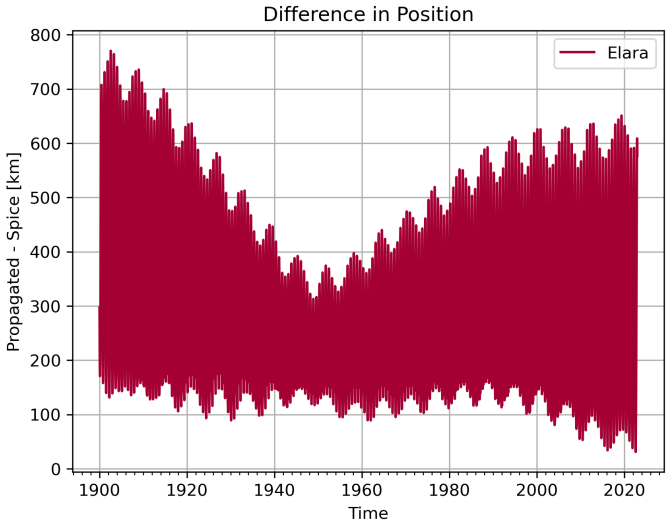

Fig. 12: Difference in the position of Elara between propagated initial state guess and SPICE kernels for the postfit without estimating the gravitational parameter of Himalia, Ela-02.

tively but also is not as accurate as required for a precise, stable, convergent solution. This problem is further aggravated by the fact that a similar residual is more influential for Amalthea as compared to the outer moons, given the closer proximity to Jupiter, thus larger angular error, while timing errors are more influential due to the higher orbital velocity.

When inspecting the correlation between RSW state entries in Figure 15, one can recognise a similar image to Figure 6 for Himalia. Indeed, there is again a clear dependency between radial position and along-track velocity, and vice versa. Once again, the out-of-plane position and velocity are almost completely decoupled from the in-plane motion and are only dependent on each other.

Unfortunately, there are no clear statistics on expected uncertainty in the ephemerides of Amalthea publically available to the best of our knowledge. However, the combination of pre-

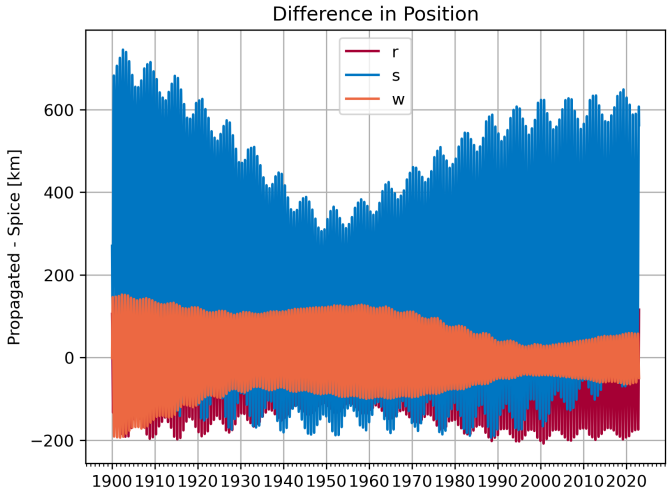

Fig. 13: Difference in the position of Elara between propagated initial state guess and SPICE kernels for the postfit without estimating the gravitational parameter of Himalia, broken down into RSW components, Ela-02.

fit and postfit results can at least give a relative image of how the postfit compares to SPICE. The main finding is that the solution without the simulated spacecraft observations performs significantly worse compared to when these missions are taken into account. This fit did not manage to accurately determine Amalthea's orbital energy and therefore drifted away from the solution by SPICE. This indicates that the data is too sparse to provide good orbital coverage, which is not improved by the high level of clustering of measurements.

5.4. Amalthea with Simualted Spacecraft Observations

The final estimation was the preliminary assessment on how the (simulated) spacecraft observations affect the orbital fit of Amalthea described in the previous section, which will be denoted by Ama-02. Remember that the solution should not be taken as an exact representation of reality, but rather as an indication of whether these observations are worth additional effort in subsequent studies. The prefit will not be analyzed as is logically exactly the same as in Figure 14a. The new postfit in turn is shown in Figure 16. The improvement with respect to Figure 14b is clear, and the postfit now closely approximates the prefit, with similar magnitude and shape in residual. This shows the importance of the spacecraft data in the orbit estimation. Furthermore, the near-perfect agreement near the end of the propagation can be explained by the concentration of accurate mission observations in that period, where Cassini and Galileo both observed Amalthea. In Figure 17, the elimination of the linear trend in the along-track direction with respect to the limited data estimation in Figure 14d is clear. Instead, there might be some remaining oscillatory motion with a period of 10 year, but this is small enough that it simply might be an artifact of the propagation method. Finally, we note that the in-orbit variation in the cross-track direction remains the same as the earlier iteration. This uniform growth might imply a slight trend in the orientation of the orbit.

The Voyager, Galileo, and Cassini mission improved the fit by providing many more observations spread across multiple months, to years for the Galileo mission. This allowed for a better estimate of the orbital energy, preventing the linear trend in error. As the epochs of these simulated measurements were

based on the times of observation that were used to generate the SPICE ephemerides, this proves the relative importance of these missions towards calculating the ephemerides of Amalthea, despite not being the objective of any of these spacecraft. However, one should keep in mind that this is a very preliminary analysis, where the observations were simulated in 3D positions and not, like the actual observations, in astrometry. These simplified observations, together with the assumptions on the quality of these spacecraft measurements might very well prove overly optimistic. This analysis does show however that a deeper study, including the real data from these missions, will prove very insightful in studying Amalthea's ephemerides.

6. Conclusion & Recommendations

This work was focused on developing and demonstrating a fully open-source framework for estimating the orbit of moons starting from raw astrometric observations. The initial states of three case studies, Himalia, Elara, and Amalthea, were estimated as a representation of the full range of minor Jovian moons. However, the framework can be extended to other satellites. The raw data was taken from the NSDC database and a processing algorithm was written to prepare these observations for the orbit estimation process. Furthermore, JPL's SPICE kernel ephemerides were used as a comparison and benchmark to evaluate the quality of the found solutions, as well as as a basis for the initial guess and simulated spacecraft observations. A least squares procedure was then used to find the best fit to the observations.

We managed to accurately estimate the state of Himalia, to well within the uncertainty of the SPICE Kernels (Brozović & Jacobson 2017) for all reported epochs. To achieve this accuracy, the oldest data had to be removed, as there were conversion errors between the old and new frames. A level of precision of 10^{-8} rad, which corresponds to 10 km was achieved for the period with data, while this grew to 10^{-7} rad or 100 km for earlier epochs. As this is well below the residuals of the observations and within the uncertainty region of the benchmark, this solution proves to be both accurate and statistically indistinguishable from SPICE. This shows the promise of the open-source procedure, as well as reinforcing the idea that the oldest observations might not significantly improve the quality of the solution. A further analysis using simulated old observations did not provide definitive answers on the contribution of these measurements, as the change in position when including them was smaller than the uncertainty of the SPICE kernel benchmark. Improvements in the reduction process and subsequent data re-reduction could increase their relevancy, however (e.g. Arlot et al. 2016).

Interestingly, this same conclusion, or reservations about the usefulness of old data, did not hold for the orbital solution of Elara. Despite having similar orbits, a 1949 close approach with the significantly more massive Himalia meant a deviation in Elara's trajectory. Old data, to which we applied an arcwise bias correction to account for the conversion errors mentioned for Himalia, then proved valuable in constraining the trajectory before the close approach. The orbit after this event is constrained more tightly by the modern observations, which means that the accuracy of old observations, and thus of the pre-1949 fit, determines how precise one can determine the gravitational parameter of Himalia. This parameter was estimated to $0.132 \mathrm{km}^3\mathrm{s}^{-2}$, similar to the value of $0.13 \mathrm{km}^3\mathrm{s}^{-2}$ found in Brozović & Jacobson (2017). Given the importance of the old data, a closer look should be taken at converting old observations, while data re-reduction initiatives could prove even more valuable than for Himalia.

Finally, estimating the orbit of Amalthea posed some additional challenges due to the limited amount and spread of observations. This prevented an accurate estimation of Amalthea's orbital energy, which manifested into the solution as a growing error in the along-track position. Simulating the observations by several missions that visited the system proved to resolve this issue and eliminate the error trend. This reduced the error from hundreds to tens of km. It is thus fair to conclude that these spacecraft play a crucial role in the quality of the current ephemerides of Amalthea, although further investigation is required to confirm these preliminary outcomes.

The promising results of these three case studies demonstrate the capabilities of the estimation framework. The solutions were proven to be high-accuracy, and any and all significant differences were related to flaws in input data. The code is available in the repository and can be easily modified to include other Jovian moons. Furthermore, it would be interesting to apply this framework to satellites of other planetary systems, although these currently do not have a predefined gravitational model implemented in Tudat. Additionally, the framework can be easily extended to allow for more parameters to estimate, of which Himalia's gravitational parameter in fitting Elara's orbit was a good example. Finally, an interesting future study would be the inclusion of diverse observation types, such as mutual events and approximations. While the availability of such data remains low for now, they could prove extremely valuable to future iterations of this type of estimation study.

References

Acton, C. H. 1996, Planet. Space Sci, 44
Arlot, J.-E., Birlan, M., & Robert, V. 2016, The Project NAROO (New Astrometric Reduction of Old Observations), Tech. rep.
Bauer, S., Hussmann, H., Oberst, J., et al. 2016, Planetary and Space Science, 129, 32
Bindschadler, D. L., Theilig, E. E., Schimmels, K. A., & Vandermey, N. 2003, in International Astronautical Congress
Bobone, J. 1953, The Astronomical Journal, 58, 172
Brown, A. G. A., Vallenari, A., Prusti, T., et al. 2021, Astronomy & Astrophysics, 55
Brozović, M. & Jacobson, R. A. 2017, The Astronomical Journal, 153, 147
Campbell, J. K. & Synnott, S. P. 1985, The Astronomical Journal, 90
Catani, L. M., Assafin, M., Morgado, B. E., et al. 2023, Monthly Notices of the Royal Astronomical Society, 526, 6145
Chyba, C. F. & Phillips, C. B. 2001, Proceedings of the National Academcis of Sciences
Chyba, C. F. & Phillips, C. B. 2002, Origins of Life and Evolution of the Biosphere
Cooper, N. J., Murray, C. D., Porco, C. C., & Spitale, J. N. 2006, Icarus, 181, 223
Dirkx, D. 2022, Tudat mathematical model definition, Tech. rep.
Dirkx, D., Lainey, V., Gurvits, L. I., & Visser, P. N. 2016, Planetary and Space Science, 134, 82
Dirkx, D., Vermeersen, L. L., Noomen, R., & Visser, P. N. 2014, Planetary and Space Science, 99, 84
Dormand, J. R. & Prince, P. J. 1980, Journal of Computational and Applied Mathematics, 19
Emelyanov, N. V. 2005a, Astronomy and Astrophysics, 435, 1173
Emelyanov, N. V. 2005b, Astronomy and Astrophysics, 438
Emelyanov, N. V., Varfolomeev, M. I., & Lainey, V. 2022, Monthly Notices of the Royal Astronomical Society, 512, 2044

Fayolle, M., Dirkx, D., Lainey, V., Gurvits, L. I., & Visser, N. A. M. 2022, Decoupled and coupled moons' ephemerides estimation strategies Application to the JUICE mission, Tech. rep.
Fayolle, M., DIrkx, D., Visser, P. N., & Lainey, V. 2021, Astronomy and Astrophysics, 652
Fayolle, M., Magnanini, A., Lainey, V., et al. 2023, Astronomy and Astrophysics, 677
Gaspar, H. S., Winter, O. C., & Vieira Neto, E. 2011, Monthly Notices of the Royal Astronomical Society, 415, 1999
Gomes-Júnior, A. R., Assafin, M., Vieira-Martins, R., et al. 2015, Astronomy and Astrophysics, 580
Heller, R., Marleau, G.-D., & Pudritz, R. E. 2015
Hernius, O., Lagerkvist, C., Lindgren, M., Williams, G. V., & Tancredi, G. 1996, Astronomy and Astrophysics Supplement Series, 115
Ianna, P. A., Seitzer, P., Levinson, F., et al. 1979, AJ, 84, 429
Jacobson, R. A. 2000, The Astronomical Journal, 120, 2679
Jacobson, R. A. 2014
Klemola, A. R. 1973, The Astronomical Journal, 78
Kolmogorov, A. 1933, Giornale dell'Istituto Italiano degli Attuari
Krivov, A. V. 1993, Astronomicheskij Zhurnal
Kulyk, I. 2008, Planetary and Space Science, 56, 1804
Kulyk, I., Jockers, K., Karpov, N., & Sergeev, A. 2002, Astronomy and Astrophysics, 383, 724
Lainey, V., Arlot, J. E., Karatekin, , & Van Hoolst, T. 2009, Nature, 459, 957
Lainey, V., Duriez, L., & Vienne, A. 2004, Astronomy and Astrophysics, 420, 1171
Ledovskaya, I. V., Jockers, K., Karpov, N. V., & Sergeev, A. V. 1999, Kinematika i Fizika Nebesnykh Tel, 15, 483
Mallama, A., Aelion, H. M., & Mallama, C. A. 2004, Icarus, 167, 320
McCord, T. B., Coradini, A., Hibbitts, C. A., et al. 2004, Icarus, 172, 104
Montenbruck, O. & Gill, E. 2000, Satellite Orbits: Models, Methods and Applications, Tech. rep.
Morgado, B., Assafin, M., Vieira-Martins, R., et al. 2016, Monthly Notices of the Royal Astronomical Society, 460, 4086
Morgado, B., Vieira-Martins, R., Assafin, M., et al. 2019, Planetary and Space Science, 179
Mulholland, J. D., Benedict, G. F., Shelus, P. J., et al. 1979, AJ, 84, 668
Mulholland, J. D., Shelus, P. J., & Abbot, R. I. 1976, The Astronomical Journal, 81
Nesvorny, D., Alvarellos, J. L. A., Dones, L., & Levison, H. F. 2003, The Astronomical Journal, 126, 398
Nicholson, P. D., Cuk, M., Sheppard, S. S., Nesvorný, D., & Johnson, T. V. 2008
Nicholson, P. D. & Matthews, K. 1991, Icarus, 93, 331
O'Neil, W. J., Ausman, N. E., Johnson, T. V., Landano, M. R., & Marr, J. C. 1993, in Congress of the International Astronautical Federation
Robert, V., Saquet, E., Colas, F., & Arlot, J.-E. 2017, MNRAS, 467, 694
Saquet, E., Emelyanov, N., Colas, F., et al. 2016, A&A, 591, 42
Shang, Y. J., Peng, Q. Y., Zheng, Z. J., et al. 2022, The Astronomical Journal, 163, 210
Sheppard, S. S. & Jewitt, D. C. 2003, Nature, 423, 261
Sheppard, S. S., Tholen, D. J., Alexandersen, M., & Trujillo, C. A. 2023, Research Notes of the AAS, 7, 100
Smith, B. A., Soderblom, L. A., Beebe, R., et al. 1979, Science, 206, 927
Smtih, B. A., Soderblom, L. A., & Johnson, T. V. 1979, Science, 204, 951
Sohl, F., Spohn, T., Breuer, D., & Nagel, K. 2002, Icarus, 157, 104
Soulie, G. 1972, Astronomy and Astrophysics Supplement Series, 6, 311
Stone, R. C. 2000, The Astronomical Journal, 120, 2124
Stone, R. C. 2001, The Astronomical Journal, 122, 2723
Stone, R. C. & Harris, F. H. 2000, The Astronomical Journal, 119, 1985
Thomas, P. C., Burns, J. A., Rossier, L., et al. 1998, Icarus, 135, 360
Veiga, C. H. 2006, Astronomy & Astrophysics, 453, 349
Veiga, C. H. & Vieira Martins, R. 1996, Revista Mexicana de Astronomia y Astrofisica Serie de Conferencias, 4, 118
Veiga, C. H. & Vieira Martins, R. 2005, A&A, 437, 1147
Veverka, J., Thomas, P., Davies, M., & Morrison, D. 1981, Journal of Geophysical Research: Space Physics, 86, 8675
Weinwurm, G. 2006, Advances in Space Research, 38, 2125
Whipple, A. L., Shelus, P. J., & Benedict, G. F. 1993, The Astronomical Journal, 105
Whipple, A. L., Shelus, P. J., Benedict, G. F., et al. 1992, The Astronomical Journal, 103, 617
Whipple, A. L., Shelus, P. J., Whited, R. W., et al. 1996, AJ, 112, 316
Yan, D., Qiao, R. C., Yu, Y., et al. 2019, Planetary and Space Science, 179
Yan, D., Qiao, R. C., Yu, Y., et al. 2020, Icarus, 337
Yizhakevych, O., Andruk, V., & Pakuliak, L. 2017, Odessa Astronomical Publications, 30, 201

Table 3: Means and standard deviations in Right Ascension and Declination of processed observations of NSDC files on the Outer Jovian satellites, along with the number and period of these observations.

NSDC Identifier	Alpha	Delta	#Obs	Observation Period	Reference
jo0001	-2.73e-08 ± 8.93e-07	-9.94e-08 ± 8.14e-07	113	1998 - 1998	Stone & Harris (2000)
jo0002	-5.99e-08 ± 8.55e-07	-5.28e-08 ± 1.35e-06	130	1998 - 1998	Stone (2000)
jo0003	1.60e-07 ± 5.00e-07	-1.38e-07 ± 2.72e-07	12	1997 - 1999	Owen comm. to NSDC (2001)
jo0004	9.10e-07 ± 2.57e-06	7.24e-07 ± 2.37e-06	59	2000 - 2000	MPC
jo0005	1.45e-07 ± 2.05e-06	1.98e-06 ± 1.74e-06	92	1992 - 2001	MPC
jo0006	1.48e-06 ± 2.38e-06	-1.07e-07 ± 3.41e-06	9	1999 - 1999	MPC
jo0007	6.41e-07 ± 1.03e-06	2.39e-07 ± 1.58e-06	48	2001 - 2001	MPC
jo0008	3.29e-07 ± 2.49e-06	9.47e-07 ± 2.89e-06	67	1993 - 2002	MPC
jo0010	-5.07e-06 ± 8.57e-07	1.20e-04 ± 4.01e-05	97	1900 - 1993	84 references
jo0011	-1.12e-06 ± 8.11e-07	-2.53e-06 ± 1.76e-06	6	1952 - 1952	Bobone (1953)
jo0012	1.51e-06 ± 2.64e-06	-5.65e-07 ± 9.74e-07	13	1967 - 1969	Klemola (1973)
jo0013	-1.85e-06 ± 6.10e-06	1.94e-06 ± 1.80e-06	4	1973 - 1973	Mulholland et al. (1976)
jo0014	-2.96e-07 ± 3.35e-06	8.91e-07 ± 3.63e-06	69	1989 - 1990	Whipple et al. (1992)
jo0015	1.64e-06 ± 2.01e-06	1.29e-06 ± 2.21e-06	82	1990 - 1992	Whipple et al. (1993)
jo0016	-5.77e-07 ± 2.49e-06	2.15e-07 ± 2.46e-06	186	1994 - 1995	Whipple et al. (1996)
jo0018	3.42e-07 ± 4.39e-06	1.11e-06 ± 2.88e-06	40	1992 - 1993	Hernius et al. (1996)
jo0019	1.36e-06 ± 2.26e-07	7.15e-06 ± 7.01e-07	3	2002 - 2002	MPC
jo0020	8.24e-06 ± 4.90e-06	-1.30e-05 ± 2.02e-06	11	1980 - 1981	IAUC comm.
jo0021	1.11e-06 ± 1.53e-06	2.95e-06 ± 4.47e-07	10	2002 - 2003	MPC
jo0022	7.19e-07 ± 2.48e-06	2.37e-06 ± 2.51e-06	276	1993 - 2003	MPC
jo0024	6.64e-07 ± 3.15e-06	1.53e-06 ± 2.50e-06	64	1998 - 2002	MPC
jo0025	-2.75e-07 ± 1.75e-06	1.13e-06 ± 1.42e-06	46	1992 - 2003	MPC
jo0026	-5.77e-07 ± 1.15e-06	6.52e-07 ± 2.67e-06	39	1998 - 2003	MPC
jo0027	1.02e-06 ± 2.62e-06	1.51e-06 ± 1.81e-06	47	2003 - 2003	MPC
jo0028	2.01e-06 ± 2.22e-06	2.08e-06 ± 2.53e-06	36	2003 - 2003	MPC
jo0029	-7.13e-07 ± 3.72e-06	-1.14e-06 ± 3.05e-06	13	1951 - 1976	IAUC comm.
jo0030	-3.91e-07 ± 7.79e-07	-4.67e-07 ± 1.47e-06	6	1951 - 1951	IAUC comm.
jo0031	7.33e-05 ± 2.05e-06	2.49e-05 ± 9.22e-07	6	1968 - 1968	Soulie (1972)
jo0033	2.13e-07 ± 1.60e-06	1.39e-06 ± 1.40e-06	156	1999 - 2002	Sokolova, in press
jo0035	1.30e-07 ± 2.54e-06	1.14e-06 ± 2.54e-06	1192	1986 - 2005	MPC
jo0036	4.27e-07 ± 1.11e-06	3.39e-07 ± 1.03e-06	215	2006 - 2006	MPC
jo0037	6.47e-07 ± 1.15e-06	3.75e-07 ± 9.10e-07	95	2006 - 2006	MPC
jo0038	-3.05e-08 ± 1.64e-06	-1.55e-07 ± 3.98e-07	118	1995 - 1998	Veiga (2006)
jo0039	2.74e-07 ± 1.50e-06	-4.32e-09 ± 1.04e-06	67	2006 - 2006	MPC
jo0041	-2.85e-07 ± 1.21e-06	-7.80e-07 ± 1.82e-06	19	2007 - 2007	MPC
jo0042	-4.12e-07 ± 1.80e-06	-5.68e-07 ± 1.82e-06	74	2007 - 2007	MPC
jo0044	2.36e-07 ± 1.33e-06	-8.04e-08 ± 1.40e-06	148	2007 - 2007	MPC
jo0045	6.47e-08 ± 1.01e-06	2.11e-07 ± 9.47e-07	132	2008 - 2008	MPC
jo0046	1.29e-08 ± 1.13e-06	9.95e-08 ± 1.17e-06	695	2000 - 2008	MPC
jo0047	1.39e-07 ± 1.52e-06	3.26e-07 ± 1.58e-06	293	2008 - 2009	MPC
jo0048	-8.33e-08 ± 1.70e-06	1.26e-06 ± 2.17e-06	276	2009 - 2011	MPC
jo0049	3.73e-06 ± 3.94e-06	6.22e-06 ± 2.27e-06	57	2010 - 2010	MPC
jo0050	-1.20e-07 ± 1.72e-06	5.42e-07 ± 1.75e-06	440	1996 - 2012	MPC
jo0051	-7.82e-07 ± 6.18e-06	6.17e-07 ± 2.85e-06	12	2010 - 2010	MPC
jo0052	9.58e-08 ± 2.55e-06	1.26e-06 ± 2.50e-06	39	2010 - 2012	MPC
jo0053	6.01e-08 ± 8.57e-07	2.22e-06 ± 7.23e-07	17	2000 - 2012	Stone (2001)
jo0054	-1.07e-07 ± 1.04e-06	2.58e-07 ± 1.04e-06	916	2010 - 2015	MPC
jo0055	1.39e-06 ± 4.75e-06	-1.93e-07 ± 2.57e-06	9	2014 - 2014	MPC
jo0056	-1.04e-08 ± 3.85e-07	-1.69e-07 ± 2.93e-07	3553	1995 - 2014	Gomes-Júnior et al. (2015)
jo0057	-6.02e-07 ± 1.11e-06	2.40e-06 ± 1.37e-06	114	2013 - 2015	Stone (2001)
jo0058	7.31e-07 ± 3.50e-07	3.20e-07 ± 4.00e-07	2	2010 - 2010	MPC
jo0059	-2.37e-08 ± 9.49e-07	4.99e-07 ± 9.96e-07	1310	2014 - 2016	MPC
jo0060	-4.77e-07 ± 6.12e-06	-1.77e-07 ± 2.69e-06	36	2015 - 2016	MPC
jo0062	-2.15e-08 ± 9.21e-07	2.58e-07 ± 8.39e-07	857	2015 - 2018	MPC
jo0063	-6.11e-07 ± 4.83e-06	5.22e-07 ± 2.42e-06	8	2017 - 2017	MPC
jo0064	-1.58e-07 ± 9.12e-07	2.32e-07 ± 8.56e-07	307	2017 - 2018	MPC

Table 4: Means and standard deviations in Right Ascension and Declination of processed observations of NSDC files on the Outer Jovian satellites continued.

NSDC Identifier	RA $\mu \pm \sigma$ (μrad)	RA $\mu \pm \sigma$ (μrad)	#Obs	Observation Period	Reference
jo0065	-1.45e-07 ± 8.39e-07	3.91e-07 ± 7.18e-07	34	2011-2019	MPC
jo0066	5.07e-07 ± 2.77e-06	-6.49e-07 ± 2.71e-06	32	1987-1993	Yizhakevych et al. (2017)
jo0067	-3.70e-09 ± 9.81e-07	-2.47e-07 ± 9.62e-07	126	2017-2019	MPC
jo0068	-6.65e-10 ± 1.25e-06	1.31e-07 ± 1.08e-06	139	2020-2020	MPC
jo0070	-2.45e-08 ± 7.35e-07	1.11e-07 ± 7.53e-07	1838	1986-2022	MPC
jo0072	2.23e-08 ± 1.09e-07	3.19e-08 ± 1.12e-07	266	2016-2018	Yan et al. (2019)
jo0073	-1.45e-07 ± 2.88e-07	-1.65e-07 ± 3.15e-07	360	2016-2018	Yan et al. (2020)
jo0074	9.19e-08 ± 1.05e-06	1.51e-07 ± 1.01e-06	1200	1986-2022	MPC
jo0075	8.08e-07 ± 6.13e-06	-2.57e-08 ± 2.82e-06	85	2010-2022	MPC

Table 5: The main properties and results of the case studies and their variations. The prefits are denoted by 00 in the case ID

Case study ID	Bias Correction	A-priori constraint	Difference with Spice [km]	Notes
Him-00	/	/	65	/
Him-01	No	No	480	/
Him-02	No	No	100	Oldest data dropped
Him-03	No	No	70	Oldest data simulated
Ela-00	/	/	400	Concurrently Estimating μ_{him}
Ela-01	Oldest data only	No	800	Concurrently Estimating μ_{him}
Ela-02	Oldest data only	No	450	Fixed μ_{him}
Ama-00	/	/	25	/
Ama-01	Yes	100 km	300	/
Ama-02	Yes	100 km	30	Simulated SC observations

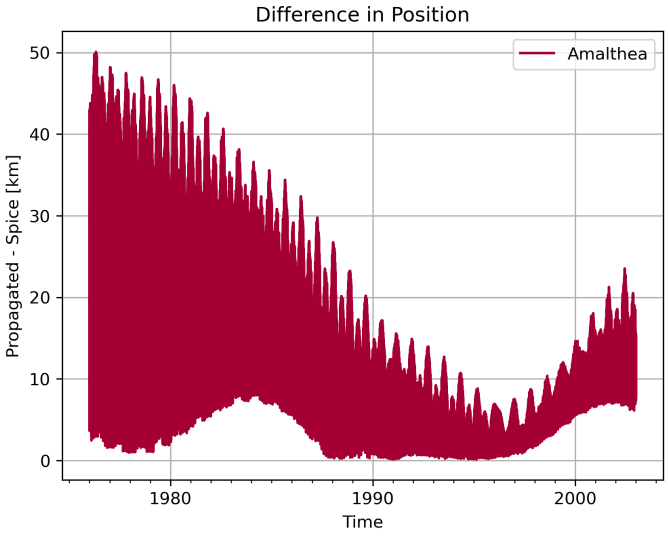

(a) Difference in the position of Amalthea between propagated initial state guess and SPICE kernels for the prefit, Ama-00.

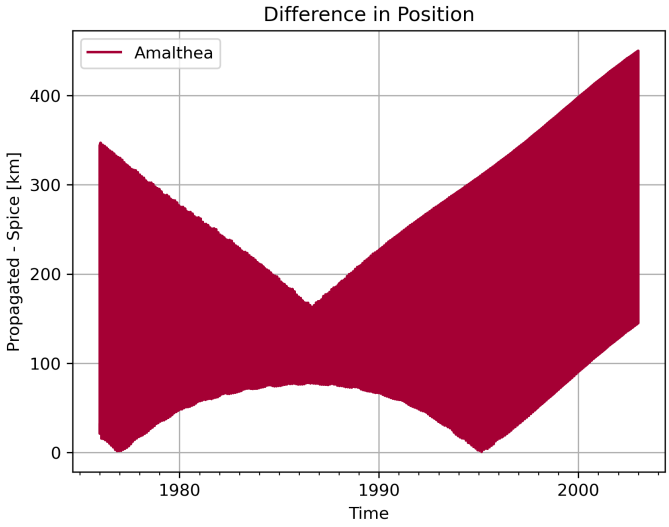

(b) Difference in the position of Amalthea between propagated initial state estimate and SPICE kernels for the postfit, Ama-01.

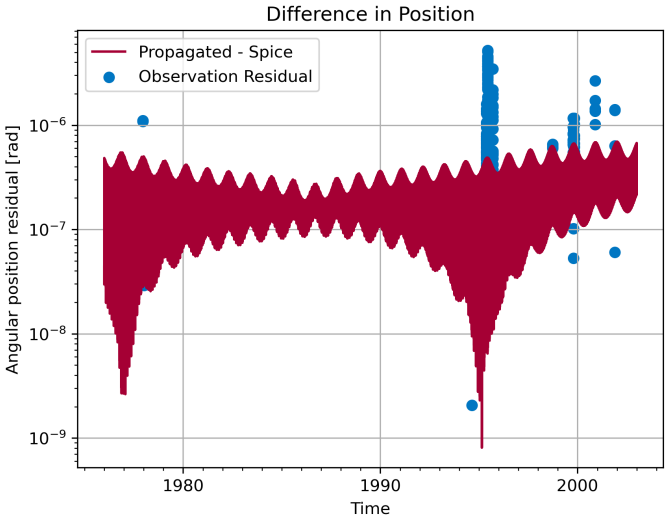

(c) Comparison between the quality of the Elara's propagated postfit initial state vs the observation residuals, Ama-01.

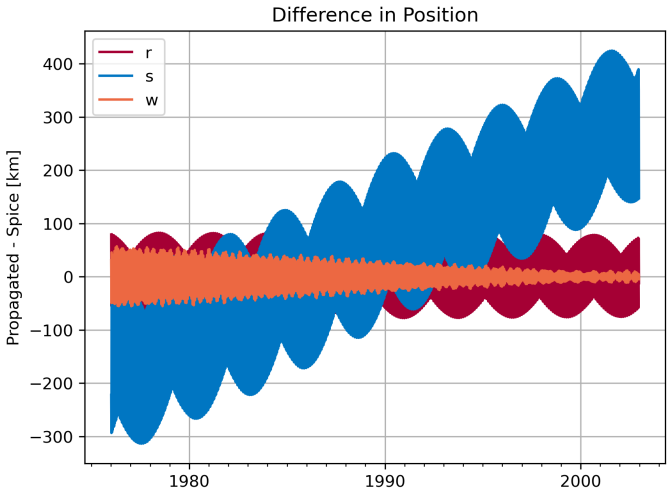

(d) Difference in the position of Amalthea between propagated initial state estimate and SPICE kernels for the postfit, broken down into RSW components, Ama-01.

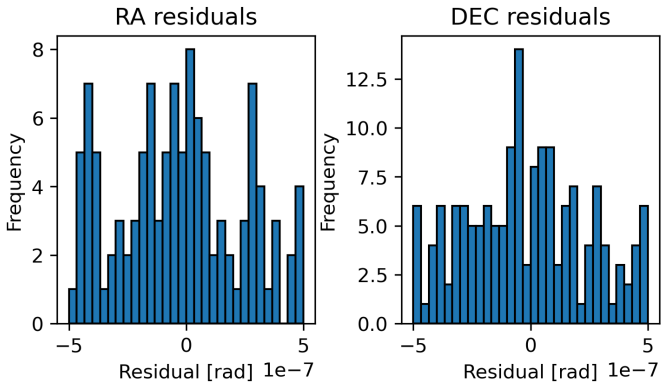

(e) The distribution of Amalthea postfit residuals per period, Ama-01.

Fig. 14: Results for the nominal run of Amalthea, Ama-01

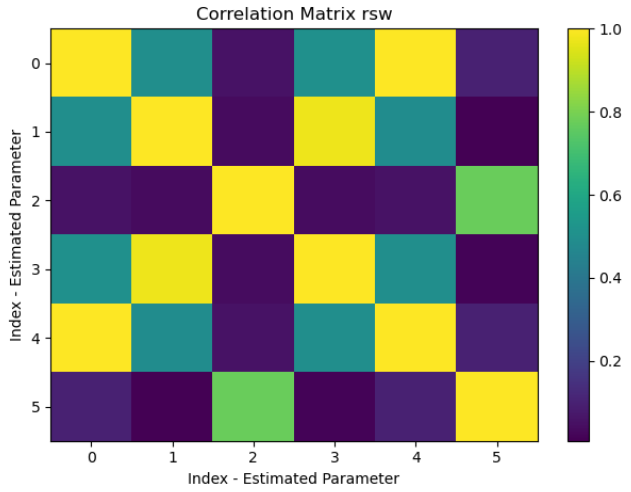

Fig. 15: Correlations between Amalthea's estimated initial state parameters, Ama-01.

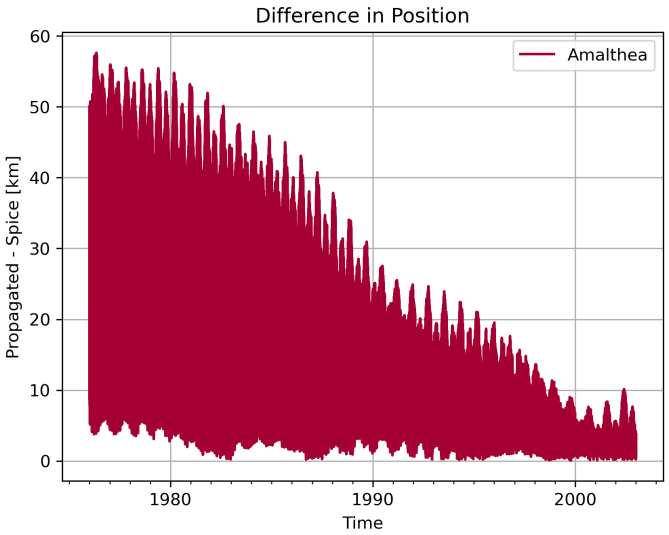

Fig. 16: Difference in the position of Amalthea between propagated initial state estimate and SPICE kernels for the postfit, including simulated mission data, Ama-02.

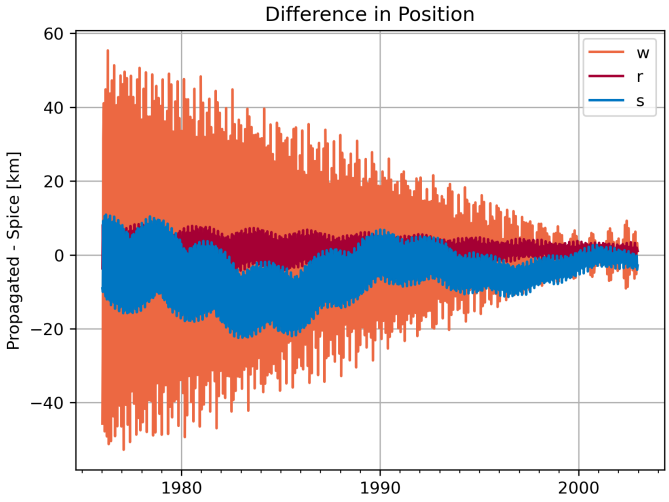

Fig. 17: Difference in the position of Amalthea between propagated initial state estimate and SPICE kernels for the postfit, broken down into RSW components, Ama-02.

Appendix A: Weights and Biases

In this appendix, an overview will be given of the applied weights and arcwise bias corrections, whenever they were applied, for each of the study cases. These weights were determined based on the squared inverse of the average residual within a 6-hour arc, as explained subsection 4.2, and were constant for all observations within that arc. A correction factor of $\sqrt{n}$ was applied to reduce the weight of individual measurements within such an arc, as they cannot be considered truly independent. The arcwise biases were simply equal to the average residual within each arc. Finally, note that within this entire section, all images only demonstrate the right ascension observations. Those for declination are omitted as they are very similar.

Appendix A.1: Himalia

Once again Himalia will be discussed first. In Figure A.1 the weights assigned to each data arc in Him-01 are shown. A few things can be noted immediately. First of all, as expected, the oldest observations have significantly lower weights, due to their poor quality. Despite this, they still proved to exert great influence on the postfit, as was demonstrated in Figure 5b. This formed part of the motivation on why it is so important to apply these weights so that more accurate observations are more dominant in the solution, as otherwise these poor observations would degrade the quality of the solution even more. Secondly, one can identity several arcs lying slightly above the majority for the modern observations. All of these contain very few observations, and thus have a randomly low residual. This is exactly why using arcwise weights instead of individual weights was necessary, as otherwise this phenomenon would be significantly worse, as can be seen in Figure A.2.

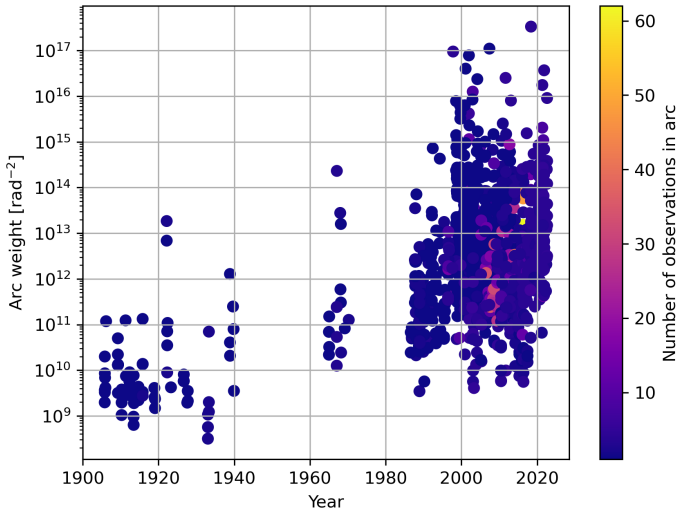

Fig. A.1: The distribution of weights for Him-01.

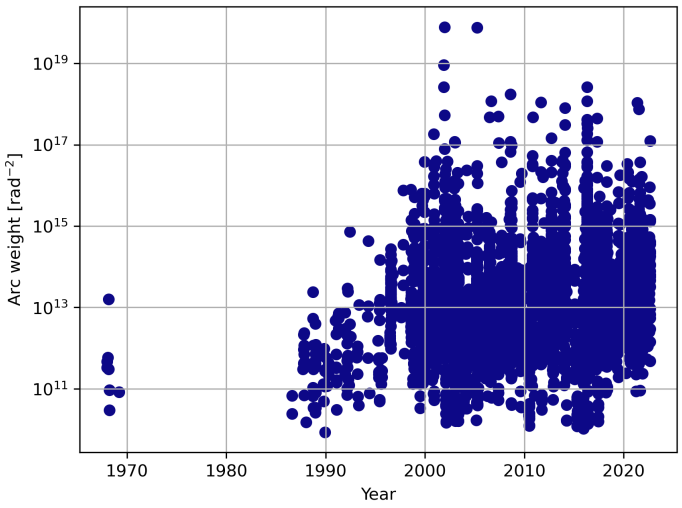

Fig. A.2: The distribution of weights for Him-01 if weights were assigned individually instead of in an arcwise basis.

Logically, the weights for the observation arcs in Him-02, where the oldest data was omitted, are exactly the same as observation residuals prefit do not influence each other, as can be confirmed in Figure A.3. One interesting comparison however is what the influence is of the correction factor $\sqrt{n}$. This effect is demonstrated in Figure A.4, where the upwards shift in weight for the lighter colored dots is clear, while arcs with just a few observations stay relatively constant.

Appendix A.2: Elara

For Elara, the distribution of weights is very similar to Himalia, as can be seen in Figure A.5. Low weights for the oldest observations, with a few outliers in weight for the modern observations by observations arcs with a low amount of observations. It is worth considering the arcwise bias with respect to SPICE, however, which is shown in Figure A.6. The observation arcs containing many measurements have very low remaining biases, as expected. The magnitude of the arcwise biases before 1949 does prove to be significant however, validating the choice to correct for them. Note that for El-01, arcwise bias corrections were only applied to the oldest observations.

Appendix A.3: Amalthea

Finally, both weights and biases paint a different picture for Amalthea. First of all, one can note that the number of arcs is extremely limited, further reinforcing the belief that this data simply lacks in quantity, as it only consists of a handful of observation campaigns of a few nights. The poorer quality of measurements also results in lower weights across the board, demonstrated in Figure A.7, as compared to those of Himalia for example. Inversely, for this same reason, the applied arcwise biases, shown in Figure A.8, are quite significant, especially considering the higher impact of small position changes.

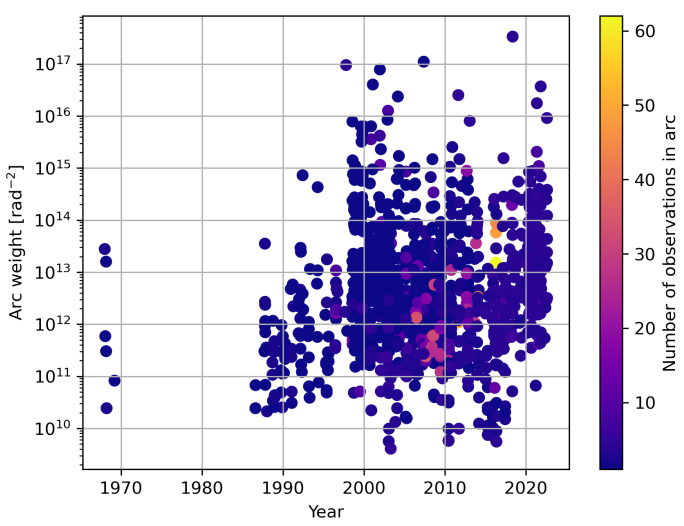

Fig. A.3: The distribution of weights for Him-02.

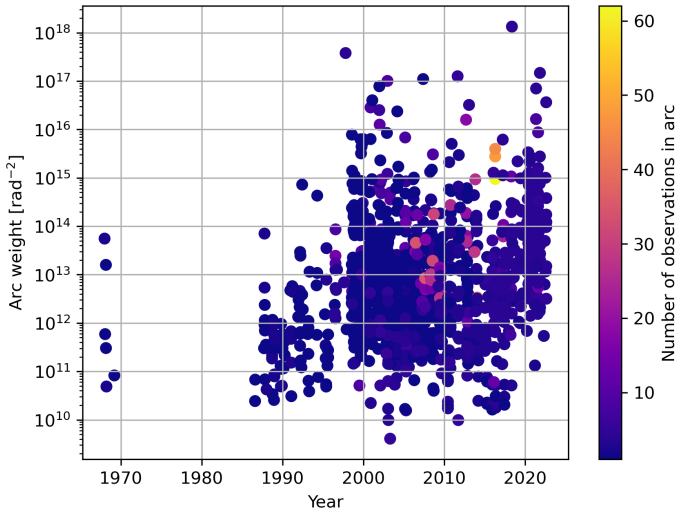

Fig. A.4: The distribution of weights for Him-02 if no correction factor would be applied for the amount of observations per arc.

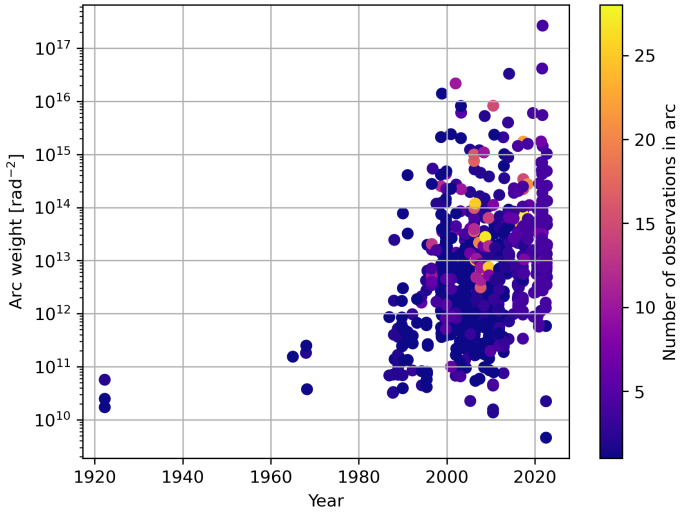

Fig. A.5: The distribution of weights for El-01.

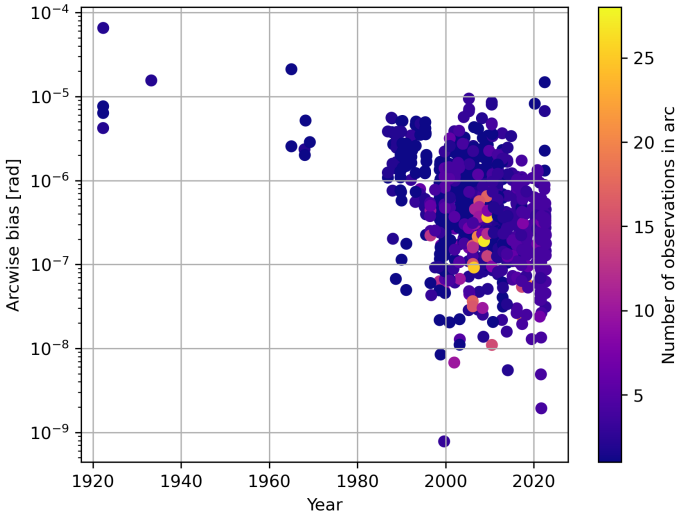

Fig. A.6: Average residual per arc for El-01, which is the bias correction. Note that this correction is only applied for arcs before 1960.

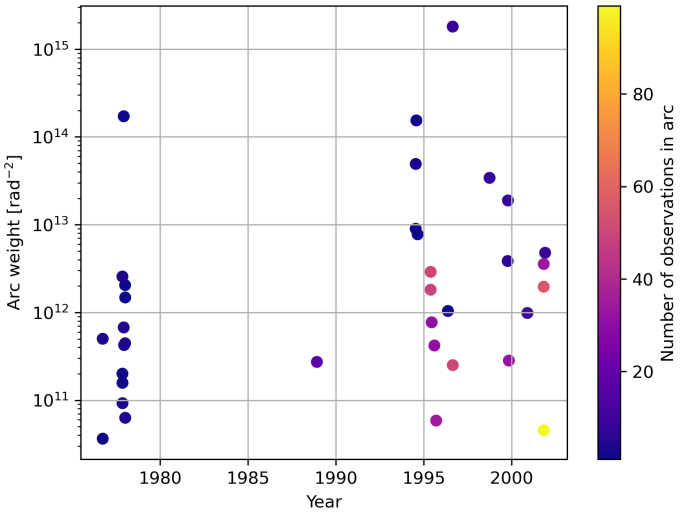

Fig. A.7: The distribution of weights for Am-01.

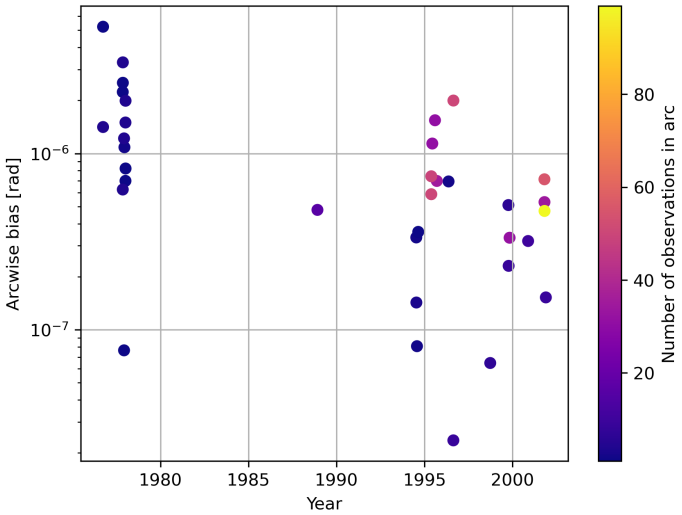

Fig. A.8: Average residual per arc for Am-01, which is the bias correction. Note that this correction is only applied for arcs before 1960.

3

Conclusions & Recommendations

The background and the main goal of this study were detailed in chapter 1, while the methodology and results were discussed in the article in chapter 2. This chapter will in turn be dedicated to highlighting the main conclusions, and the recommendations to the brave souls continuing this work in the future.

3.1. Conclusions

In section 1.1 the goals of this study were detailed. We will now look back and evaluate the extent to which these objectives were achieved, by assessing the completion of the exhaustive subgoals.

- **To Process the raw observations into uniform tudat-readable files.**

A versatile data processing algorithm was developed that was able to process any NSDC observation set of the Jovian moons. This algorithm relies on some metadata to understand how to process the observations, but apart from that operates independently. It works by first uniformizing the time into seconds since J2000 in the Barycentric Dynamic Time, before converting all measurements into an absolute expression consisting of right ascension and declination. Finally, all observations are rotated to the ECLIPJ2000 frame. At this point, any outliers are removed, the data is separated by observatory and target body, and saved in CSV files that can be easily loaded into tudat-compatible observation sets. The processed observations were compared to the SPICE benchmark and verified with expected accuracy from literature, except for measurements taken prior to 1950, to which there was a remaining bias due to conversion from old frames. Although the magnitude of this bias has been discussed previously (Jacobson, 2000), the proper correction was not detailed. Additionally, this algorithm was tested with observations of natural satellites of different gas giants to assess its robustness. The algorithm proved to be capable of accurately converting these data as well, although some small modifications were required due to differences in formatting.

- **To accurately model the dynamic environment of the (selected) Jovian moons.**

The accuracy of the dynamical model is best seen in the prefit, where the ideal initial state is estimated to minimize the difference in trajectory with respect to SPICE. For Amalthea and Himalia this discrepancy with SPICE remained extremely small across the period of propagation, with 30 km and 60 km respectively, most likely due to the minor differences in the integration or propagation, such as the zonal harmonics up to degree 8 being taken into account, rather than degree 6 for SPICE (Brozović and Jacobson, 2017) or the difference in integrator. These values are well within the uncertainty of the SPICE ephemerides (Brozović and Jacobson, 2017). Thus, for these two case studies, the error in the prefit is dominated by the quality of these ephemerides, while differences in dynamical modeling explain the existing discrepancies between prefit and SPICE.

For the dynamical model of Elara, the situation is slightly more complex, as the 1949 close approach with Himalia inflates any existing errors in the model. Concurrently estimating Himalia's gravitational parameter led to a significant reduction in this error, but a remaining residual of 400 km indicated that the dynamics of this close approach were still not captured exactly. However, this agreement was deemed sufficient for the purposes of this study. Note however that the discrepancy remains below 50 km from the event onwards.

- **To reach a convergent estimate of the orbit of the (selected) Jovian moons.**

For all of the study cases, a convergent estimate was reached, although the specifics differed a bit per moon. For Himalia the estimation process proved the easiest. The results showed a reasonable fit, that was dominated by a linear trend in the along-track direction. This drift was caused by the poor quality of the old data, related to the remaining bias with respect to SPICE in the conversion from old frames. After removing this data, however, an excellent agreement with the JPL ephemerides was found. For the period where plenty accurate observations were available, this difference stayed below 25 km, while it rose to 100 km for earlier epochs. Cleary, this challenges the relevancy of the older observations, given the uncertainty in these results is larger than the difference, i.e. these solutions are statistically indistinguishable. The estimation of Elaras orbit was once again limited by the accuracy at the close approach. Here the old data proved crucial in constraining the trajectory of Elara before the event. The inaccurate and sparse observations cause an error of several hundred km. Finally, the estimation process proved most difficult for Amalthea. The observations were limited and not well distributed. This, together with the rapid dynamics, means the inversion is almost ill-defined. An a-priori covariance matrix is then required to provide stability, which constrained the step in initial state to 100 km, which was a rough estimation of the uncertainty of the SPICE ephemerides in absence of concrete published results. This produced a difference with SPICE of hundreds of km, once again dominated by a linear trend in the along-track direction. This indicates that the input data is not sufficient to accurately model the orbital energy, which is highly sensitive due to the limited orbital period, and thus causes a clear drift.

- **To perform a preliminary assessment of the influence of Spacecraft observations on the generation of Amalthea ephemerides.**

One important difference between our solution for Amalthea and that published by JPL was the usage of mission data. To account for this dissimilarity, the Amalthea observations of Voyager, Galileo and Cassini were simulated based on the SPICE kernels, by including an artificial Gaussian error proportional to the expected accuracy. This turned out to have a significant effect on the ephemerides and reduced the discrepancy to a maximum of 50 km. The solution turned out to be most accurate, to only a few km, around the start of this millennium, when both Cassini and Galileo conducted valuable observations. These results should be put in the proper context, however. While very promising, these simulated observations were simplified versions of reality, directly representing Amalthea with a 3D position, rather than astrometric observations as is the case in reality. Furthermore, the uncertainty in these observations was estimated based on very limited data. This means that these results might very well be overly optimistic. They do prove however that further studying these observations is warranted in order to improve the quality of Amalthea ephemerides.

- **To determine the mass of Himalia.**

The final goal was to verify the published results on the mass of Himalia (Brozović and Jacobson, 2017; Emelyanov, 2005b). As mentioned before, this mass can be estimated from estimating the orbit of Elara, specifically around 1949, due to its close approach with Himalia. The gravitational parameter was determined to be equal to 0.144 km^{3}s^{-2} in the prefit and 0.132 km^{3}s^{-2} in the postfit. Both these values are in excellent agreement with that published by Brozovic at 0.13 ± 0.02 km^{3}s^{-2} and within the given uncertainty region. Emelyanov reported a value about a factor of two larger. However, the change in residuals is not statistically significant (Brozović and Jacobson, 2017).

3.2. Recommendations

Throughout this work, some interesting topics for future topics have been noted. These recommendations will be discussed in this section.

The first recommendation is to examine the oldest observations more closely and try to eliminate the remaining biases, or at least quantify their influence. It was demonstrated that this data has a significant effect on the quality of the ephemerides of Elara, and could help in studying the dynamics of close approaches between moons. This study should involve a deeper review of the old reference frames and the conversion required to more modern alternatives, and modify the data processing algorithm accordingly. Specifically, investigating the conversion related to the transformation from Newcomb's equinox to FK4 could prove beneficial, as briefly touched upon in Jacobson, 2000.

Secondly, the data processing algorithm should be expanded to allow for the conversion of raw space-based astrometrical observations to a tudat-compatible format. This study has relied on simulated measurements based on the limited amount of public knowledge about their accuracy. While it is by no means a perfect representation, it showed the influence of this data. A future study could now incorporate the real observations, which would result in a clearer image of the exact relation between Earth-based and in-situ observations.

Similarly, a promising expansion of the processing algorithm would be the incorporation of Space Telescope observations. The increasing quality of these telescopes allows for more faint bodies, which include many of the minor moons, to be observed. Many more natural satellite measurements are expected by Gaia and James Webb in the coming years and are estimated to be twice as precise as ground-based alternatives (Yan et al., 2019).

The rise in new observation methods could prove interesting as well to future iterations of this thesis. While there was not enough data available from mutual events and approximations involving small moons to make it worthwhile to incorporate it in this study, this availability is expected to rapidly change in the future. These methods allow us to measure the state of the bodies significantly more accurately, and subsequently will greatly improve future estimation processes.

In this study, the estimation process was limited to three case studies. There are however many more interesting moons that would be interesting to study. Furthermore, this framework can be expanded to different planetary systems. It will be interesting to study how their different dynamics influence the conclusions drawn here and the quality of the fit. Along the same lines, the set of parameters that are estimated can be expanded to include more properties describing the dynamical model. The gravitational parameter of Himalia proved to be a great example of the relevancy of studying such parameters, leading to a better understanding of the solar system dynamics. Each of these parameters that can be estimated accurately will improve the reliability of the long-term ephemerides and our knowledge of the evolution of the solar system.

Finally, future efforts should include the addition of an integrator that is better suited to the long-term propagation of the bodies. The integrators considered for this study were limited to those available in Tudat, which are not able to capture long-term dynamics.

References

Brozović, M., & Jacobson, R. A. (2017). The Orbits of Jupiter's Irregular Satellites. *The Astronomical Journal*, *153*(4), 147. https://doi.org/10.3847/1538-3881/aa5e4d

Chyba, C. F., & Phillips, C. B. (2002). Europa as an Abode of Life. *Origins of Life and Evolution of the Biosphere*.

Dirkx, D., Gurvits, L. I., Lainey, V., Lari, G., Milani, A., Cimò, G., Bocanegra-Bahamon, T. M., & Visser, P. N. (2017). On the contribution of PRIDE-JUICE to Jovian system ephemerides. *Planetary and Space Science*, *147*, 14–27. https://doi.org/10.1016/j.pss.2017.09.004

Dirkx, D., Lainey, V., Gurvits, L. I., & Visser, P. N. (2016). Dynamical modelling of the Galilean moons for the JUICE mission. *Planetary and Space Science*, *134*, 82–95. https://doi.org/10.1016/j.pss.2016.10.011

Emelyanov, N. V. (2005a). Ephemerides of the outer Jovian satellites. *Astronomy and Astrophysics*, *435*(3), 1173–1179. https://doi.org/10.1051/0004-6361:20042264

Emelyanov, N. V. (2005b). The mass of Himalia from the perturbations on other satellites. *Astronomy and Astrophysics*, *438*(3). https://doi.org/10.1051/0004-6361:200500143

Emelyanov, N. V., Varfolomeev, M. I., & Lainey, V. (2022). New ephemerides of outer planetary satellites. *Monthly Notices of the Royal Astronomical Society*, *512*(2), 2044–2050. https://doi.org/10.1093/mnras/stac586

Fayolle, M., Dirkx, D., Lainey, V., Gurvits, L. I., & Visser, N. A. M. (2022). *Decoupled and coupled moons' ephemerides estimation strategies Application to the JUICE mission* (tech. rep.). https://sci.esa.int/web/juice

Fayolle, M., Magnanini, A., Lainey, V., Dirkx, D., Zannoni, M., & Tortora, P. (2023). Combining astrometry and JUICE-Europa Clipper radio science to improve the ephemerides of the Galilean moons. *Astronomy and Astrophysics*, *677*. https://doi.org/10.1051/0004-6361/202347065

Hadjifotinou, K. G., & Gousidou-Koutita, M. (1998). Comparisson of Numerical Methods for the Integration of Natural Satellite Systems. *Celestial Mechanics and Dynamical Astronomy*, *70*, 99–113.

Jacobson, R. A. (2000). The Orbits of the Outer Jovian Satellites. *The Astronomical Journal*, *120*, 2679–2686.

Jacobson, R. A. (2014). The Orbits of the Regular Jovian Satellites.

Kulyk, I., Jockers, K., Karpov, N., & Sergeev, A. (2002). Astrometric CCD observations of the inner Jovian satellites in 1999-2000. *Astronomy and Astrophysics*, *383*(2), 724–728. https://doi.org/10.1051/0004-6361:20011770

Lainey, V., Arlot, J. E., & Vienne, A. (2004). New accurate ephemerides for the Galilean satellites of Jupiter II. Fitting the observations. *Astronomy and Astrophysics*, *427*(1), 371–376. https://doi.org/10.1051/0004-6361:20041271

Lainey, V., Arlot, J. E., Karatekin, Ö., & Van Hoolst, T. (2009). Strong tidal dissipation in Io and Jupiter from astrometric observations. *Nature*, *459*(7249), 957–959. https://doi.org/10.1038/nature08108

Lieske, J. H. (1980). *Improved Ephemerides of the Galilean Satellites* (tech. rep.). ASTRONOMY and ASTROPHYSICS.

Sohl, F., Spohn, T., Breuer, D., & Nagel, K. (2002). Implications from Galileo observations on the interior structure and chemistry of the Galilean satellites. *Icarus*, *157*(1), 104–119. https://doi.org/10.1006/icar.2002.6828

The Astropy Collaboration, Price-Whelan, A. M., Lim, P. L., Earl, N., Starkman, N., Bradley, L., Shupe, D. L., Patil, A. A., Corrales, L., Brasseur, C. E., Nöthe, M., Donath, A., Tollerud, E., Morris, B. M., Ginsburg, A., Vaher, E., Weaver, B. A., Tocknell, J., Jamieson, W., … Zonca, A. (2022). The Astropy Project: Sustaining and Growing a Community-oriented Open-source Project and the Latest Major Release (v5.0) of the Core Package*. *The Astrophysical Journal*, *935*(2), 167. https://doi.org/10.3847/1538-4357/ac7c74

Yan, D., Qiao, R. C., Yu, Y., Cheng, X., Zhange, H. Y., Lana, Z. G., Yang, B. P., & Luo, H. (2019). New precise astrometric positions of Himalia in 2016 - 2018 based on Gaia DR2. *Planetary and Space Science*, *179*.

Zeebe, R. E. (2023). OrbitN: A Symplectic Integrator for Planetary Systems Dominated by a Central Mass—Insight into Long-term Solar System Chaos. *The Astronomical Journal*, *166*(1), 1. https://doi.org/10.3847/1538-3881/acd63b

A

Observation Processing Algorithm

The data found in the NSDC satellite observation database was provided in a wide range of different formats. To convert this data to a uniform format that could directly be input into the Tudat estimation process, a conversion and sorting algorithm was developed. Its general structure and working principle will be discussed here.

A.1. Meta Data

Due to the wide variety in formatting of the data, the first step was efficiently organizing the metadata describing the format and contents of every file. As the layout of the files describing the contents of each data file varied as well, which makes automatically reading these files difficult, we opted to insert the metadata at the top of the datafile manually. Sixteen entries were needed to robustly cover all variations in formatting, to specify the type of observable, the observed body or where to find it, the central body, how to properly describe the timing of the observation and most importantly where to find everything, amongst others. These 16 entries were directly loaded into Python as variables. Based on these variables, the algorithm will determine which path to take in processing the observations through straightforward if statements. The template for this metadata, including a definition per variable, can be found in the repository.

A.2. Time

The estimation process in Tudat was done in the Barycentric Dynamical Time (TDB) timescale, where an observation time is reported in seconds since the J2000 epoch. Thus, any observation reported in a different way, which is all of them, has to be converted. For all the files covered, which include the Jovian minor moon files and some additional Saturn satellite files to test the robustness of the algorithm, we faced four different types of time notation system: Julian Date (JD), Modified Julian Date (MJD), Gregorian date with 3, 4, 5 or 6 entries, and a single study chose to denote the epoch of observations by specifying the minutes since a reference JD. Conversion between these and the desired system is straightforward and was readily available in Tudat's 'time_conversion' module. In some instances, the direct conversion was not available, in which an intermediate step was added, for example, the MJD first being converted into a JD. On the other hand, conversion between time scales was not as straightforward. For this, we again relied on tudat functionality. The problem lay in converting observations before 1960. The Tudat function in question relies on first converting the observations to UTC, before a second conversion to TDB is made. However, UTC is only defined for epochs after 1960. Earlier observations where therefore converted using tudat's SPICE interface. The time module from the Astropy software library was successfully used to verify the correct conversions (The Astropy Collaboration et al., 2022). Finally, it is worth mentioning that some datasets used a timescale offset, for example UTC-3, which was resolved by adding this offset to the metadata. These time conversions were the necessary first step before accurate corrections can be made.

A.3. Angles

After successfully uniformizing the observation times, the observables can now be transformed as well. There are two main ways that these observables were reported in: absolute and relative, each with several variations. As all angular positions were to be converted to a decimal RA-DEC system, the easiest conversion was for absolute observations. These were provided with either 1 or 3 entries per angle. Note that these three entries vary between RA α and DEC δ. For the right ascension, these three entries are hours, minutes and seconds, while the declination is reported in degrees, arcminutes and arcseconds, a factor 15 smaller units. Both variations are then simply converted to decimal radians. Relative observations on the other hand rely on knowing the position of a second body, preferably with a lower uncertainty than the observations. The position of this relative body is requested from SPICE, similar to the benchmark used in this study, as explained in subsection 2.1 of the article. The only major difference is that the position here is requested in the orientation of the observation, instead of in ECLIPJ2000. In principle, converting these observations to absolute ones then simply consists of adding the angular position of the body and the relative angle. However, this angle was again reported in a multitude of ways. The easiest were observations in $\Delta\alpha$ and $\Delta\delta$, which could be added straightforwardly. Other datasets where reported in $\Delta\alpha * cos(\delta_{rel})$ and $\Delta\delta$, or in $\Delta\alpha * 10^5$ and $\Delta\delta * 10^5$. We have chosen to discard one file (ji0006) containing the angular separation as observable as it was significantly out of the line of this work, while not adding much to the eventual quality.

A.4. Rotation

Finally, the absolute observations have to be converted to the ECLIPJ2000 orientation, as it will be used in the estimation process. The raw data was available in several orientations. The majority was in B1950 or J2000, but several files had their date or year as the reference equinox. Within the algorithm at hand, the uniformization process consisted of two steps: converting any older files (i.e. those not in J2000) to J2000, and converting all files from J2000 to ECLIPJ2000. While the latter conversion is a simple rotation, the former proved more complex. We once again employed the astropy software library, in this case the flexible SkyCoord function to transform between the older observations in the fk4 frames to the fk5 frame with the J2000 equinox.

A.5. Postprocessing

After processing all observations, each dataset is analyzed as a whole. First of all, the mean and standard deviation are calculated. Any set that has a mean higher than the standard deviation is removed from consideration as it is likely that a bias is remaining in the data that was not accounted for. Although we realize that this affects small datasets disproportionally, the amount and volume of the remaining data make this a non-issue. Furthermore, any outliers (z>3) are removed as well. Finally, the files are filtered per observed moon and per observatory, to comply with Tudat's link end requirements, and saved in a csv file, along with the difference between the point and the calculated position of the body from the SPICE kernel.

A.6. Validation

To validate the data, the observations are compared to the SPICE kernels, which can be taken as truth at the precision level of a single observation, and as a good comparison for the data set as a whole. The averages and standard deviations where compared to the order of magnitude of expected results (e.g. Jacobson, 2000). Subsequently, some individual sets, that had clear publications including the quality of data, were used in confirming they have been processed correctly. One example is noted in Table A.1 based on datasets ji0002 and ji0004 (Kulyk et al., 2002), note that better accuracy is in part due to the outlier removal. Furthermore, one can observe that these values are not exactly the same, which is due to a difference in benchmark, but are sufficiently close together to confirm that there is no statistically significant difference.

Table A.1: Comparisson between results of the processing algorithm and those reported by Kulyk et al., 2002

Satellite (year)	α (mrad)	δ (mrad)	α Kulyk (mrad)	δ Kulyk (mrad)
Thebe (1999)	-0.049 ± 0.818	-0.089 ± 0.560	-0.097 ± 0.776	-0.291 ± 0.582
Amalthea (1999)	-0.336 ± 0.534	-0.292 ± 0.416	0.145 ± 0.485	-0.291 ± 0.242
Amalthea (2000)	-0.319 ± 1.066	-0.216 ± 0.799	-0.339 ± 1.067	-0.291 ± 0.873
Metis (1999)	-0.953 ± 1.334	0.907 ± 1.219	-1.406 ± 1.164	0.388 ± 1.212
Metis (2000)	-0.386 ± 2.168	0.366 ± 1.298	-0.727 ± 1.551	0.194 ± 1.309
Adrastea (2000)	-2.018 ± 4.091	0.537 ± 2.623	-0.727 ± 4.266	0.533 ± 3.006

B

Integrator and propagator set-up

In section 3 of the article, the equations of motion were discussed. One has to rely on numerical methods to solve these differential equations and advance the state of the estimated bodies through time, as most often an analytical solution does not exist. To set up this integration of the equations of motion, adequate integrator and propagator settings have to be defined to minimize both errors and computational requirements, which often require a trade-off. This propagation error can be broken down into multiple causes, which we will cover one by one. The first error consists of inaccuracies in the equations of motion or the dynamical model itself. These modeling errors come from inaccurate gravitational parameters, accelerations that were not taken into account, or other factors that cause a discrepancy between the equations of motion and reality. Logically, these errors are always present but should be kept below a defined precision level. A second source of errors stems from inaccurately integrating these differential equations. In order to be able to make meaningful conclusions about the quality of the estimation, which will be in the range of tens of km in the best-case scenario, the propagation errors should be at least an order of magnitude smaller. This appendix will discuss the settings required to achieve the necessary accuracy, specifically focussed on Amalthea, as it is the most sensitive out of the case studies. The reasoning behind adequate settings to accurately propagate the states of both Himalia and Elara are then kept short, as they largely follow the same reasoning. The first step is to define a benchmark as a reference for the magnitude of the errors.

B.1. Benchmark Generation

This benchmark was roughly based on an existing tudat example code, which covered a similar estimation process for the Galilean moons with simulated data [1]. For the benchmark, a Cowell propagator was chosen for its reliability and its capability to handle orbits with low eccentricities and inclinations, although it is not the most computationally efficient. In the same spirit, the 8th-order Runge-Kutta Dormand-Prince method with fixed step size is used as integrator to ensure accuracy of the benchmark over computational efficiency. One remaining setting for the benchmark is then the time step. For this multiple time steps were compared in Figure B.1a, which shows the growth of integration error over time for different time steps, and Figure B.1b, which shows the maximum error per time step. The integration error is evaluated with respect to a similar propagation with half the timestep. Finally, the propagation is limited here to 1 year due to computational limitations.

These figures both show that the intersection between the dominance of truncation and rounding errors lies in the orders of minutes. In the left figure, this can be seen by looking at the transition from smooth and uniform growth to more erratic behavior with decreasing time steps. The figure on the right further reinforces this idea by demonstrating the shift from broken, rapid changes to a linear trend. A suitable time step for the benchmark is then taken slightly before the change from rounding to truncation error

[1] https://github.com/tudat-team/tudatpy-examples/blob/feature/galilean_moons_state_estimation/estimation/galilean_moons_state_estimation.ipynb

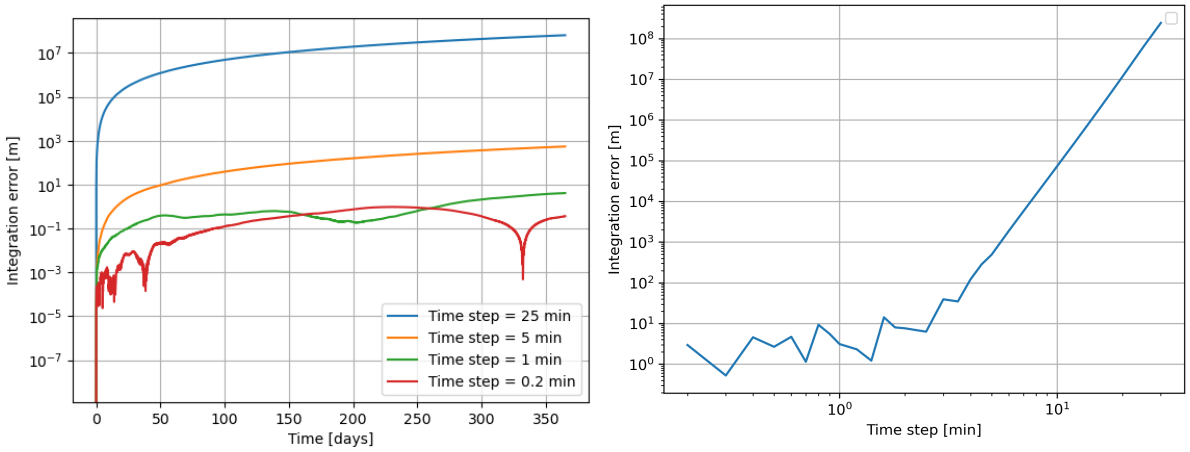

(a) Integration errors of different time steps over time.

(b) Max integration error for different time steps.

Figure B.1: Analysis of the appropriate time step for propagating Amalthea.

at 1 min. Furthermore, we already note that a time step of 6 min would be a good candidate for the integrator as it returns an integrator error in the order of kilometers, which is the desired accuracy.

A similar analysis was done for Himalia, using the same integrator and propagator. The main difference logically is the necessary time step. Although the figure is slightly less clear than for Amalthea, Figure B.2 demonstrates that a time step of 120 min proves sufficiently accurate to serve as benchmark.

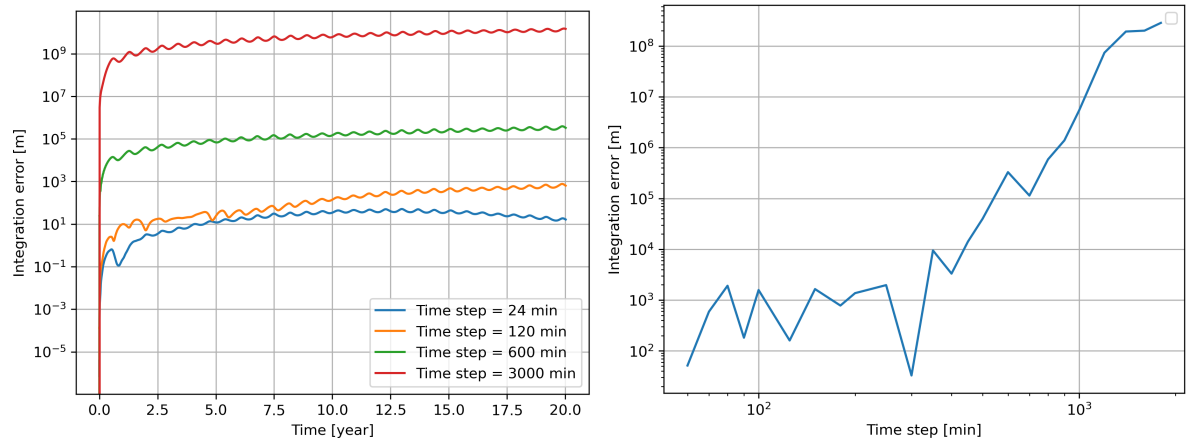

(a) Integration errors of different time steps over time.

(b) Max integration error for different time steps.

Figure B.2: Analysis of the appropriate time step for propagating Himalia.

B.2. Integrator & Propagator Analysis

We now have a high-accuracy benchmark that can be used to estimate the integration error of less precise propagations. This in turn allows for the selection of an appropriate integrator. corresponding to the desired accuracy level while minimizing the computational requirements. For this study, we will limit the selection to the integrators implemented in Tudat. Those include integrators from the Runge-Kutta, Bulirsch-Stoer, Adams-Bashforh-Moulton, and Euler families. These are some of the most common integrators and amongst the best for short periods of propagation, i.e. up to a few years for accurate solutions during a mission lifetime. These integrators are then a logical choice to include in Tudat, given a large part of earlier simulations were dedicated to the upcoming JUICE and Europa Clipper missions (e.g. Dirkx et al., 2016, 2017; Fayolle et al., 2022, 2023). This, however, does not correspond to the needs of this study, where integrators are required to be accurate over significantly longer periods

of time, i.e. more than 100 years. This automatically disqualifies many of the integrators available in tudat, for example the Euler method and the lower-order Runge-Kutta options. Furthermore, this suggests the optimal integrator might actually lie outside of tudat's capabilities. This idea is reinforced by comparing to similar ephemeris determination studies, that have opted for more accurate alternatives such as the Runge–Kutta–Nystrom or the Gauss–Jackson method (e.g. Brozović and Jacobson, 2017; Jacobson, 2000). Even more accurate might be the implementation of Recurrent Power Series (RPS, e.g Hadjifotinou and Gousidou-Koutita, 1998) or symplectic integrators, which are better at maintaining the energy of the system (e.g. Zeebe, 2023).

In order to prevent significant discrepancies in integrator error between the results of this study and the SPICE kernels that will be used as a comparison, the choice is made to continue with the 8th-order Dormand-Prince integrator as in the benchmark. This choice is not motivated numerically due to the lack of access to these more accurate long-term integrators, thus any conclusion from comparing with the benchmark would be moot. From Figure B.1b, it can be seen that 6 minutes will be an adequate time step for propagating Amalthea, keeping the integration error at the specified accuracy level. Similarly, a time step of 180 minutes was decided upon for both Himalia and Elara, resulting in a comparable integration error.

A similar reasoning is used in motivating the retention of the Cowell propagator. This option is a solid choice for all types of natural satellites, albeit not the most efficient. Other propagators, for example those employing Keplerian elements, face singularities for orbits with low eccentricities or inclinations. Encke's method on the other hand would be a good option for orbits with low perturbation. However, the trajectory of the outer Jovian satellites is significantly affected by the gravitational attraction of the sun. Thus, in this complex motion, the Cowell method is preferred. To keep this estimation framework uniform, this propagator option will be applied across the board, even though there might better options for individual cases.

B.3. Environment Model

Finally, an assessment is made of which accelerations are relevant to this study. For this, the difference between runs with and without a certain force will be compared. When the resulting difference in position over time stays below a few km, this effect is ignored. Otherwise, it is deemed necessary to include in the environment and will be used in the estimation process in the study. Once again the time of propagation is limited to one year. Note that the results of this estimation are preliminary and should not seen as exact values, rather as a simple way to decide with accelerations are relevant to this study. Especially for accelerations resulting in a small difference, it is impossible to separate their effect from the integration error.

Firstly the effects of the point masses of some celestial bodies are evaluated, specifically on Amalthea. To quantify the impact of these accelerations, the states over time resulting from a propagation taking them into account are compared to a reference solution, which in this case is a simple Keplerian orbit. This comparison is shown in Figure B.3a. Then, based on the assumption that these forces are uncorrelated, only the perturbations for which the change in propagated position is significant are added to the environment. From this figure, it can be concluded that the attractions by the Galilean satellites and the Sun prove highly influential, whereas the effect of the gravity of Saturn, Uranus, Neptune and the (other) minor Jovian moons, remains well below the the expected quality of the estimation. Therefore, one is lead to the conclusion that they can be ignored for the purposes of this analysis, at least for the Amalthea case study.

As Jupiter is not a perfect uniform sphere, the variations in its gravitational field have a significant effect on the orbit of the Jovian satellites, especially on the inner moons considering their close proximity to the primary. Therefore, it is important to estimate what level of precision is required in modeling this gravitational field, i.e. how many spherical harmonic terms (as explained in section 3 in the article) should be taken into account. For Jupiter this search is limited to the amount of degree terms that should be included, i.e. the variations in gravity field parallel to the rotational axis. Due to the rapid rotation and axial symmetry, the variations at a given latitude are insignificant. In Figure B.3b, the change in position with increasing degree is shown, each compared to the previous, i.e. degree 2 is compared to 0, degree 4 to 2, and so on. This figure demonstrates that the terms up to degree

8 are relevant to this study, as these cause a significant difference in orbit. Later terms were not properly implemented in tudat, but this decreasing trend in coefficient continues, as measured by the Juno mission (Parisi2020ResolvingFunctions), supporting the choice of including zonal terms up until degree 8.

Finally, the effects of some other possible accelerations are estimated for completeness' sake. First of all, a reference solution is again defined by considering the environment discussed earlier, including Jupiter's Spherical Harmonics up to degree 8 and order 0, and the point masses of the Galilean satellites and the Sun. Figure B.3c demonstrates the effect of the adding spherical harmonics up to degree and order 2 to the Galilean satellites, solar radiation pressure, and simplified models of relativistic and tidal effects. From these four, only the relativistic effects, for which Schwarzschild correction was used, came close to the desired accuracy of 1 km. To ensure that this correction can indeed be ignored, the propagation was extended to 13 years, as shown in Figure B.3d. This demonstrates that the error remains stable at a few km. Therefore the relativistic correction will not be applied in this study.

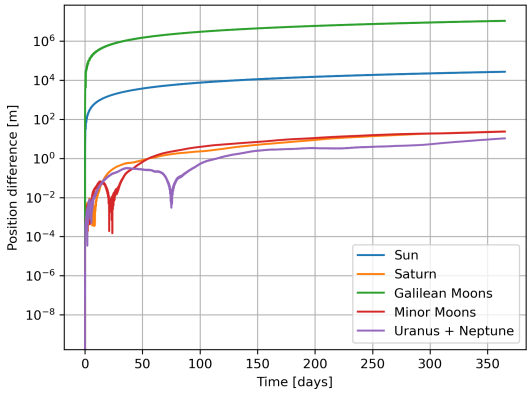

(a) Perturbation in position over time by the point mass of third bodies.

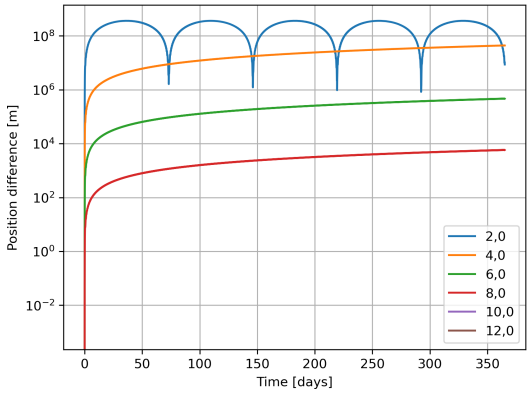

(b) Perturbation in position over time by th Jupiter Spherical Harmonics.

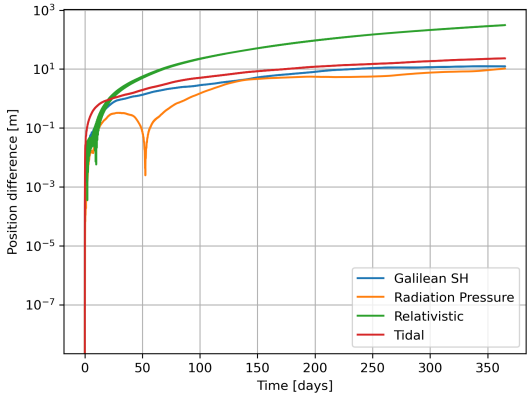

(c) Perturbation in position over time by other (pseudo-)forces.

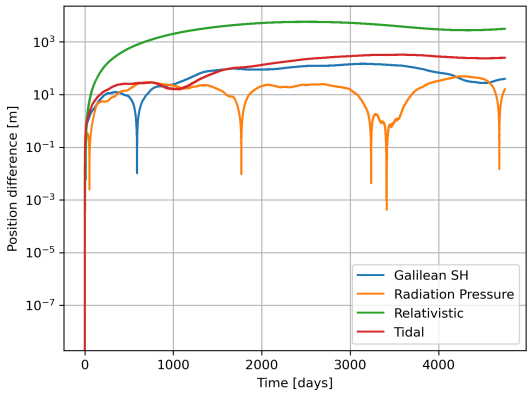

(d) Perturbation in position over time by other (pseudo-)forces over an extended timeline.

Figure B.3: Perturbations on Amalthea's position over time, based on groups of different types of accelerations.

For the outer moons, Himalia and Elara, a similar analysis yields slightly different results. Note that only one sets of results, namely those for Himalia are displayed, as Elara's plots show almost exactly the same image. One exception is Figure B.4d, which only applies for Elara, and will be explained later. The time of propagation was extended to 20 years for a better representation of the quality of the long-term propagation. One characteristic of outer moons is that they are more strongly perturbed by forces stemming from outside the planetary system as compared to regular satellites, considering their relatively weak attraction to the central body. This theory is confirmed in Figure B.4a, where the Sun proves to exert the highest perturbation, while Saturn can no longer be neglected. Due to their high mass, the Galilean Moons should also be added to the acceleration model in order to accurately propagate these outer satellites. On the other hand, the zonal terms of Jupiter's gravity field become

significantly less influential due to the aforementioned large distance. Logically, with increasing distance, the angular size of Jupiter decreases, and thus the effects of the spherical harmonics terms with them. In this case, the degree 2 term proves accurate enough for the study at hand. Similarly to Amalthea, none of the accelerations considered in Figure B.4c are significant enough to take into account for the rest of the study. There is one difference however between Himalia and Elara, due to their relative mass. As Himalia is significantly more massive, it influences Elara's orbit, specifically during their 1949 close approach. In Figure B.4d a propagation from 1945 to 1955 is demonstrated. Around the middle of this plot, a sharp increase in position difference between including or excluding Himalia's gravitational attraction on Elara can be seen, which corresponds to the event. Note that no plot was added to depict Elara's gravitational influence of Himalia, as no reliable values for Elara's mass are available. It is however safe to conclude that this perturbation is negligible.

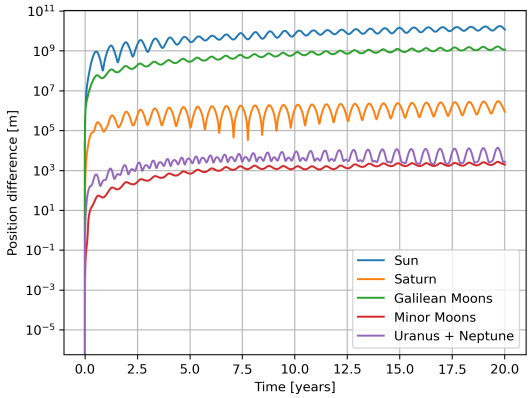

(a) Perturbation in position over time by the point mass of third bodies.

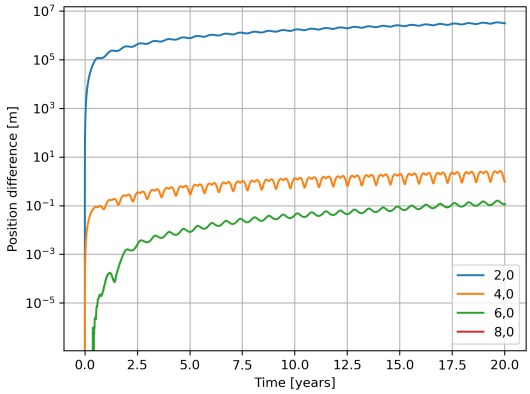

(b) Perturbation in position over time by th Jupiter Spherical Harmonics.

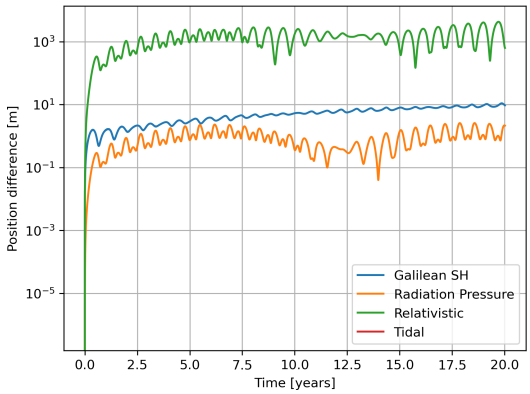

(c) Perturbation in position over time by other (pseudo-)forces.

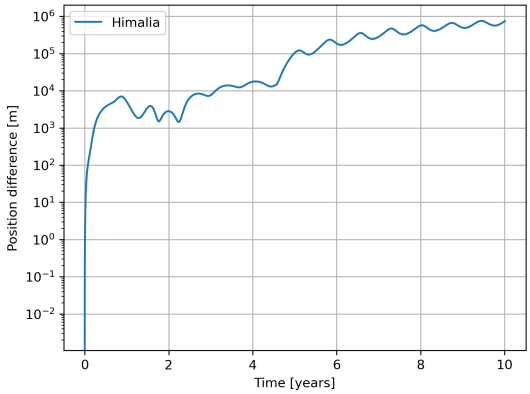

(d) Perturbation on Elaras position by Himalia, in the 10 years surrounding the close approach.

Figure B.4: Perturbations on Himalia's and Elara's position over time, based on groups of different types of accelerations.

Note that these conclusions on the outer moons might vary per family or even per individual moon, and this process should thus always be repeated for other study cases.

For the sake of uniformising the study, the same environment model was used for all study cases, except for Elara's special case. This means in practice that for all moons, the following accelerations were used:

- Jupiter spherical harmonics gravity field with degree and order 8,0
- Sun point mass gravity
- Saturn point mass gravity
- Galilean moons point mass gravity

While this means a more extensive Jupiter gravity field for the outer moons and the addition of the

Saturn point mass to the inner moons than technically required, the benefits in increased usability due to standardization outweigh the small increase in computational cost.

C

Additional Data

Out of the more than 400 runs, this appendix will be dedicated to highlighting some results that do not directly reinforce the flow and conclusion of the article, but could help in understanding the depth and the context of the work and the set-up decisions. The case studies covered in the article will be revisited, and some alternative runs will be discussed for each of them. Logically only the post-fit will be considered, given that all the settings affecting the pre-fit were already covered in Appendix B.

C.1. Himalia

Once again Himalia will be considered first. In the article, specifically when discussing the set-up, it was explained that no arcwise biases were applied to the data for Himalia, unlike Elara. Here this choice will be revisited and its effect demonstrated, amongst others. First, the effect of applying arcwise biases is demonstrated in Figure C.1a. Comparing this error to the paper, it becomes clear that the quality of the fit over the last 40 years deteriorates, while the earlier error is the same. This behavior is related to the way the weights are defined. This weighting is based on the average quality of an arc before correcting for biases. The improvement in residual is not uniform across all observations, however. Arcs with a small amount of observations and/or a low variance will be significantly improved by applying this bias, whereas larger datasets with higher variances are less impacted by these corrections. However, as the weights are assigned based on original quality, these observations still pull the solution towards their inaccurate direction. This effect is clearly seen in the early observations in Figure C.1b, where the arcs containing a larger variance continue to do so after correcting, only centered around 0. Furthermore, as these sets contain more data, as well as having their average closer to 0, which means a higher weight, they dominate the final solution.

To verify that this behaviour is indeed caused by the weighting methodology, a subsequent similar run was done, without weighting the observations, while still applying arcwise biases. The results are demonstrated in Figure C.2. While the residuals are minimally different, the fit to SPICE shows a significant improvement. This is because the few arcs with a large number of measurements with a low average residual but high standard deviation no longer dominate the solution, instead contributing equally. Conversely, however, this also means that the more accurate arcs, as compared to SPICE, no longer contribute more to the solution, which results in a post fit that resembles the SPICE solution less than the final fit covered in the article, where the oldest data was simply ignored.

Furthermore, while this incompatibility of weighting technique and bias correction is theoretically present in both old and new data, this behavior is believed to be most extreme for the data-rich periods, considering the observations are packed more closely. Therefore, the next attempt to properly estimate Himalia's orbit was to only apply an arcwise bias to the oldest observations, as was done in the article for Elara. Results for both the weighted and unweighted versions of this set-up are shown in Figure C.4. Although there are minor differences between the two, it can be concluded that correcting weighted observations does not prove problematic in this case. One may wonder why it was then chosen to not

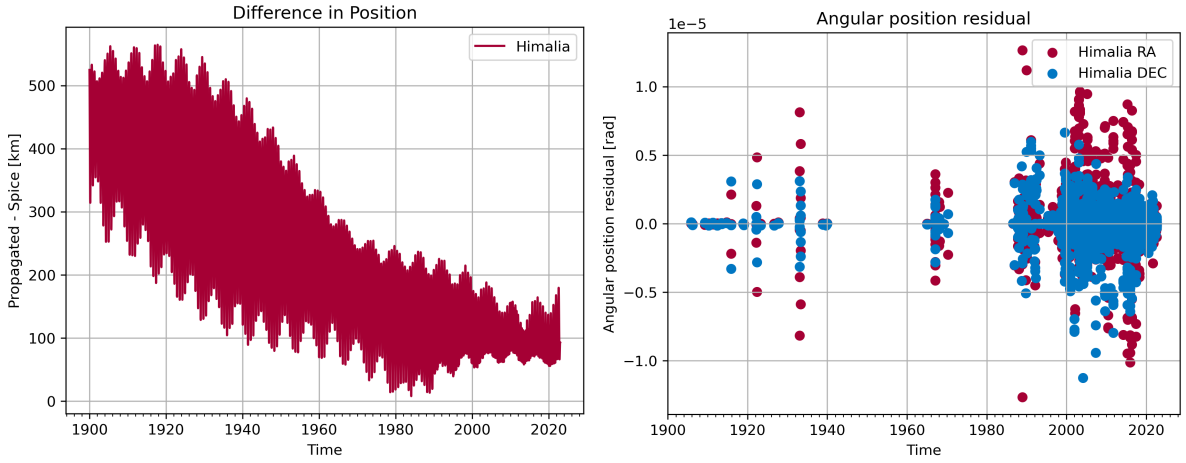

(a) Difference in position between postfit and SPICE kernels.

(b) Postfit observation residuals, broken down into RA and DEC.

Figure C.1: The results of estimating Himalia's orbit when applying arcwise corrections.

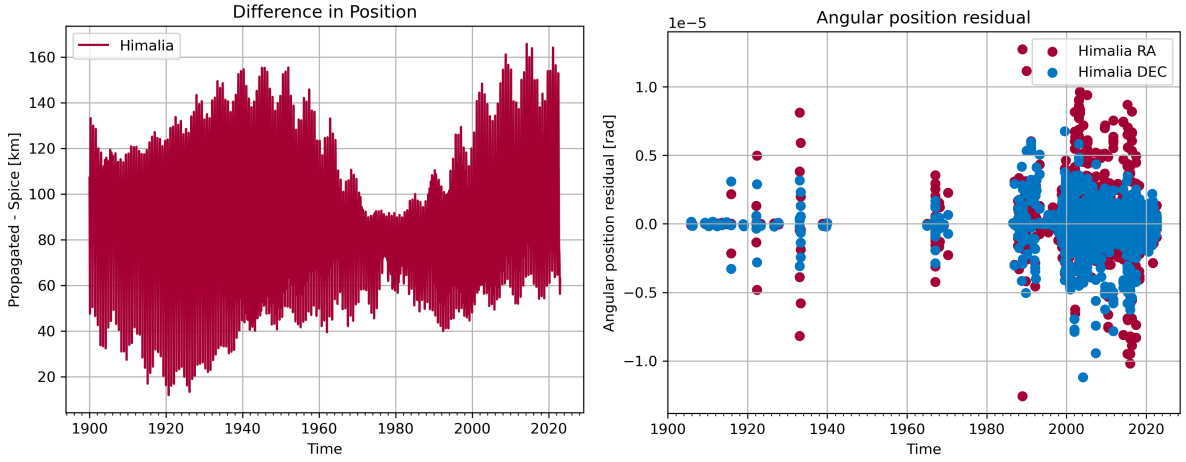

(a) Difference in position between postfit and SPICE kernels.

(b) Postfit observation residuals, broken down into RA and DEC.

Figure C.2: The results of estimating Himalia's orbit when applying arcwise corrections, without assigning weights.

apply this arcwise correction to these old observations, as was the case for Elara. This is due to the fact that applying such arcwise correction yields a skewed image when working with sparse datasets, such as these very old observations. Looking back at e.g. Figure C.3b, one can see that many of the residuals lie on, or close to the x-axis, indicating near-perfect observations, whereas these observations are significantly less accurate than their modern counterparts in reality. Applying arcwise corrections to a very limited amount of observations logically just sets them equal to the reference. Furthermore, this very reference is then used as a benchmark to determine the quality of the fit, returning an overly optimistic result. For this reason, the choice was made to retain the original values in the article, despite knowing there is a remaining bias, to demonstrate the effect of their relatively poor quality.

Finally, the effect of applying a correction of factor $\sqrt{n}$ to the noise in weighting arcs, to avoid crowded passes dominating the solution, is revisited. This analysis is made both for the estimation process with (Figure C.4a) and without (Figure C.4b) the oldest observations, like in the article. Omitting this correction factor proves to aggravate the conclusions drawn in the article. Starting with the version without the oldest observations, it is noted that the solution approaches SPICE even closer than the final result of the article, and only differs minimally from the prefit. This is related to the massive amounts of the most modern and accurate data monopolizing the solutions. Their weights are assigned based on their correspondence to SPICE, so the specific arcs that contain many observations and lie closest to SPICE pull the solution towards this very benchmark, explaining the agreement with the prefit. While it makes

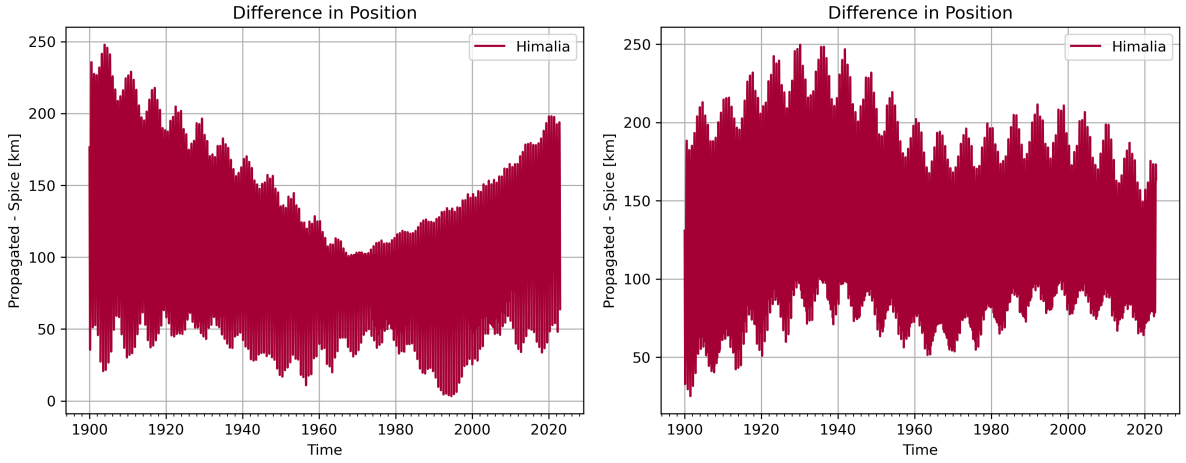

(a) Unweighted **(b)** Weighted

Figure C.3: The results of estimating Himalia's orbit when applying arcwise corrections only to the oldest datasets.

sense to assign these accurate measurements a significant weight, the factor $\sqrt{n}$ proves necessary to prevent rewarding these arcs twice. On the other hand, when including the oldest observations, it becomes clear that this correction factor also helps in mitigating the influence of the few inaccurate arcs before 1960. The discrepancy with SPICE, which can be taken as the truth at this precision level, grows by more than 40% by omitting this correction. This behavior is explained by realizing the poor fit is dominated by a few arcs with multiple observations, thus logically but unintentionally, decreasing the weight of these observations by a factor n improves the solution.

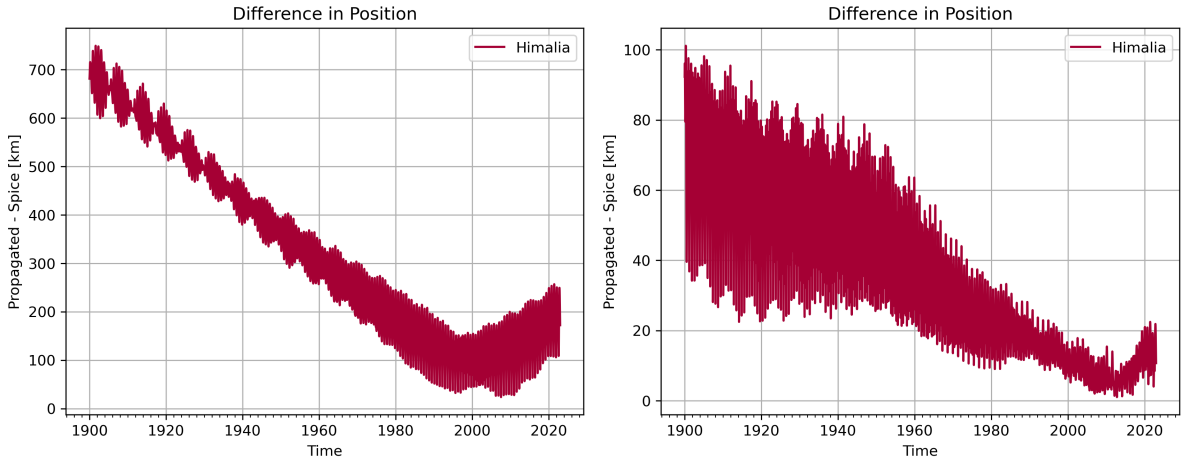

(a) With oldest observations **(b)** Without oldest observations

Figure C.4: The results of estimating Himalia's without applying a correction for the number of observations per arc, both with and without the oldest datasets.

C.2. Elara

Throughout both the article and the extra results discussed in the previous section for Himalia, it has been mentioned multiple times that no arcwise biases were applied to the oldest observations to give a realistic image of their effect on the estimation process. However, this same reasoning was not applied to Elara, where the quality of early observations is highly influential in constraining the orbit pre-1949, as demonstrated in Figure C.5. These figures represent the result of the estimation process when no arcwise biases are applied. A hard break can be seen at the epoch of closest approach, where the error quickly grows to 50000 km. Furthermore, Figure C.5b better demonstrates how the least-

squares solution agrees with the residual of the few old observations, demonstrating their influence. This warrants the application of arcwise biases, despite yielding an overly positive image, as more accurate data is required to estimate the orbit of Elara.

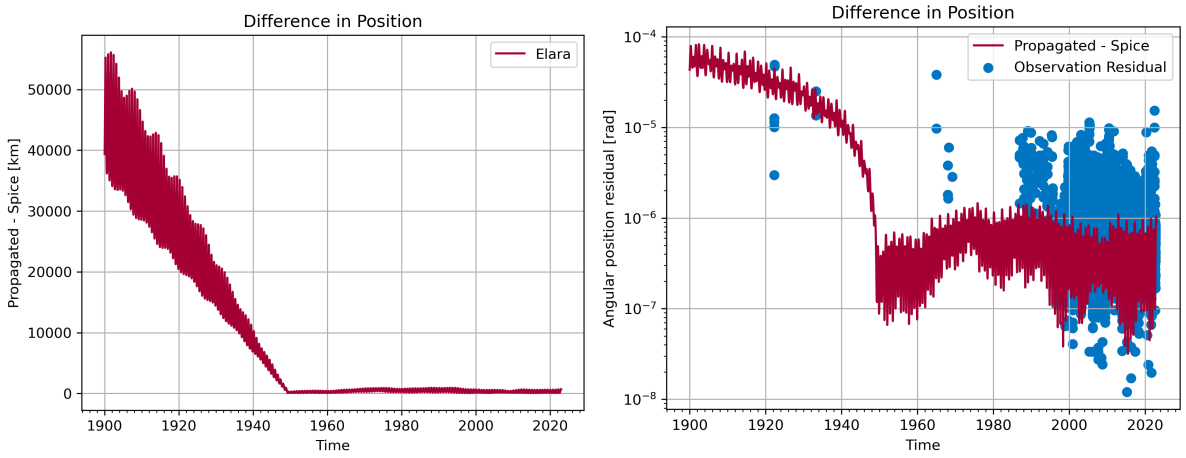

(a) With oldest observations

(b) Without oldest observations

Figure C.5: The results of estimating Himalia's without applying a correction for the number of observations per arc, both with and without the oldest datasets.

Secondly, the opposite can be considered, namely what the postfit would look like when applying these biases on all arcs. Much like it was the case for Himalia, Figure C.6 depicts a large discrepancy between SPICE and the postfit positions when combining the weighting methodology with applying arwise bias corrections. In this case, the magnitude of this difference is even larger, due to the balance of modern to old data being even more extreme compared to Himalia, together with the unique dynamics due to the close approach. For completeness' sake, a similar estimation, now without assigning weights to the observations is shown in Figure C.7. This image once again displays that the fit, logically, aligns closer to SPICE when applying arcwise biases. Furthermore, this reinforces the conclusion that applying these arcwise biases is not complementary with the weighting methodology. Finally, note that while this postfit better agrees with SPICE than the equivalent in the article, this bears no statistical significance until the processing of the early observations is improved, such that Himalia's gravitational parameter can be better approximated in turn.

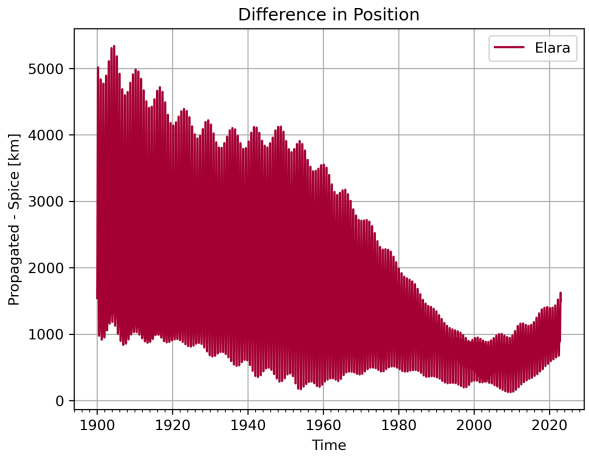

Figure C.6: Difference in position between postfit and SPICE kernels when estimating the orbit of Elara while correcting for arcwise biases everywhere.

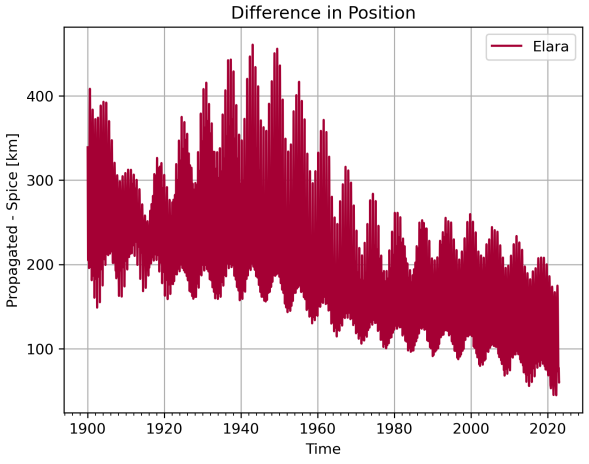

Figure C.7: Difference in position between postfit and SPICE kernels when estimating the orbit of Elara while correcting for arcwise biases everywhere, without assigning weights to the observations.

C.3. Amalthea

Finally, the reasoning behind the setup of the final case study, Amalthea, used in the article, will expanded upon. One of the main differences with the outer moon case studies was the difficulty in reaching a convergent solution. To improve convergence, some specific data was removed, while an apriori covariance matrix was specified to constrain the update in initial state per iteration. First, the effect of these removed datasets is shown in Figure C.8. A distinction is made between applying a tight apriori covariance constraint (20 km) and a looser one (200 km).

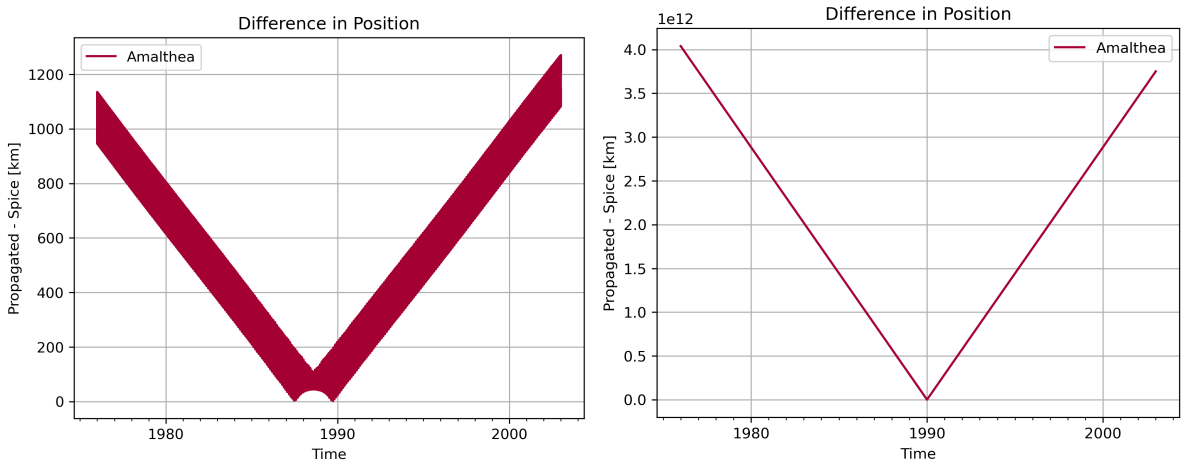

(a) With tight a-priori covariance constraints

(b) With loose a-priori covariance constraints

Figure C.8: Estimation of the orbit of Amalthea, including the datasets that were discarded in the article.

When applying these tight constraints, as demonstrated in Figure C.8a, the solution does not converge, instead the initial state is changed by tens of km between every iteration. Such constant steps between iterations are expected when the a-priori constraint is set too tight. However, in this case, the first two iterations do not follow suit, instead, they have a significantly larger, close to 100 km, change in initial state, before settling on these constant steps. The image depicts the quality of the fit with respect to SPICE after 5 iterations, but this figure continues to worsen for further iterations. If the constraint is loosened on the other hand, the updates to the initial state rapidly spiral out of control, leading to a terrible solution, as shown in Figure C.8b. Thus, these specific sets, of which the 'ji0013' is the most prominent, were removed to improve the quality and convergence of the fit. Although this is thought to be related to them leading the inversion to be ill-posed, it is not clear why these specific sets cause this behavior.

Secondly, the effect of applying the a-priori covariance matrix is assessed. Looking at Figure C.9a, one can quickly realize that this is almost exactly the same figure as the one that was presented in the paper. Logically, one may then wonder what the point is of bothering with applying such an a-priori constraint, given that it does not seem to do much. However, the reason for keeping this constraint is more complex. While it is true that it does not affect the final run, it provided stability and convergence for many earlier iterations of the estimation process, as will be seen in the rest of this section. It turns out that the chosen final set-up, which includes weighted observations, correction for arcwise biases, and the elimination the disturbing datasets, is more stable compared to earlier versions, but it would have been impossible to find this exact configuration without the a-priori matrix, as it prevented the solution from immediately creating a position difference of millions of km with respect to SPICE. For this reason, the constraint was kept, even though it was not technically required anymore for this specific run, which could not be known beforehand.

However, retaining the a-priori covariance matrix does pose a problem, namely what magnitude it should be. While 100 km was found to be a suitable level for the problem at hand, as it is the rough level of knowledge available on the orbits of Amalthea, one has to be wary of the risks. If the constraint is too loose, the solution rapidly diverges to several millions of km away from the true orbit, comparable to as was seen earlier in Figure C.8b. Conversely, placing the constraint too tight does not allow

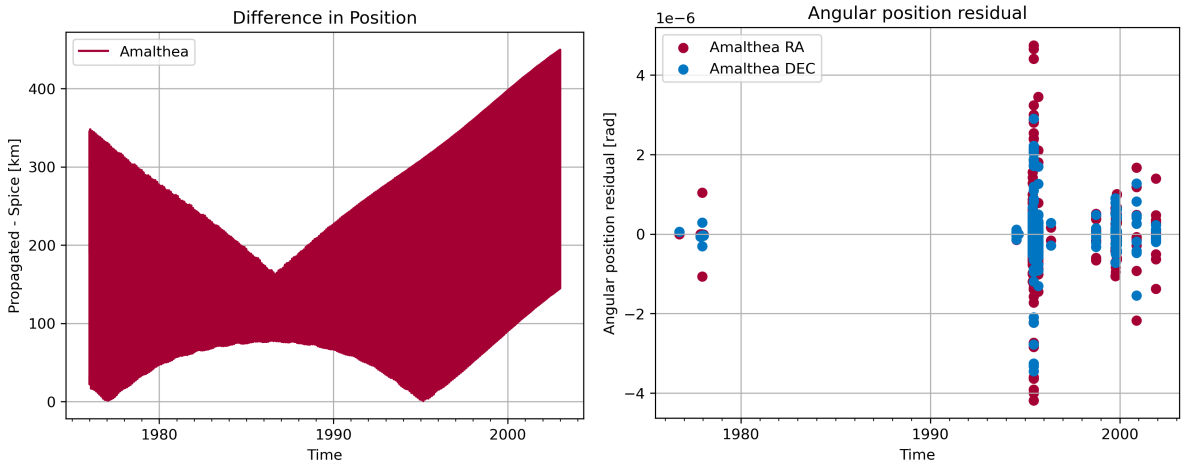

(a) Difference in position between postfit and SPICE kernels

(b) Postfit observation residuals, broken down into RA and DEC

Figure C.9: Estimation of the orbit of Amalthea, without posing an a-priori covariance matrix constraint.

the initial state estimate to deviate sufficiently from the initial guess, resulting in solutions such as Figure C.10. Depending on how much too tight this constraint is, the solution will resemble the prefit (such as Figure C.10a or true postfit (such as Figure C.10b) more, where true refers to the postfit if the perfect a-priori constraint was defined.

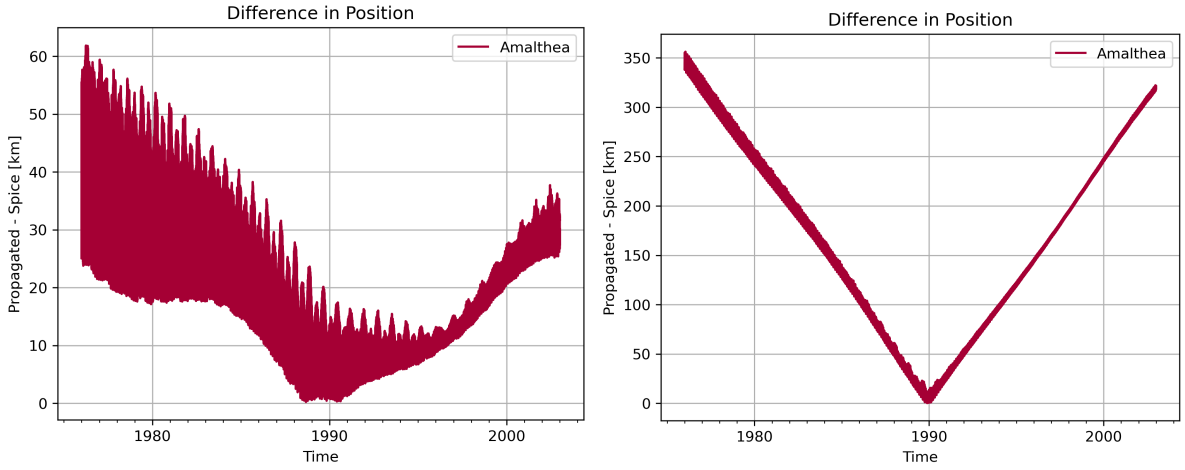

(a) covariance of 10 m

(b) covariance of 1 km

Figure C.10: Estimation of the orbit of Amalthea, with a overly tight constrain on the a-priori covariance.

Another design decision for the estimation process used in the paper was to apply corrections for arcwise biases. Unlike Elara, and despite the conclusions drawn in the earlier sections of this appendix, this correction was applied for all Amalthea data. However, it is important to realize the significantly different nature of the case studies. For Himalia and Elara, the problem turned out to be the massive cluster of modern data, where the combination of the weighting methodology and bias correction proved incompatible, which led to some arcs adversely impacting the quality of the fit. However, when looking for example at Figure C.9b, one can quickly realize that the situation is vastly different for Amalthea. The data is divided into a limited number of clear arcs. Additionally, it is important to realize the significantly higher effect of any remaining biases, as compared to the outer satellites. While the magnitude might be similar to those seen before, the angular size of such an error is way more significant to Amalthea, thus eliminating these biases is very important for a good fit. This reasoning is confirmed in Figure C.11, where the orbit of Amalthea was estimated without applying an arcwise bias. Two things can be noted from these plots. First of all, it is clear that the solution can safely be considered significantly worse,

given the large discrepancy with respect to SPICE. Secondly, Figure C.11b demonstrates an increased spread in residuals, as well as demonstrating clear biases, whereas the arcs were centered around the x-axis in Figure C.9b.

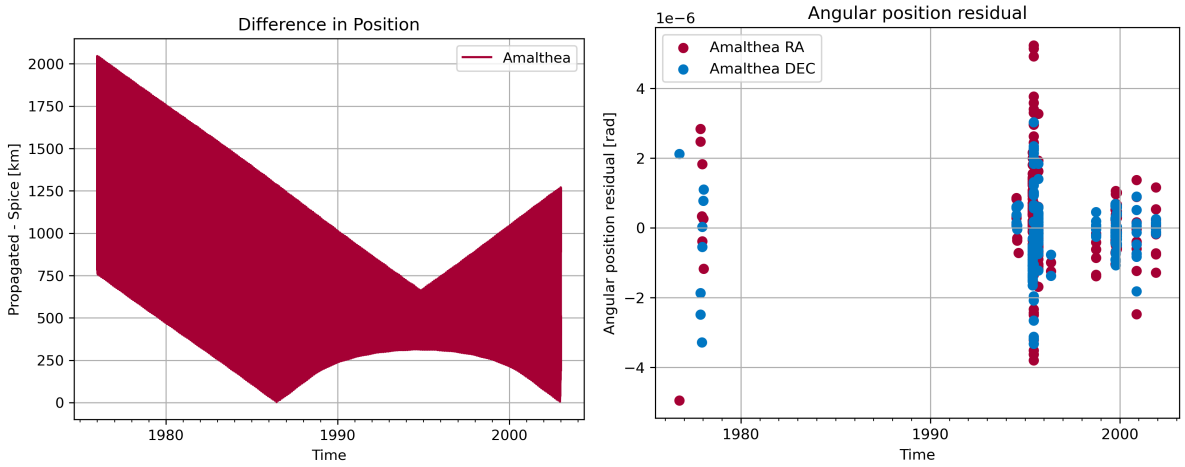

(a) Difference in position between postfit and SPICE kernels

(b) Postfit observation residuals, broken down into RA and DEC

Figure C.11: Estimation of the orbit of Amalthea, without correcting for remaining arcwise biases.

So far, the value of the arcwise bias has simply been set equal to the average residual within the arc. However, it is possible to estimate the value of this correction concurrently with the initial state, much like was the case for Himalia's gravitational parameter when estimating Elara's orbit. Despite the promise of this setup, it did not improve the quality of the least-squares solution, as can be seen in Figure C.12. This might be due to the fact that the initial guess is already close to the optimal value. Note that when estimating the magnitude of these arcwise biases, it is necessary to apply an a-priori covariance matrix. In this case, a constraint of 10^{-7} rad was chosen to prevent excessively large variations in the estimation of the bias. Higher values led to divergence.

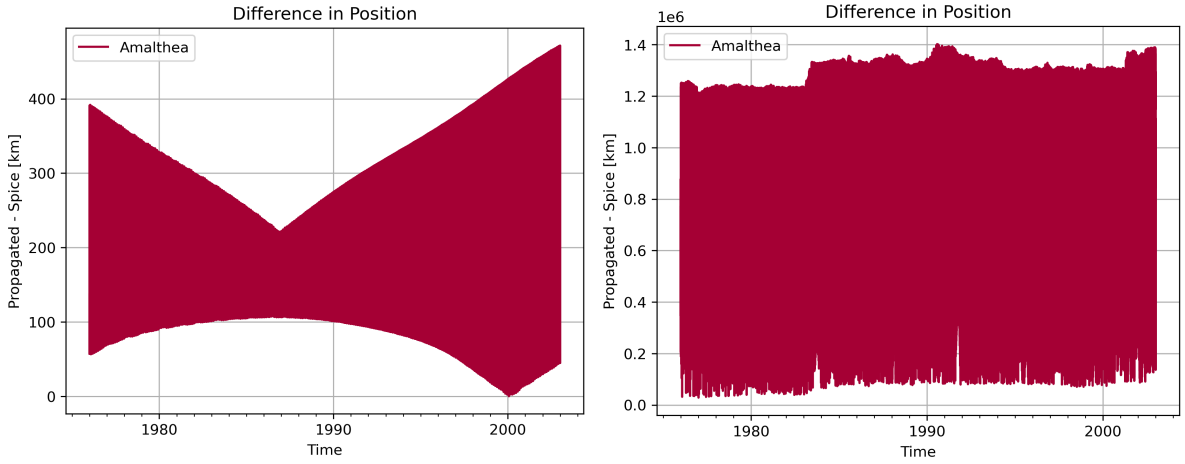

Figure C.12: Difference in position between postfit and SPICE kernels when estimating the orbit of Amalthea while concurrently estimating the arcwise bias.

Figure C.13: Difference in position between postfit and SPICE kernels when estimating the orbit of Amalthea without assigning weights to the observations.

Finally, Figure C.13 demonstrates the importance of including weighted observations for the Amalthea case study. Due to the relatively large spread in observation residuals, in combination with the sensitive nature of the Amalthea dynamic environment, it is crucial to assign higher importance to the more accurate observation(arcs). Failing to do so, as seen in the figure, quickly results in an orbit that is vastly different from reality.

In this appendix, the set-up of the case studies in the article was contextualized, and some further attempts were demonstrated. The choice to avoid correcting for arcwise biases for the outer moons, except where absolutely required, was explained. On the other hand, the importance of assigning correct weights was shown, including the normalization for data-rich arcs. Finally, the sensitivity of Amalthea, where the solution rapidly diverges to millions of km with inappropriate setup settings, was presented. An attempt was made to further improve the solution by estimating the magnitude of the arcwise bias, but this, surprisingly, turned out to have a negligible effect on the results.